Graduate School ETD Form 9
(Revised 12/07)

PURDUE UNIVERSITY
GRADUATE SCHOOL
Thesis/Dissertation Acceptance

This is to certify that the thesis/dissertation prepared

By SOUMINI VASAN

Entitled
CASCADES OF GENETIC INSTABILITY RESULTING FROM COMPROMISED BREAK-INDUCED REPLICATION

For the degree of Master of Science

Is approved by the final examining committee:

DR. ANNA MALKOVA
Chair

DR. SIMON ATKINSON

DR. ANDREW KUSMIERCZYK

To the best of my knowledge and as understood by the student in the *Research Integrity and Copyright Disclaimer (Graduate School Form 20)*, this thesis/dissertation adheres to the provisions of Purdue University's "Policy on Integrity in Research" and the use of copyrighted material.

Approved by Major Professor(s): DR. ANNA MALKOVA

Approved by: DR. SIMON ATKINSON 08/07/2013
Head of the Graduate Program Date

CASCADES OF GENETIC INSTABILITY RESULTING FROM COMPROMISED BREAK-INDUCED REPLICATION

A Thesis

Submitted to the Faculty

of

Purdue University

by

Soumini Vasan

In Partial Fulfillment of the

Requirements for the Degree

of

Master of Science

December 2013

Purdue University

Indianapolis, Indiana

I dedicate this to my parents.

ACKNOWLEDGEMENTS

I would like to express my deepest gratitude to my mentor, Dr. Anna Malkova for giving me an opportunity to work in her lab. She has been an absolutely amazing teacher, motivating and encouraging me throughout. Her strong passion for science is very inspiring and I truly admire her insightful approach towards solving problems. I thank her for all the guidance and support. I would also like to thank my hard-working, ambitious and friendly lab members Cynthia, Sreejith, Sandeep, Yu-Hsiang, Rajula and our lovely freshmen workers and undergraduate researchers for making my research experience here enjoyable.

I would also like to use this opportunity to thank our collaborator Dr. Lucas Argueso for his suggestions and ideas. He made working on a new and interesting territory like array-CGH easy for me.

I thank my committee members Dr. Simon Atkinson and Dr. Andrew Kusmierczyk for showing enthusiastic interest in my work and for providing valuable inputs and suggestions through the course of my research.

My achievement here would not be possible if it were not for the support of my father, Mr. S. Vasan Subramanian, my mother Mrs. Vyjayanthi Vasan, my brother Dr. Bharath Karthik Vasan, his wife Mrs. Harini Sundararaman Bharath and my sister Ms. Aishwarya Ramamurthy. I thank them for their unconditional love, encouragement and support. I love you all beyond words!

I give my special thanks to my extended family and friends here. The ones that have always been there for me and those that helped me sail through difficult times. I wish for all of them to find happiness and success in all their endeavors.

TABLE OF CONTENTS

Page

Page

Page

LIST OF TABLES

LIST OF FIGURES

Figure Page

Appendix Figure

Appendix Figure Page

LIST OF ABBREVIATIONS

ALT	Alternative Telomere Lengthening
BIR	Break-induced replication
CGH	Comparative Genomic Hybridization
Chr	Chromosome
CL	Chromosome Loss
CNV	Copy-number Variations
CR	Chromosomal Rearrangement
DNA	Deoxyribonucleic acid
DSB	Double-strand Break
DSBR	Double-strand Break Repair
dsDNA	Double-stranded DNA
Et Br	Ethidium Bromide
FACS	Fluorescence-activated Cell Sorting
GC	Gene Conversion
GCR	Gross Chromosomal Rearrangement
HC	Half Crossover
HCC	Half Crossover Cascades/ Half Crossover instability-Cascades
HR	Homologous Recombination

MHEJ	Microhomology-mediated end joining
NHEJ	Non-homologous End Joining
NRT	Non-reciprocal Translocation
PCR	Polymerase Chain Reaction
PFGE	Pulsed-field Gel Electrophoresis
Pol	Polymerase
PIKK	phosphoinositol-3-kinase-related kinase
SDSA	Synthesis-dependent Strand Annealing
SSA	Single-strand Annealing
ssDNA	Single-stranded DNA
WT	Wild type

ABSTRACT

Vasan, Soumini. M.S., Purdue University, December 2013. Cascades of genetic instability resulting from compromised break-induced replication. Major Professor: Anna Malkova.

Break-induced replication (BIR) is a mechanism to repair double-strand breaks (DSBs) that possess only a single end that can find homology in the genome. This situation can result from the collapse of replication forks or telomere erosion. BIR frequently produces various genetic instabilities including mutations, loss of heterozygosity, deletions, duplications, and template switching that can result in copy-number variations (CNVs). An important type of genomic rearrangement specifically linked to BIR is half crossovers (HCs), which result from fusions between parts of recombining chromosomes. Because HC formation produces a fused molecule as well as a broken chromosome fragment, these events could be highly destabilizing. Here I demonstrate that HC formation results from the interruption of BIR caused by a defective replisome or premature onset of mitosis. Additionally, I document the existence of half crossover instability cascades (HCC) that resemble cycles of non-reciprocal translocations (NRTs) previously described in human tumors. I postulate that HCs represent a potent source of genetic destabilization with significant consequences that mimic those observed in human diseases, including cancer.

CHAPTER 1. INTRODUCTION

1.1 Objectives

The overall goal of this research was to demonstrate the effects of reduced quality of DNA synthesis and checkpoint control during break-induced replication (BIR), a homologous recombination (HR) pathway of chromosome double-strand break (DSB) repair. This research is described with respect to the following specific aim:

To analyze the effects of impaired replicative polymerases and defective DNA-damage checkpoint response in BIR repair.

1.2 Organization

This thesis begins with a literature review (Chapter 2) where topics in DNA repair, HR repair mechanisms and genetic instabilities are introduced to the reader. Materials and methods used in this research work are described in Chapter 3. Results obtained from all my experiments are described in Chapter 4 followed by Discussion (Chapter 5), where I summarize and discuss findings relevant to my results.

CHAPTER 2. LITERATURE REVIEW

2.1 DNA double strand breaks

DNA double strand breaks (DSBs) are lesions physically disrupting and impairing both the strands of DNA. DSBs are primarily hazardous to the cell because they can lead to chromosomal rearrangements or cell death. DSBs can be caused by 1) exogenous factors like environmental toxins (example: heavy metals, organic pollutants like polychlorinated biphenyls (PCBs) etc.,), ultraviolet light, and gamma radiation or 2) endogenous factors such as reactive oxygen species or during repair mechanisms notably base excision repair and nucleotide excision repair. DSBs can also result from mechanical stresses in the cell. For example, the formation of dicentric chromosomes (chromosome with two centromeres) can result in breaks during anaphase leading to breakage-fusion bridge (BFB) events [1]. DSBs are also known to arise at stalled replication forks when the progressing replication fork encounters pre-existing nicks or lesions in the DNA double helix [2; 3]. DSB-induced changes to the genome have been implicated in promoting various human diseases, including cancer, which emphasizes the importance of proper repair of such lesions [4]. Multiple pathways of DNA repair have evolved and this research concentrates mainly on DSB repair by one Homologous Recombination pathway called Break-induced Replication (BIR).

2.2 Yeast *Saccharomyces cerevisiae* as a model organism to study DSB repair

Budding yeast *S. cerevisiae* was used as a model organism in this research where a system was employed to investigate DSB repair because of its comparatively small and completely sequenced genome which can be easily manipulated. Budding yeast can exist in two states - either haploids or diploids and they can also multiply rapidly making it greatly convenient for genetic analysis. DSBs and DSB repair are being studied in yeast and the studies related to repair genes and pathways are widely conserved in yeast and other higher eukaryotes, making studies in DSB repair highly relevant to the conditions in mammals and humans.

Many experimental systems have evolved to study DSB repair in yeast. In our experimental system to study DNA repair, DSBs are generated by a galactose-inducible HO endonuclease (see Chapter 4 for a detailed description). The DSB is initiated by a very specific HO-endonuclease (encoded by an HO gene) which causes a 4bp cut at a 24bp recognition site [5]. The HO gene was placed under the regulation of a galactose promoter [6]. Using this method of manipulating the GAL/HO promoter in our system serves as a useful tool for studying different pathways of DSB repair.

2.3 DSB repair pathways in *S. cerevisiae*

Multiple pathways of DSB repair have evolved but all of them can be mainly categorized into: 1) Non-Homologous End Joining (NHEJ) and 2) Homologous

Recombination (HR). NHEJ is a repair mechanism where there is simply a ligation of the broken DNA ends produced after a DSB without the requirement of any homology whereas HR mechanisms exclusively rely on homology to repair the DSBs.

2.3.1 Non-Homologous End Joining (NHEJ)

NHEJ is one of the two primary repair mechanisms wherein two non-homologous broken ends of a DNA molecule fuse together after a DSB (Fig 2.1). NHEJ is an error-prone repair mechanism. If the ends of the broken DNA molecules are compatible, NHEJ repairs the breaks [7] but this often results in small DNA insertions and deletions that can be destabilizing. Defects in NHEJ repair are also associated with carcinogenesis (reviewed in [8]).

Many studies aim to understand NHEJ in yeast and another alternative mechanism called Microhomology-Mediated End Joining (MMEJ), similar to NHEJ was identified, which occurs in the absence of Ku, an essential NHEJ repair protein which binds to DSB ends to initiate and mediate NHEJ repair. The MMEJ pathway also repairs DSBs by the principle of end-joining but requires very-short homology between the overhanging ends (Microhomology) [9].

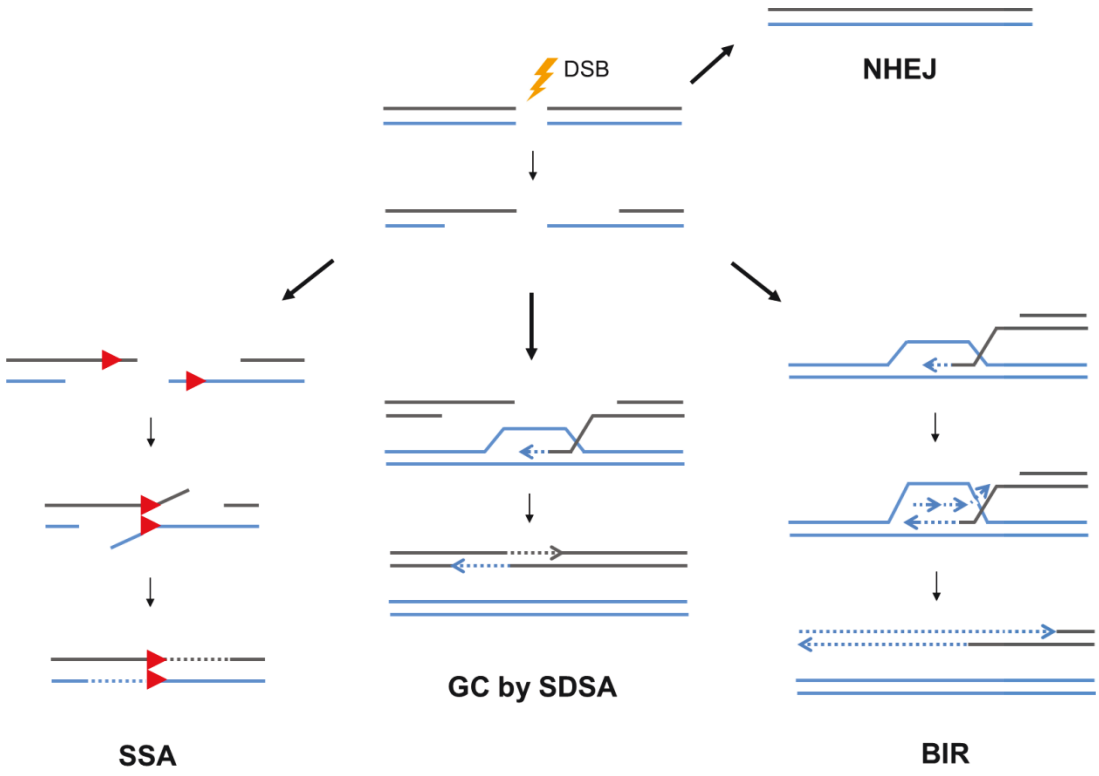

Figure 2.1. DSB repair pathways in *S. cerevisiae*. DSBs can be repaired by either HR (SSA, GC or BIR) or by NHEJ. The choice of repair depends on many factors, like the cell cycle, the extent of resection etc. GC can proceed by two possible ways, DSBR or SDSA, which are depicted in Fig. 2.2. See text for further details.

While HR mechanism is described as the most dominant DSB repair pathway in yeast; NHEJ and MMEJ are reported to occur more frequently in mammalian cells [reviewed in 10].

2.3.2 Homologous Recombination

Homologous Recombination (HR) is a DNA repair mechanism that uses genetic information from a homologous DNA sequence as a template to repair DNA breaks. HR requires at least 50 - 100 kb of homology between the recombining molecules. The choice of template sequence employed determines the genetic consequences of DNA repair. When sister chromatids are involved, the identical and intact sister chromatid is the preferred template for recombination and this type is thought to be the most secure form of repair which preserves genomic integrity [11]. The three main types of HR are Gene Conversion (GC), Break-Induced Replication and Single Strand Annealing (SSA) (Fig. 2.1).

2.3.2.1 Gene Conversion

The most preferred and safe HR mechanism to repair DSBs is gene conversion (GC) [12]. During GC repair, a small length of broken DNA fragments is repaired by filling the gap in the ruptured DNA; hence also known as Gap Repair. Gene conversion can be categorized into two types: GC with crossing over of flanking DNA sequences and GC without crossing over.

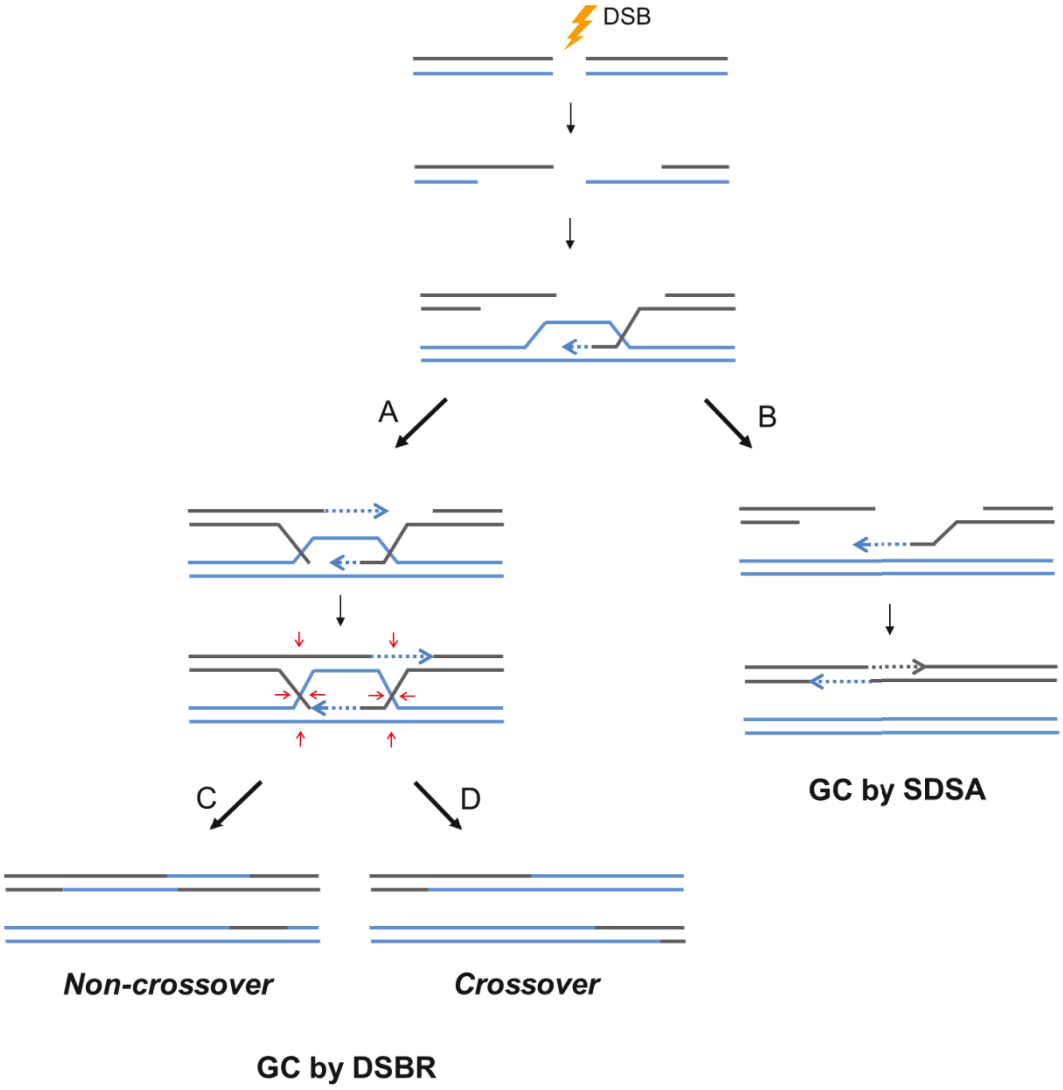

Figure 2.2. Two pathways of GC repair. DSBs can repair by GC through two mechanisms: DSBR or SDSA. DSBs induced during meiosis require the resolution of Holliday junctions either by crossing over or non-crossing over - GC by DSBR. DSBs induced in vegetative cells do not require Holliday junction resolution and repair by invasion on one side of the break - GC by SDSA. See text for further details.

The GC associated with crossing over is known to frequently occur in meiotic cells and is best explained by the Szostak model (1999) [13]. This kind of GC is also more commonly referred to as double-strand break repair (DSBR) (Fig. 2.2). In DSBR, upon DSB induction, 5' to 3' resection of the ends follows and the resulting 3' ends initiate recombination by invading a homologous template to begin new DNA synthesis. Two Holliday Junctions are formed and enzymatic resolution of the joint molecules is necessary for the repair to be completed (Fig. 2.2A) [14, 15]. The two Holliday junctions are independently resolved either by cutting the crossed strands or uncrossed strands, resulting in crossover (Fig. 2.2D) or non-crossover (Fig. 2.2C) products respectively. DSBR is also known to occur rarely in vegetative cells.

The GC associated without crossing over occurs more frequently when DSBs are induced in vegetative cells and is also known as synthesis-dependent strand annealing (SDSA) (Fig. 2.2B) [16, 17]. Mitotic GC or SDSA does not involve the formation of Holliday junctions. Upon 5' to 3' resection (on both sides of the break), at least one of the ssDNA ends invades the donor molecule and new DNA synthesis is carried out using the donor molecule sequence template. The heteroduplex molecule dissociates and the broken molecules are re-annealed using the newly synthesized sequences. The repair is completed by sealing of the single-strand gaps.

2.3.2.2 Single-strand annealing

Single-strand annealing (SSA) is a type of repair which is associated with DSBs that occur between two homologous regions that form direct repeats. The DSBs are repaired when complementary sequences on either sides of the lesion are annealed (Fig. 2.1) [18]. This mechanism was first proposed by Lin et al., (1995) [19] in mammalian cells. SSA proceeds by resection of the DSB ends that results in long single stranded tails. This results in the exposure of complimentary strands in a way that assists in their annealing. Annealing of the complimentary strands gives rise to extra flaps near the junction that are clipped off (Fig. 2.1) [20]. The resultant gap is filled by gap repair (or GC).

The consequences of this process include deletion of one of the direct repeats involved in annealing as well as the Interceding sequences. Such deletions make SSA a dangerous and unfavorable pathway when compared to GC. However, while comparing efficiencies between GC and SSA, even when a homologous sequence for GC is available, SSA predominates resulting in nearly 30% of the DSB repair outcomes [21]. SSA also shows approximately 100% efficiency with respect to repair of homologous regions flanking the DSBs in the range of 400 bp. SSA is a slow process when compared to GC and takes about 6 hours to complete [20].

2.3.2.3 Break-induced Replication

Break-induced replication is an alternative HR repair pathway that in contrast to GC, utilizes only one side of the DSB for HR (Fig. 2.1). A BIR-like recombination was first observed and identified in bacteriophage T4 [22]. This mechanism was previously known as recombination-dependent DNA replication (RDR) and was confirmed in *Escherichia coli* [23]. Further investigations in yeast revealed analogous mechanisms of DSB repair in eukaryotes where the 3' single-stranded end invades a homologous sequence followed by extensive DNA synthesis till the end of the donor molecule sequence [24, 25, 26, and 27].

The exact mechanism of BIR is still being understood but BIR is known to initiate in a manner similar to GC (Fig. 2.1). Upon DSB induction, the ends of the DNA are resected in a 5' to 3' direction followed by invasion of the 3' ssDNA broken end into a homologous donor sequence (Fig. 2.3). BIR differs from GC in the steps that follow where BIR has the ability to participate in repair only on one side of the DSB. As a result, the ends cannot re-anneal and ligate. However, the intermediate resulting from the one-ended invasion becomes a substrate for the assembly of a repair-related replication fork. New DNA synthesis now begins along the length of the donor template and the repair is completed when the donor template is copied till the end (Fig. 2.3). Although the complete composition of this replication fork remains unclear, the requirement for all the replication initiation factors [28] combined with a rate of replication similar to the

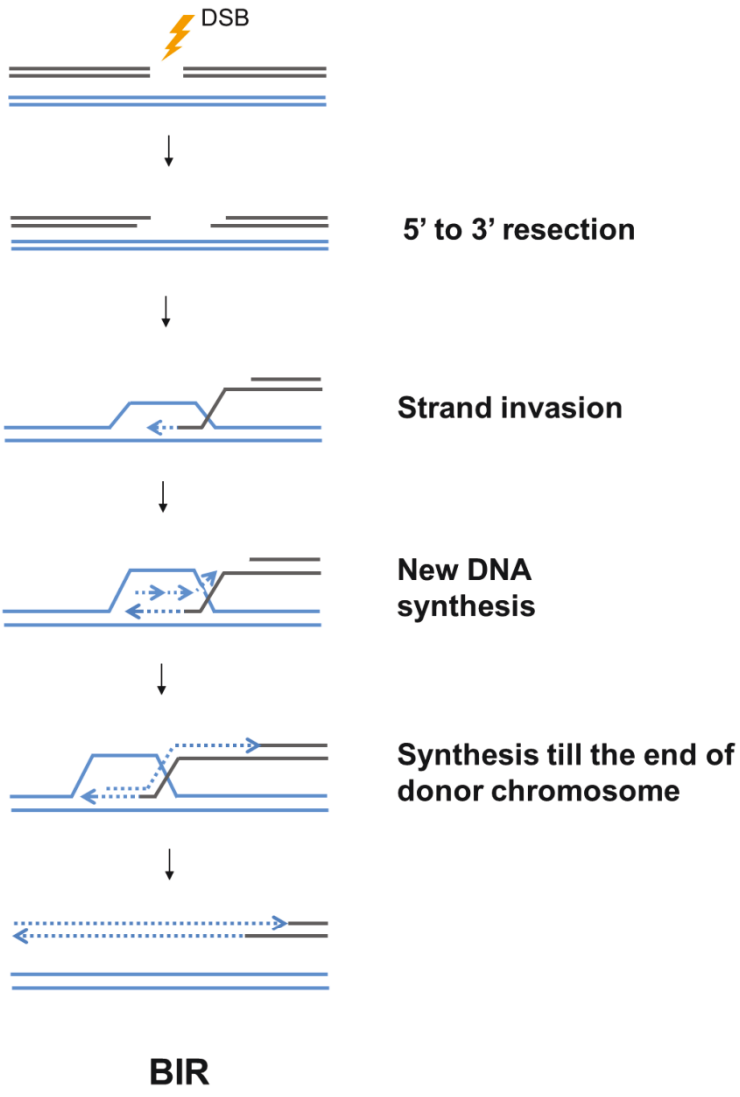

Figure 2.3. DSB repair by Break-induced Replication (BIR). This schematic shows the mechanism of BIR. See text for further details.

one observed in S-phase replication [29] suggest that a processive replication fork is assembled during BIR.

BIR is known to be important in preserving the stability of the genome. In the absence of telomerase, BIR aids in telomere maintenance (alternative telomere lengthening) [30, 31 and 32]. It was suggested that collapsed replication forks are rescued by HR mechanisms like BIR where the relevance was based on the structure of a stalled replication fork [33]. The collapsed replication forks are converted to DSBs by certain recombination pathways that further resolve these structures. A new replication fork can be formed when the broken chromosome recombines with an intact chromosome [34] and this suggests that BIR could be involved in the restart of collapsed replication forks.

BIR is a significant repair pathway for other reasons as well. For example, it has been observed that gap repair can proceed through BIR [35] and, for reasons that are not entirely clear yet; the frequency of BIR is known to increase in aged cells [36]. BIR is initiated by strand invasion, which occurs with kinetics similar to those of the GC pathway [35]. However, after strand invasion, progress stalls and DNA synthesis is delayed by 4 or more hours [37]. The exact reason for this pause is not known, but several possibilities have been proposed, including slow replication fork assembly, unstable D-loop formation, and the existence of a “recombination checkpoint”, discouraging BIR repair (reviewed in [38 and 39]). The delay in BIR initiation leads to the establishment of a checkpoint-mediated

G2/M arrest, which allows cells to complete BIR prior to cell division. Once DNA synthesis associated with BIR is initiated, it is fast and processive, similar to normal S-phase DNA replication [37]. It has been demonstrated that the initiation of BIR DNA synthesis involves the majority of proteins required for initiation of S-phase DNA replication [40] (See chapter 2.4.3).

2.4 The mechanism of Homologous Recombination in yeast and the proteins and replicative polymerases involved

The initial stages in HR include the DNA lesion processing stage where a Rad51-ATP-ssDNA filament (nucleoprotein filament) is formed, followed by synapsis where the filament executes a homology search and DNA strand exchange leading to D-loop formation. DNA synthesis begins and the stages that follow vary from pathway to pathway.

Many proteins have been identified to be involved in HR in yeast, many of which belong to the *RAD52* epistasis group of genes. This group constitutes of *RAD50*, *RAD51*, *RAD54*, *RAD55*, *RAD57*, *RAD59*, *MRE11*, *RDH54*/*TID1* and *XRS2*. This brief review will pertain to important proteins associated with GC, SSA and BIR in relation to the different stages of HR mentioned above.

2.4.1 Presynapsis

Upon DSB induction, the ends of the broken molecule need to be made available for resection since DNA resection is the crucial step differentiating HR from NHEJ [41 and 42]. The 3' ssDNA tails form substrates for the *RAD51* strand exchange protein. The switch from a DSB to ssDNA is also necessary for the activation of Mec1p and Tel1p checkpoint response. This resection occurs during the S and G2 phases of the cell cycle where the sister chromatid is available to provide an accurate template for HR repair.

The MRX complex comprising of Mre11p, Rad50p and Xrs2p is responsible for recognizing the DSBs in *S. cerevisiae*. Rad50p plays a role in holding the broken ends of the DSB together [43], while Mre11 cuts the ends of the DSB prior to 5' to 3' resection by other proteins. Xrs2p is known to assist Rad50p and Mre11p in recognizing the break site. The MRX complex in association with Sae2p removes short oligonucleotides from the 5' end of the broken DNA [44]. Incidentally, MRX and Sae2p are also responsible for inhibiting Ku protein (protein responsible for carrying out NHEJ) from the ends of the DSB [45]. MRX and Sae2p have another important task of assembling exonuclease Exo1p and helicase Sgs1p, along with endonuclease Dna2p to the broken DNA ends where they resect the ends further [44].

The 3' end of the ssDNA overhang is now exposed due to extensive resection and this exposed DNA attracts RPA which quickly binds to the ends protecting

the ssDNA from forming secondary structures. For SSA repair, the RPA-coated ssDNA is bound by Rad52p which completes the repair process by assisting in the annealing of the exposed ends and later in ligation [46]. For GC and BIR, the ssDNA is further processed. Nucleoprotein filament formation is necessary and this is accomplished by Rad51p which displaces RPA and binds to the exposed ssDNA. This process is mediated by Rad52p, which belongs to a class of mediator proteins (Rad52p/Rad55p/Rad57p) [47]. Rad52p assists Rad51p in displacing RPA from the ssDNA ends. It also helps in strand exchange by pairing the nucleoprotein filament with the donor chromosome [48]. Rad55p and Rad57p form a heterodimer that assist in the formation of the Rad51p nucleoprotein filament [47].

2.4.2 Synapsis

There have been observations pertaining to the importance of Rad54p in this pathway where Rad54p is believed to enhance the process of strand exchange [49] along with being associated to chromatin remodeling during HR [50]. *RDH54/TID1* appears to play a similar role in HR but has more significance during meiotic recombination [51].

2.4.3 Post synapsis and replicative polymerases

The post synaptic phase of HR involves strand exchange, initiation of DNA synthesis and branch migration. A DSB is fully repaired when new DNA is synthesized. For GC and SSA, repair synthesis proceeds in the absence of a replication fork and it involves the polymerization by processive polymerases δ

(*POL3*) and ε (*POL2*) [52 and 53]. Polymerase δ (Rad30p) and translesion polymerase ε (Pol ε) are also known to be involved in the repair synthesis but their specific roles are yet to be completely understood [54]. During SSA, since there is no template chromosome available, the repair is restricted to the broken molecule. Interestingly, during GC, new DNA synthesis proceeds by copying information from the broken molecule [55]. However, *Rad1/Rad10* endonucleases are involved in cleaving the 3' nonhomologous overhangs in both GC and SSA repair [20]. Dn14p or Cdc9p ligases then bind the DNA strand together.

DNA synthesis during BIR involves the formation of a replication fork with both leading and lagging strands differentiating it from SSA and GC. Many observations made have led to this understanding. Initiation of BIR DNA synthesis requires all essential S-phase replication factors except for those that are involved in recognizing the origin; namely Cdc45p, the GINS complex, Mcm2p as well as Cdt1. All three major replicative polymerases that are involved in S-phase replication are suggested to participate in BIR DNA synthesis [28] - Pol α, Pol δ and Pol ε. Pol δ, plays a crucial role in BIR DNA synthesis [28, 32 and 56]. However, the role of Pol ε and Pol α, in BIR remains unclear [28], (also reviewed in [39]). It was also observed that Pol α is not very essential for other kinds of HR repair [53].

It was observed and characterized that BIR repair can proceed without the presence of Rad51p [24a and 57]. The *RAD51*-independent pathway is observed to be *RAD52*-dependent and is also shown to follow the genetic requirements of SSA [24].

2.5 The DNA Damage Checkpoint in yeast DSB Repair

As mentioned earlier, BIR is a slow and long repair process and requires a prolonged G2/M arrest [16]. The initiation of BIR takes much more time when compared with GC. In case of BIR, upon DSB induction, the cells stay arrested in G2/M for about 4-5 hours in order to facilitate repair. This arrest is initiated and maintained by cell cycle checkpoints. When DSBs are induced by different internal or external factors, the DNA damage checkpoint machinery is responsible for assessing the type and amount of damage that is caused to the DNA. However, the primary role of checkpoints is to trigger cell cycle arrest and this provides time for the cells to assemble appropriate repair machinery components that can repair damaged chromosomes before they enter mitosis.

Two primary checkpoints exist in *S. cerevisiae*: the S-phase checkpoint that monitors the cell cycle at times of replication stress [58] or DNA damage [59] and the G2/M checkpoint that is associated with the cellular response to DNA damage and monitors the prevention of sister chromatid separation prior to repair [reviewed in 60].

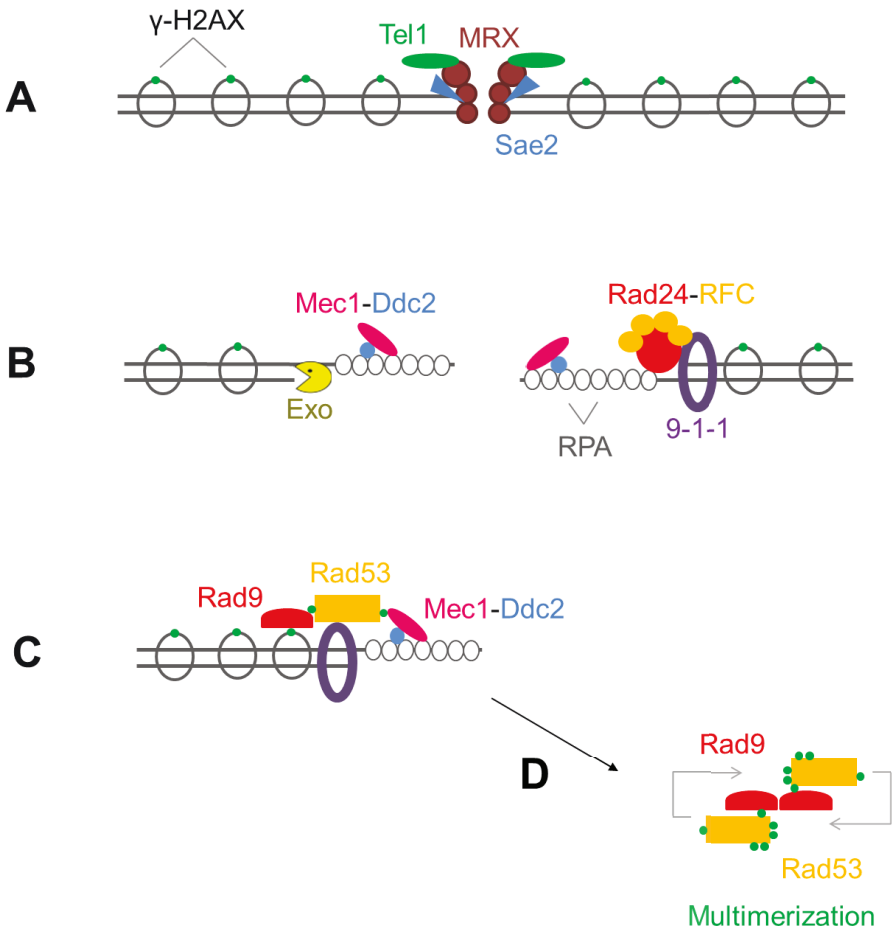

Figure 2.4. Checkpoint proteins associated with DSB. (A) Checkpoint proteins associated with identifying and interacting with a DSB initially are depicted here; namely Mre11p, Rad50p and Xrs2p (MRX) (brown) along with Tel1p (green) and Sae2p (blue). **(B)** DNA resection carried out by MRX and Exo (yellow). Resected DNA coated by RPA (white circles) and Rad24p (red) in association with Rfc2-5 (orange) loads the 9-1-1 (purple) clamp, which slides only over dsDNA and not over RPA coated ssDNA. Mec1p-Ddc2p (pink and blue) activate the checkpoint cascade. **(C)** Phosphorylated Rad9p (red) recruits Rad53p for phosphorylation, facilitated by the 9-1-1 complex. **(D)** Multimerization of Rad9p and Rad53p for full activation of Rad53p. Schematic re-drawn based on a review by Harrison and Haber, 2006 [61].

The G2/M checkpoint is also commonly known as the DNA damage checkpoint (DDC). The DDC is initiated when DNA damage is inflicted on the cells. The MRX complex is responsible for recognizing the DSB initially after which DNA resection is initiated following stabilization of the DSB (Fig. 2.4A).

Mec1p and Tel1p, two phosphoinositol-3-kinase related kinase (PIKK) proteins (homologs of human ATR and ATM respectively) aid in mediating the DDC. The MRX complex directly recruits Tel1p to the break site, where it phosphorylates histone protein H2AX [reviewed in 61]. The phosphorylated H2AX (γH2AX) further recruits various chromatin remodeling proteins that assist in the repair of the damage (Fig. 2.4A). Mec1p, like Tel1p is also associated with the phosphorylation of H2AX and is apparently a more important protein during the DDC. Mec1p is also likely to be related to the cell cycle-related regulation of post-DSB resection by Cdk1 [41]. Ddc2p, bound to RPA-coated ssDNA, interacts with Mec1p and aids in the recruitment of Mec1p to the damage site after 5’ to 3’ resection (Fig. 2.4B) [62 and 63].

The checkpoint clamp or 9-1-1 clamp (Rad17p/Mec3p/Ddc3p) is loaded onto dsDNA by the clamp loader. This does not depend on the localization of Mec1p to the damage site [64 and reviewed 61]. The clamp loader consists of Rad24p in complex with Rfc-2p and is recruited to DSB sites where it loads the 9-1-1 clamp (Fig. 2.4B) [32, 56, 65] which is known to be strongly required for checkpoint activation and cell cycle arrest [25]. Activation of Mec1p kinase activity initiates a

phosphorylation signal where Rad9p localizes to γH2AX (Fig. 2.4C). Phosporylated Rad9p interacts with effector kinase Rad53p recruiting it near Mec1p for phosphorylation (Fig. 2.4C) [66]. The 9-1-1 clamp is also responsible for the phosphorylation of Mec1-dependent phosphorylation of another effector kinase Chk1; where the phosphorylation is mediated through interactions with Rad9p. Both the effector proteins play a key role in maintaining cell cycle arrest [67] and are also required for the transcriptional activation of damage-related genes [68]. A complex of Rad9p and Rad53p multimerizes to allow further auto-phosphorylation and full activation of Rad53p for inducing cell cycle arrest (Fig. 2.4D).

2.6 Genetic instabilities associated with DSB repair

DSBs increase overall genetic instability [69]. While homologous recombination is a crucial mechanism for damage tolerance, the tolerance is achieved through conservative repair like GC. It has been demonstrated in yeast that mutations in Rad51p reduce the efficiency of GC, increase the rates of SSA, a non-conservative HR mechanism, leading to genetic instabilities in the form of translocations and rearranged chromosomes [70].

DNA resection plays an important role in the choice of repair between HR and NHEJ (also see Section 2.4.1). NHEJ is a preferred choice when the ends of the DSB are compatible for joining. Resection initiates to prepare substrates for HR if the compatibility check of DSB ends for NHEJ fails [71]. The formation of tumorigenic rearrangements in mammalian cells depends on the extent of DNA

end resection [71] and mutations in resection proteins are known to lead to genetic instabilities [72]. NHEJ is known as an error-prone repair mechanism, since it can lead to deleterious chromosomal rearrangements. NHEJ often leads to mutations in the breakpoint junctions and is also shown to be highly mutagenic [73].

It is known that HR repair is more preferred than NHEJ, with GC being the safest among all the HR pathways. BIR, an alternative HR pathway and the main pathway studied in this research is demonstrated to have hazardous outcomes. While the end result of BIR is repair of the DSBs, the mechanism of BIR increases the likelihood of a variety of deleterious outcomes that may have destabilizing consequences in the genome. Among these are loss of heterozygosity, deletions, duplications, translocations, copy-number variations, and a significantly elevated mutation rate [37, 65, 74 - 82].

During BIR repair, if there are disturbances and the progression is interrupted, it leads to the formation of outcomes that are termed as “Half crossovers” (HC). HC are chromosome fusions initially identified in *rad51Δ* and *rad52Δ* mutants [56, 83-86] and were recently demonstrated to occur in wild type and various mutants following initiation of BIR repair upon DSB induction [32 and 56].

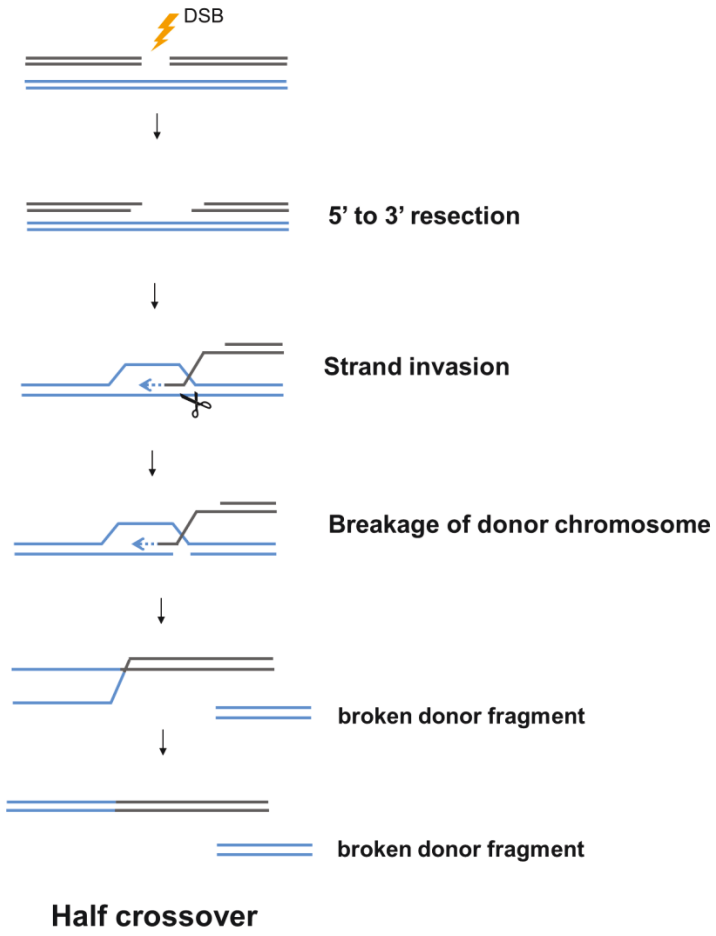

Figure 2.5. Half crossover formation. This schematic shows the mechanism of formation of half crossover (HC) outcomes. See text for further details.

BIR-induced HC formation is initiated by strand invasion, but the resulting intermediate ruptures prior to repair to yield a rearranged chromosome consisting of fused pieces of the recipient and donor molecules, as well as a destabilized fragment of the broken donor (Fig. 2.5). Accordingly, HC formation requires proteins involved in the strand invasion step of BIR, however the impairment of proteins involved in BIR after strand invasion promotes HCs [32]. Thus, HCs are markedly elevated in two mutants affecting the function of Polδ, *pol32Δ* and *pol3-ct*, which interfere with successful initiation of DNA synthesis [32 and 56]. It was proposed that the failure to initiate DNA synthesis promotes resolution of the Holliday junction (HJ) formed during strand invasion. The exact mechanism of HJ resolution remains unknown, though the resolvase Mus81p has been implicated as one protein capable of resolving HJs and therefore may contribute to HC formation [56].

HCs result in the breakage of a previously intact donor chromosome, which can have deleterious repercussions by initiating recurrent cycles of HCs. Analogous cycles (called NRTs, for non-reciprocal translocations) have been described in mammalian tumors where broken chromosomes initiate recombination with an intact donor, which in turn leads to breakage of the donor [87]. While the molecular mechanism of NRTs remains undefined, we have previously proposed [32] that cycles of NRTs are mediated by cascades of HCs that continue until the donor fragments are either stabilized or lost.

Thus, further investigation into how half crossovers are formed and the possible cascades of genetic instability that may result is warranted.

To further define mechanisms of HC formation and the effects of HCs on genetic instability, I hypothesize that various factors that interrupt ongoing BIR replication may induce HC formation in a manner similar to mutations that prevent initiation of BIR replication. I and some lab members show that interruption of BIR synthesis due to a defective replisome results in a dramatic increase in HCs. Moreover I observed that disruption of BIR imposed by premature onset of mitosis in cells increased HC formation. Finally, I document the occurrence of half crossover instability cascades (HCCs) that closely resemble NRT cycles observed in cancer cells.

CHAPTER 3. MATERIALS AND METHODS

3.1 Strains and media

3.1.1 Strain construction

All the strains used in this study are shown in Table 3.1 along with their respective genotypes. All the yeast strains were isogenic to AM1003 (described in [56]), which is a chromosome III disome with the following genotype: *hmlΔ::ADE1/hmlΔ::ADE3 MAT***a**-*LEU2*-tel/*MATα-inc hmrΔ::HYG* FS2Δ::*NAT*/FS2 *leu2/leu2-3,112 thr4 ura3-52 ade3::GAL::HO ade1 met13*. In this strain, the *HO* endonuclease-induced DSBs introduced at *MAT***a** are predominantly repaired by BIR because the portion of the chromosome centromere-distal to *MAT***a** is truncated to leave only 46 bp of homology with the donor sequence [40, 56]. This also ensures a low frequency of repair by GC.

The majority of single-gene deletion mutants were constructed by transformation with a PCR-derived *KAN-MX* module flanked by terminal sequences homologous to the sequences flanking the open reading frame of each gene [88]. Also see Table 3.2 for the list of primers used in strain construction and characterization.

Table 3.1. List of strains used in this study

Strain name	Genotype	Source
AM1003	*hmlΔ::ADE1/hmlΔ::ADE3 MAT**a**-LEU2-tel/MATα-inc hmrΔ::HYG FS2Δ::NAT/FS2leu2/leu2-3,112 thr4 ura3-52 ade3::GAL::HO ade1 met13*	Malkova lab
AM1017	AM1003, but *rad24::KAN*	Malkova lab
AM1228	AM1003, but *rad9::KAN*	Malkova lab
AM2426	AM1003, but *rad9::KAN*	Malkova lab
AM1239	AM1228, but *rad50::hisG-URA3-hisG*	Malkova lab
AM2566	AM2426, but *sgs1::hisG-URA3-hisG*	Malkova lab
AM2568	AM1017, but *sgs1::hisG-URA3-hisG*	Malkova lab
AM1014	AM1003, but *pol32::KAN*	Malkova lab
AM1386	AM1003, but *pol3-t*	Malkova lab
AM1596	AM1003, but *pol31-WRRGW*	Malkova lab
AM1241	AM1003, but *pol3y-708A*	Malkova lab
AM2305	AM1003, but *pol1-1*	Malkova lab
AM2866	AM1003, but *pol2-1*	Malkova lab
AM1423	AM1003, but *pol2-Y831A*	Malkova lab
AM2432	AM1003, but *pol2-9*	Malkova lab

Table 3.2. List of primers used in this study

Malkova Lab Database Name	5' to 3' Sequence	Description
OL26	CCTCGACATCATCTGCCC	Used to confirm insertion of *KAN-MX* (Wach et al.) to delete gene function. Within TEF terminator, 174 bp from the MX18 primer pointing towards the MX18 primer
OL27	CAGCGAGGAGCCGTAATTTT	Used to confirm insertion of *KAN-MX* (Wach et al.) to delete gene function. Within the TEF promote, 269 bp from the MX19 primer pointing towards the MX19 primer
OL370	CGAAGGCTCACGGTAAATCTTCCA	P1 to amplify *rad24::KAN* fragment
OL371	CAAGGAATCTATAGAAGAAGATCC	P2 to amplify *rad24::KAN* fragment
OL372	GCACAGGCCCTGTCCCATATCCTT	P1 to confirm integration of *rad24::KAN* fragment
OL373	GGTGAAGCTAGTACAAGCTGCACC	P2 to confirm integration of *rad24::KAN* fragment
OL478	GGCCTACTGTCGCTAGACTGGATG	P1 to amplify *sgs1::KAN* fragment
OL479	GATTGCCCGGCTTCGGCTGCCAGG	P2 to amplify *sgs1::KAN* fragment
OL480	GAGGTTATACCCGTGAAGAAGCCG	P1 to confirm integration of *sgs1::KAN* fragment
OL481	GTGACATTCGCAGCCACATGCTCC	P2 to confirm integration of *sgs1::KAN* fragment
OL666	TGGTGGTACGAACATCCAATGAAG	P1 to confirm integration of *URA3* (antisense)

Table 3.2. Continued.

Malkova Lab Database Name	5' to 3' Sequence	Description
OL667	CTTCATTGGATGTTCGTACCACCA	P1 to confirm integration of URA3
OL668	CCTGTAGAGACCACATCATCCACG	P2 to confirm integration of *URA3* (antisense)
OL669	CGTGGATGATGTGGTCTCTACAGG	P2 to confirm integration of *URA3*
OL741	CAAGATGCAAGCCTAAAATATATGC	P1 to amplify *rad9::KAN* fragment
OL742	CGGCTTTGAATTTTCAGAGTGCAG	P2 to amplify *rad9::KAN* fragment (antisense)
OL743	TGCGGGAGAACACCGATCTTATCT	P1 to confirm integration of *rad9::KAN* fragment
OL744	GCTCCCCATCAAAATAAGGTCTAA	P2 to confirm integration of *rad9::KAN* fragment
OL785	TATGGCCACTTGCTCCAAACAATT	P1 to confirm elimination of wt *RAD24*
OL786	AGGGACAGAAGGCTTCGCATGTTG	P2 to confirm elimination of wt *RAD24*
OL795	TGCCCAAAGTACTGGAACAAAATC	P1 to confirm elimination of *SGS1*
OL796	GTTGGTCCAGATGCAGGAATGCTG	P2 to confirm elimination of *SGS1*
OL809	GCGCAGGTAGAATGCTTACAATTG	P1 to confirm elimination of wt *RAD9* (antisense)
OL810	CATCATGTCTTGGACTCTCGTCAAG	P2 to confirm elimination of wt *RAD9*
OL1773	ATGGTTCTAACCGATGCCGAAGAA	P3 used for PCR Breakpoint analysis (*YCL021W-A*-specific)

Table 3.2. Continued.

Malkova Lab Database Name	5' to 3' Sequence	Description
OL1774	CCGTTAATGTGGTTTTGCCGACAT	P4 used for PCR Breakpoint analysis (*RHB1*-specific)
OL1775	AAAACGCTGACCAAGCTTGCTACA	P5 used for PCR Breakpoint analysis *(KCC4*-specific)
OL1776	ATGGGGTAGATTTCGCTAAATCTC	P6 used for PCR Breakpoint analysis *(CIT2*-specific)
OL1780	GGAAAATCATCAATCTATGGCAGG	P1 to amplify Probe 2 fragment (*YER134C*-specific)
OL1781	ACCTGGTTCATTCACCACTTTTCA	P2 to amplify Probe 2 fragment (*YER134C*-specific)
OL1782	CTACTAGAAGGCTGGAAGCAATAC	P1 to amplify Probe 4 fragment (*KCC4*-specific)
OL1783	CATCGTATTGTCCATTTGGGGATC	P2 to amplify Probe 4 fragment (*KCC4*-specific)
OL1784	AGTCTGGGATACAGCCCTATTTTC	P1 to amplify Probe 5 fragment (*CIT2*-specific)
OL1785	AGTTTACCCGGAGGTCATCATTCT	P2 to amplify Probe 5 fragment (*CIT2*-specific)
OL1794	TCCTTCCCAAATCAGCTTTGGTAC	P1 to amplify Probe 3 fragment (*RHB1*-specific)
OL1795	TCGTAGAATCGCGGTTCGTTGAAT	P2 to amplify Probe 3 fragment (*RHB1*-specific)
OL1906	GAGGTTATACCCGTGAAGAAGCCG	P1 to confirm elimination of wt *SGS1*
OL1907	ATTAGAGTGGGAGCACTGATTTAA	P2 to confirm elimination of wt *SGS1*
OL1992	GTAGCCTTCAAGATTGTTTGCTTC	FP used for PCR Breakpoint analysis *(SRD1*-specific)

Table 3.2. Continued.

Malkova Lab Database Name	5' to 3' Sequence	Description
OL1993	TTTCTTCGTAATACTGGCAGACCG	RP used for PCR Breakpoint analysis *(SRD1*-specific)
OL1994	GCCTCCTGGGACATTCTTATAGTG	RP used for PCR Breakpoint analysis (*MAK3* -specific)
OL1995	GAGATTCCGATGACCGTGAATACC	RP used for PCR Breakpoint analysis (in between *MAK32* and Ty's in Chr III)
OL1996	CCTCGCTTGATAGACGATAGTTGG	RP used for PCR Breakpoint analysis (in between deltas and *YER134C* in Chr V)
OL1997	CCAACACTATTGATTCCTGCCATAG	RP used for PCR Breakpoint analysis *(YER134C*-specific)
OL1998	TGTGACGAACATGAACCTTAACCC	RP used for PCR Breakpoint analysis *(YER134C*-specific)
OL1999	AAGGCAAGCTGGGGGTAGAAAGAA	FP used for PCR Breakpoint analysis (*GLC7*-specific)
OL2000	ACGTCTTCCTTTGGCTTTGAACCC	FP used for PCR Breakpoint analysis (in between *GLC7* and deltas in Chr V)
OL2001	CAAAATATACAGCCCTCATCAGCA	FP used for PCR Breakpoint analysis (in the deltas in Chr V)
OL2002	TGCTGATGAGGGCTGTATATTTTG	RP used for PCR Breakpoint analysis (in the deltas in Chr V)

3.1.2 Media and growth conditions

For non-selective growth of yeast strains, rich medium (yeast extract-peptone-dextrose [YEPD]) was used. Synthetic complete medium, with bases and amino acids omitted as specified in Guthrie, 1991 [90] were used for the selection of yeast auxotrophic markers. YEP-lactate (YEP-Lac), a glucose-free medium contained 1% yeast extract and 2% Bacto peptone supplemented with 3.7% lactic acid (pH 5.5). YEP-galactose (YEP-Gal) medium contained 1% yeast extract and 2% Bacto peptone supplemented with 2% (w/v) galactose and was used to induce GAL::HO DSB. Plate media was prepared similarly to liquid media, but contained 25 g/L of granulated agar. Yeast cultures were grown at 30°C or at 20°C (in the case of yeast strains bearing polymerase mutations, which rendered them temperature-sensitive). Media containing antibiotics of interest were prepared by adding the drug to YEPD medium in the following amounts: G418 (KAN): 0.3 g/L or 0.5 g/L; Nourseothricin sulphate (NAT) 0.1 g/L. These drugs were dissolved in 5 mL of ddH20 and filter-sterilized before adding to the autoclaved YEPD media which was cooled to 55°C prior to addition.

3.2 Methods employed

3.2.1 Transformation methods

3.2.1.1 One step transformation of yeast

Strains constructed using the one-step-transformation protocol were mostly simple deletion strains (either using *KAN-MX* replacement or insertion of a linearized plasmid like in the case of *pol2-9*). 5 mL of saturated liquid yeast culture was grown overnight at 30°C in YEPD medium on a rotary shaker. The cultures were centrifuged at 3,500 rpm for 4 minutes and the pellet-cells were collected and re-suspended in 100 µl of one-step-buffer (100 mM dithiothreitol and 0.2 M lithium acetate in 40% poly-ethylene glycol). 30 µg of sonicated salmon sperm (single-stranded DNA) previously denatured at 100°C and placed on ice was added to this mixture following which, 50 ng-1 µg of DNA was added. This mixture was incubated at 45°C for 30 minutes followed by plating on selective media where only the transformants grew or on non-selective media (YEPD). The plates were incubated at 30°C for 3-4 days after which they were replica-plated on selective media or antibiotic-containing media. In cases of obtaining Ura^- transformants, the cells were replica-plated from YEPD on to 5-fluoro-orotic acid media where only the Ura^- transformants could grow. All the transformants obtained from one-step-transformation were confirmed either by PCR or by the use of genetic markers.

3.2.1.2 Transformation of *E. coli*

Various plasmids were transformed in Competent *E.coli* cells (XL1 Blue Cells -Stratagene Corporation) as per the manufacturer's manual. In particular, 100 µl of cells were thawed on ice and mixed with 1.7 µL β-mercaptoethanol and incubated on ice. This mixture was gently mixed occasionally for 10 minutes. 0.1 - 50 ng of plasmid DNA was added to the cells after incubation, gently mixed, and placed on ice for 30 min. The samples were then heat-pulsed for 45 seconds at 42°C and immediately placed on ice for 2 minutes. 0.9 mL of pre-warmed (42°C) Luria broth was added to these samples, and they were grown for 1 hr at 37°C on a rotary shaker. Cells were plated on Luria broth plates containing 100 µg/mL ampicillin and grown overnight at 37°C.

3.2.2 DNA purification

3.2.2.1 Genomic DNA extraction using Glass beads

5 mL of saturated liquid yeast culture was grown overnight at 30°C in YEPD medium on a rotary shaker. The cultures were centrifuged at 3,500 rpm for 4 minutes and the pellet-cells were collected and re-suspended in a lysis buffer (1% sodium dodecyl sulfate, 10 mM Tris (8.0) and 1 mM EDTA (pH 8.0)). 600 µl of this mixture was added to a microfuge tube containing 300 µl of sterile glass beads (Sigma-Aldrich). 400 µL of Tris-buffered 50% phenol, 48% chloroform, 2% isoamyl alcohol was added to the microfuge tube and vortexed for about 2 minutes and then placed on ice. The tubes were vortexed for an additional 1

minute before centrifuging for 15 minutes at 12,000 rpm and at 4°C. The clear aqueous phase obtained was carefully transferred to fresh microfuge tubes and 400 µL of Tris-buffered 50% phenol, 48% chloroform, 2% isoamyl alcohol was added again and mixed well by inverting several times. This mixture was centrifuged again and the new aqueous phase obtained was transferred to fresh microfuge tubes and mixed with 50 µl of 3M sodium acetate (pH 6.5). 600 µL of isopropanol was added to this mixture and centrifuged to obtain a DNA pellet which was re-suspended in 300 µL 1x TE buffer, treated with RNase (3 µL of 10 mg/mL). This mixture was incubated at 37°C for 30 minutes. After incubation, the DNA was precipitated by the addition of 3M ammonium acetate (5.5) followed by addition of 300 µl isopropyl alcohol and then centrifuged. The supernatant is discarded and the DNA pellet obtained was washed with 500 µl of 80% ethanol and then re-suspended in 100 µL of double-distilled water.

3.2.2.2 Chromosomal DNA extraction for Pulse Field Gel Electrophoresis (PFGE)

50 mL of saturated liquid yeast culture was grown overnight at 30°C in YEPD medium on a rotary shaker. The cultures were centrifuged at 3,500 rpm for 4 minutes and the cell-pellets were collected. In case of time-course experiments, cell-pellets that were washed in 50 mM EDTA (8.0) and frozen at -80°C were thawed and prepared for extraction. The pellet-cells were re-suspended in 400 µL of SCE solution (1 M sorbitol, 0.1 M sodium citrate (5.8), 10 mM EDTA (7.5)) containing 1 mg zymolase (100T) and 25 µL β-mercaptoethanol. This mixture

was briefly incubated at 45°C after which 500 µL was mixed with 1.2% low-melting-point molten agarose in SCE cooled to 45°C and pipetted into plug molds (as described in a manual by Sambrook and Russel [91]). The plugs were allowed to solidify and then expelled in 50 mL polypropylene tubes containing Solution 2 (0.5 M EDTA (7.5), 10 mM Tris (8.0), 7% β-mercaptoethanol, 1 µL/mL of 10 mg/mL RNaseA). The plugs in Solution 2 were then incubated at 37°C for an hour after which the solution was removed and replaced with 5 mL of Solution 3 (1% N-lauroyl sarcosine in 0.5 M EDTA (9.0) and 1 mg/mL proteinase K) and incubated at 50°C overnight. After incubation, the solution is removed, washed with 50X TE buffer and stored in 50% glycerol at -20°C.

3.2.2.3 Plasmid DNA extraction

The Qiagen Maxiprep Kit (Qiagen) was used to isolate plasmids from *E.coli*. A 5 mL culture of the desired strain was grown overnight at 37°C in LB medium containing 100 µg/mL ampicillin on a rotary shaker. The inoculum was transferred to 250 mL of LB containing 50 µl/mL of ampicillin and grown for 16 hours at 37°C. The cultures were centrifuged at 6,000 rpm for 15 minutes at 4°C and the pellet-cells were collected and re-suspended in 20 mL of Buffer P1 (50 mM Tris-HCl, 10 mM EDTA (8.0), 100 µg RNaseA). 20 mL of Buffer P2 (200 mM NaOH, 1% (w/v) SDS) was then added and the samples were mixed by gently inverting several times after which they were incubated at room temperature. To this mixture, 20 mL of chilled Buffer P3 (3M potassium acetate (5.5)) was added

and mixed again by inverting several times. The samples were then subjected to centrifugation at 20,000 rpm for 30 minutes at 4°C to remove cell debris. The supernatant containing plasmid DNA was transferred to a Quiagen-tip 500 column that was equilibrated with 10 mL of QBT buffer (750 mM $NaCl_2$, 50 mM MOPS and 15% ethanol (7.0)). The column was then washed twice with 30 mL Buffer QC (1.25 M $NaCl_2$, 50 mM Tris-HCl and 15% ethanol (8.5)). Plasmid DNA was precipitated with 0.7 volumes isopropanol and centrifuged at 15,000 rpm for 30 minutes at 4°C. The pellet obtained was washed with 70% ethanol and centrifuged as previously. The DNA obtained was re-suspended in 200 µL double-distilled water and stored at -20°C.

3.2.3 Yeast Recombinant DNA techniques

3.2.3.1 Polymerase Chain Reaction (PCR)

Polymerase Chain Reactions (PCR) were performed to amplify fragments of DNA either in 25 µL or 50 µL reaction set-up. The reaction mixture for most of the PCRs typically contained two oligonucleotide primers specific for sequences in each strand (50 µM each), template DNA (10 - 50 ng), dNTPs (10 mM), $MgCl_2$ (7.5 mM), Go Taq Buffer (proprietary mixture), double-distilled water and 1 unit of Taq-DNA polymerase (Promega or Sib Enzyme). For amplification of long and complex DNA fragments, PCR reaction mixtures were carried out using 1X Ex-Taq buffer, $MgCl_2$ (2.0 mM), dNTPs (0.2 mM), two oligonucleotide primers specific for sequences in each strand (50 µM each), template DNA (10 - 50 ng)

and 1 unit of Ex-Taq polymerase (all components from TaKaRa Bio Company). Colony PCRs were performed in cases where transformants had to be checked using whole cells as a source of DNA. All reactions were run on a BIORAD MyCycler thermocycler machine. A standard PCR cycle consisted of an initial denaturation step (temperature set at 94°C for 1 minute) followed by 40 denaturing cycles at 94°C for 30 seconds, an annealing step varying from 55°C-65°C for 1 minute and an extension step at 72°C for 1.5 minutes. Finally, after an extension step at 72°C for 10 minutes, the PCR products were either stored at 4°C or checked by running on an agarose gel.

3.2.3.2 Restriction Digestion of DNA

Restriction digestion of DNA was performed for various purposes like DNA probe preparation, strain construction and verifying chromosomal re-arrangements. Commercially available enzymes were used for digesting DNA (New England Biolabs or Fermentas). Appropriate buffers provided by the company were used to aid the reaction. Typically, 5 to 10 units of enzyme were allowed to digest approximately 1 µg of plasmid DNA for about 2 hours. For genomic DNA digests, additional 5 to 10 units of enzyme were added after approximately 5 hours and allowed to incubate overnight at suggested temperatures. The digested DNA samples were later precipitated to concentrate the DNA and then confirmed using agarose gel electrophoresis or Southern-blot analysis.

3.2.4 Pulse Field Gel Electrophoresis (PFGE)

3.2.4.1 PFGE for separation of chromosomal DNA

For PFGE gel electrophoresis, 50-ml aliquots of growing cultures were removed and the extraction of DNA embedded in 0.55% agarose plugs was performed as described by Sambrook and Russell [91]. PFGE was performed by running genomic DNA embedded in the 0.55% agarose plugs at 6V/cm, for 40 hours (initial switch time 10s; final switch time 35s) using 0.5X TBE buffer with the buffer constantly circulating at 10°C. After the run is completed, separated bands were visualized in UV light after 30 min incubation in 0.5x TBE with ethidium bromide.

3.2.4.1.1 Southern hybridization of PFGE-separated chromosomal DNA

After capturing an image of the separated fragments under UV light, DNA on the PFGE gel is transferred to a nylon membrane (Hybond N_+, Amersham). Characterizing the repair products separated on the PFGE gel is accomplished by Southern blotting followed by hybridizing using ^{32}P-labeled specific DNA probes containing either an *ADE1* (*Sal*I fragment from pJH879) or *ADE3* (obtained by PCR amplification of chromosome VII from 907,979–908,735) sequence. Blots were analyzed using a GE Healthcare Typhoon™ FLA 9500 phosphor-imager. The kinetics of accumulation of BIR product was measured using an *ADE1*-specific fragment as a probe. To account for variation in DNA loads, intensities of the bands corresponding to the intact chromosome III, as

well as to the repaired chromosome III, were normalized to intensities of the bands corresponding to chromosome I, which also hybridizes to the *ADE1*-specific probe. The efficiency of BIR repair, presented as the percentage of truncated chromosome III that was converted to BIR product, was calculated by dividing the normalized intensity of a repair band by the normalized intensity of uncut, truncated chromosome III. Results of three time-course experiments were used to calculate the average ±SD BIR efficiency at each time point for each strain. BIR efficiencies between strains were concluded to be statistically significantly different if SDs did not overlap.

3.2.4.2 PFGE for separation of DNA fragments after Restriction Digestion

PFGE was performed by running DNA samples after restriction digestion with various enzymes. Sample DNA was precipitated and concentrated after restriction digestion and diluted with 25 µL distilled water. 6X loading dye was used to visualize the running of DNA. A typical PFGE program in the CHEF DRII machine, followed to separate fragments that were in the range of 2 kb to 80 kb had the following settings: single block; Initial Switch time: 1.7 seconds; Final Switch time: 2.6 seconds; Total run time: 22 hours; Voltage: 6V/cm; Buffer: 0.5x commercial grade TBE; Temperature 14°C; Gel: 1% BioRad Molecular Biology Certified agarose. After the run is completed, separated bands were visualized in UV light after 30 min incubation in 0.5x TBE with ethidium bromide.

3.2.4.2.1 Southern hybridization of PFGE-separated digested DNA fragments

After capturing an image of the separated fragments under UV light, DNA on the PFGE gel is transferred to a nylon membrane (Hybond N_+, Amersham). Characterizing the repair products separated on the PFGE gel is accomplished by Southern blotting followed by hybridizing using ^{32}P-labeled specific DNA probes that were generated by PCR amplification using 24-bp primers and genomic DNA of AM1003 as a template. The locations of these probes on chromosome III were as follows: (1) *SRD*1, 148247-148549 (probe 1); (2) *RHB1*, 167594-167893 (probe 3); (3) *KCC4*, 82015-82365 (probe 4); and 4) *CIT2*, 123682-123981 (probe 5). The location of the *YER134C*-specific probe on chromosome V is 436745-437044 (probe 2). Also see Table 3.2 for a list of all the primers used in the making of these probes. For all probes mentioned above, the starting and ending coordinates on the corresponding chromosomes are derived from the Saccharomyces Genome Database (SGD).

3.2.5 Analysis of cell cycle arrest by Flow Cytometery

The kinetics of DSB repair was examined in time-course experiments. YEP-Lac (500 to1000 mL was inoculated with approximately $2x10^6$ cells/mL. Cultures were grown at 30°C overnight to reach a concentration of approximately $5x10^6$ cells/mL. *HO* endonuclease was induced by the addition of galactose to achieve a final concentration of 2%. For fluorescence-activated cell sorter (FACS) analyses, 5-mL aliquots were removed, cells were spun, diluted, and fixed by the addition of 70% ethanol, and stored at 4°C.

Flow Cytometery analysis was performed using propidium iodide with a Becton Dickinson fluorescence-activated cell analyzer (as described in [92]).

3.2.6 Analysis of DSB repair outcomes in wildtype and all mutants

3.2.6.1 Analysis of DSB repair outcomes

To monitor the repair of *HO*-induced DSBs, I harvested logarithmically growing cells grown in YEP-Lac at 30^{o}C and plated them on YEP-Gal. Cells were grown at 30^{o}C and the resulting colonies were then replica plated onto omission media to examine the heterozygous *ADE1*, ADE3, *LEU2*, and *NAT* markers of these strains. When temperature-sensitive strains bearing *pol3-t* or *pol1-1* polymerase mutations were used, the cells were grown in YEP-Lac at 20^{o}C. Following plating on YEP-Gal, the cells were incubated at 30^{o}C for 24 hours (a length of time sufficient to complete BIR), then incubated at 20^{o}C until the colonies were full-grown. To test the effect of DNA damage on formation of HCs, AM1003 was grown to log phase in YEP-Lac medium, incubated in galactose-containing media for 30 minutes (to induce the *HO*-created DSB). Repair events were identified by a phenotypic analysis after replica plating onto omission media to examine the heterozygous *ADE1*, *ADE3*, *LEU2*, and *NAT* markers, and also confirmed by PFGE (Fig. 3.1).

Gene conversion (GC) outcomes displayed an Ade^{+}Leu^{+} phenotype and contained two copies of chromosome III: a 356-kb chromosome that hybridized to an *ADE3*-specific probe and a short (217 kb) chromosome that hybridized to

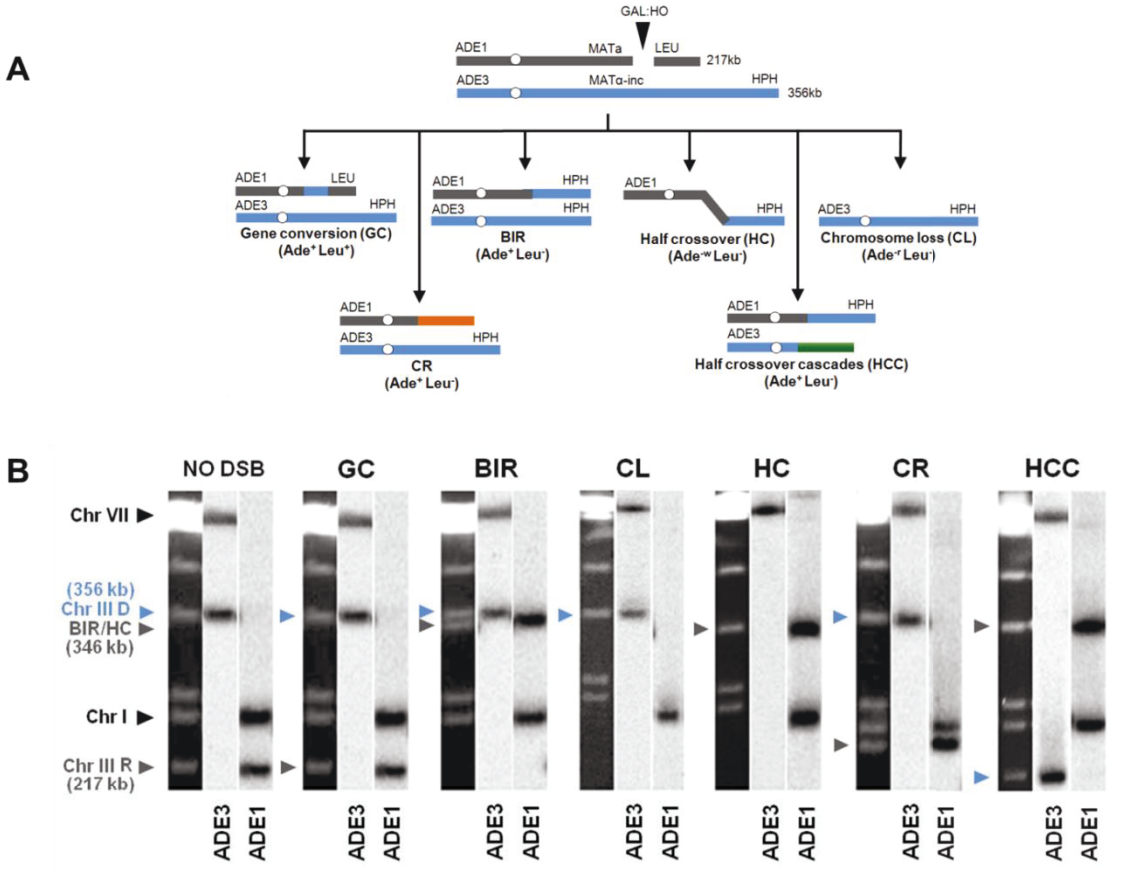

Figure 3.1. Analysis of DSB repair outcomes. (A) Schematic diagram depicting the following DSB repair outcomes: gene conversion (GC), break-induced replication (BIR), chromosome loss (CL), half crossover (HC), chromosome rearrangements (CRs) resulting from stabilization of the broken recipient chromosome via ectopic recombination or by *de novo* telomere formation, and half crossover cascades (HCC) initiated by HC and resulting from stabilization of the broken donor chromosome. (B) PFGE analysis of the DSB repair outcomes listed in A. Light bands correspond to chromosomes stained with ethidium bromide, while dark bands correspond to hybridization with *ADE1* (recipient-specific) or *ADE3* (donor-specific) probes marked by grey and blue arrowheads, respectively.

an *ADE1*-specific probe (Fig. 3.1). The absence of repair led to Chromosome Loss (CL), which was detected by formation of $Ade^{-r}Leu^{-}$ colonies containing a single, 356-kb chromosome III, which hybridized to the *ADE3*-specific probe. Formation of $Ade^{-w}Leu^{-}$ colonies or colony sectors indicated formation of Half Crossovers (HCs). These colonies contained a single, 346-kb chromosome III that hybridized to the *ADE1*-specific probe. $Ade^{+}Leu^{-}$ phenotypes could result from several repair outcomes: BIR, HC (when it co-segregates with an intact copy of the donor chromosome during mitosis, from CRs or from HCC events). CRs and HCC events were identified by PFGE (Fig. 3.1). CRs carried a 356 kb band that hybridized to the *ADE3*-specific probe and a band of any size (different from 346 kb) that hybridized to *ADE1*. HCC contained a single, 346 kb band that hybridized to an *ADE1* probe in addition to a band of varying size that hybridized to *ADE3*. PFGE could not distinguish between $Ade^{+}Leu^{-}$ BIR and events where a HC co-segregated with an intact donor chromosome because both classes carried a 356 kb band that hybridized to *ADE3* and a 346 kb band that hybridized to *ADE1*. Therefore, I assumed the number of $Ade^{+}Leu^{-}$ HCs to be equal to the number of $Ade^{-w}Leu^{-}$ HCs based on the idea that an HC product should co-segregate with an intact copy of the donor chromosome in half of the cases of HC formation. Overall, the formula to calculate the number of BIR events was as follows: BIR = (number of $Ade^{+}Leu^{-}$) - (GCR+HCC+HC).

In total, the following number of colonies were scored in experiments aimed to determine the effect of defective polymerases on half crossover formation for

each subsequent strain: Pol$^+$ (wt) – 1192 colonies; *pol3Y-708A* – 2428 colonies; *pol3-t* – 1240 colonies; *pol31-WRRGW* – 776 colonies; *pol2-Y831A* – 2491 colonies; *pol2-1* – 896 colonies; *pol2-9* - 2819 colonies and *pol1-1* – 454 colonies. The number of colonies scored in experiments aimed to determine the distribution of repair outcomes in checkpoint-deficient mutants was as follows: Rad$^+$ (wt) – 718 colonies, *rad24Δ* – 756 colonies; *rad9Δ* – 465 colonies; *rad24Δsgs1Δ* - 339 colonies; *rad9Δsgs1Δ* - 338colonies; and *rad9Δrad50Δ* - 340 colonies. Finally, the number of simple (s) and multiple (m) repair events scored during analysis of the effect of checkpoint- deficient mutants was as follows for each strain background: wild type (wt): 1353s; *rad24Δ*: 671s and 1782m; *rad9Δ*: 473s and 946m; *rad24Δsgs1Δ*: 677s; *rad9Δsgs1Δ*: 450s and 515m; *rad9Δrad50Δ*: 508s and 346m.

3.2.6.2 Analysis of individual colonies and sectors

The distribution of various types of repair among all repair events was determined differently for simple colonies (containing <2Ade$^-$ sectors) and for multi-sectored colonies (containing ≥2 Ade$^-$ sectors). The frequency among simple colonies was determined as previously described in [40]. The frequency of each repair outcome in multi-sectored colonies was determined as the sum of all sectors belonging to this phenotypic class divided by the total number of sectors analyzed. The physical analysis of repair in individual colonies was performed by PFGE. The PFGE analysis of random repair events was performed on 10 to 60

random representatives for each class of repair outcomes. In the case of random analysis, no more than one representative of each individual class from every colony was analyzed.

3.2.7 Analysis of half-crossover cascade (HCC) events by Array-CGH

The analysis of copy number variation associated with the HCC events was conducted as described recently [93]. Briefly, genomic DNA was prepared from the same agarose-embedded full length chromosome material used in the PFGE analysis. DNA from the parental strain was labeled with dUTP-Cy3 and DNA from the derivative strains carrying genome rearrangements was labeled with dUTP-Cy5. The labeled DNAs were mixed and competitively hybridized to custom Agilent 60-mer oligonucleotide microarrays. The arrays were scanned, the images were analyzed, and the CNV regions were identified using GenePix 6.0 and Nexus Copy Number software, respectively.

CHAPTER 4. RESULTS

4.1 Experimental system

To assay the efficiency of BIR and the frequency of half crossovers in DSB repair, I employed our disomic experimental system in yeast, *Saccharomyces cerevisiae,* wherein a galactose-induced DSB is initiated at the *MAT***a** locus on the truncated copy of chromosome III (recipient chromosome) (Fig. 4.1A) [56]. The second full copy of chromosome III contains the uncleavable *MAT*a-inc allele and serves as a template for DSB repair (donor chromosome). Upon induction of the DSB, DNA is repaired predominantly by BIR (Fig. 4.1B) because only one end of the DSB has large homology to the full-length donor copy of chromosome III. The ends of both chromosomes that participate in BIR repair are marked by *ADE1, LEU2, ADE3* or *HPH*; such that repair outcomes can be determined using appropriate selective media. Also, a *NAT* cassette was used to replace a region 30 kb centromere-proximal to *MAT***a** that contained two Ty1 elements (FS2) in the recipient chromosome [79].

Using these genetic markers, it was determined that more than 75% of DSB repair outcomes displayed an $Ade^{+}Leu^{-}$ phenotype, indicating BIR repair of the galactose-induced DSB (Fig. 4.1B, Fig. 4.8A; Fig. 4.13, Fig. 4.4).

Figure 4.1. Experimental system to study BIR and half crossover formation. (A) Strain disomic for Chromosome (Chr) III (AM1003) [12]. A DSB is created at *MAT***a** in truncated Chr III (recipient (upper) chromosome) by a galactose-inducible *HO* endonuclease. The *MAT*α-inc chromosome (donor (lower) chromosome) is full-length and is resistant to cutting by *HO*. The ends of the recombining chromosomes are marked by *ADE1*, *LEU2*, *ADE3* and *HPH*. Two copies of Ty1 elements (Ty1α and Ty1β), comprising the FS2 region located ~30 kb centromere proximal from *MAT***a**, are replaced by a *NAT* cassette in the recipient chromosome. The positions of two other Ty elements (Ty1γ and Ty1ε) comprising the FS1 region are shown. **(B)** Schematic representation of an $Ade^{+}Leu^{-}$ **(**Break-Induced Replication (BIR)) outcome. **(C)** $Ade^{+}Leu^{+}$ (Gene Conversion (GC)) outcome. **(D)** $Ade^{-r}Leu^{-}$ (Chromosome Loss (CL)) outcome. **(E)** $Ade^{-w}Leu^{-}$ (Half Crossover (HC)) outcome.

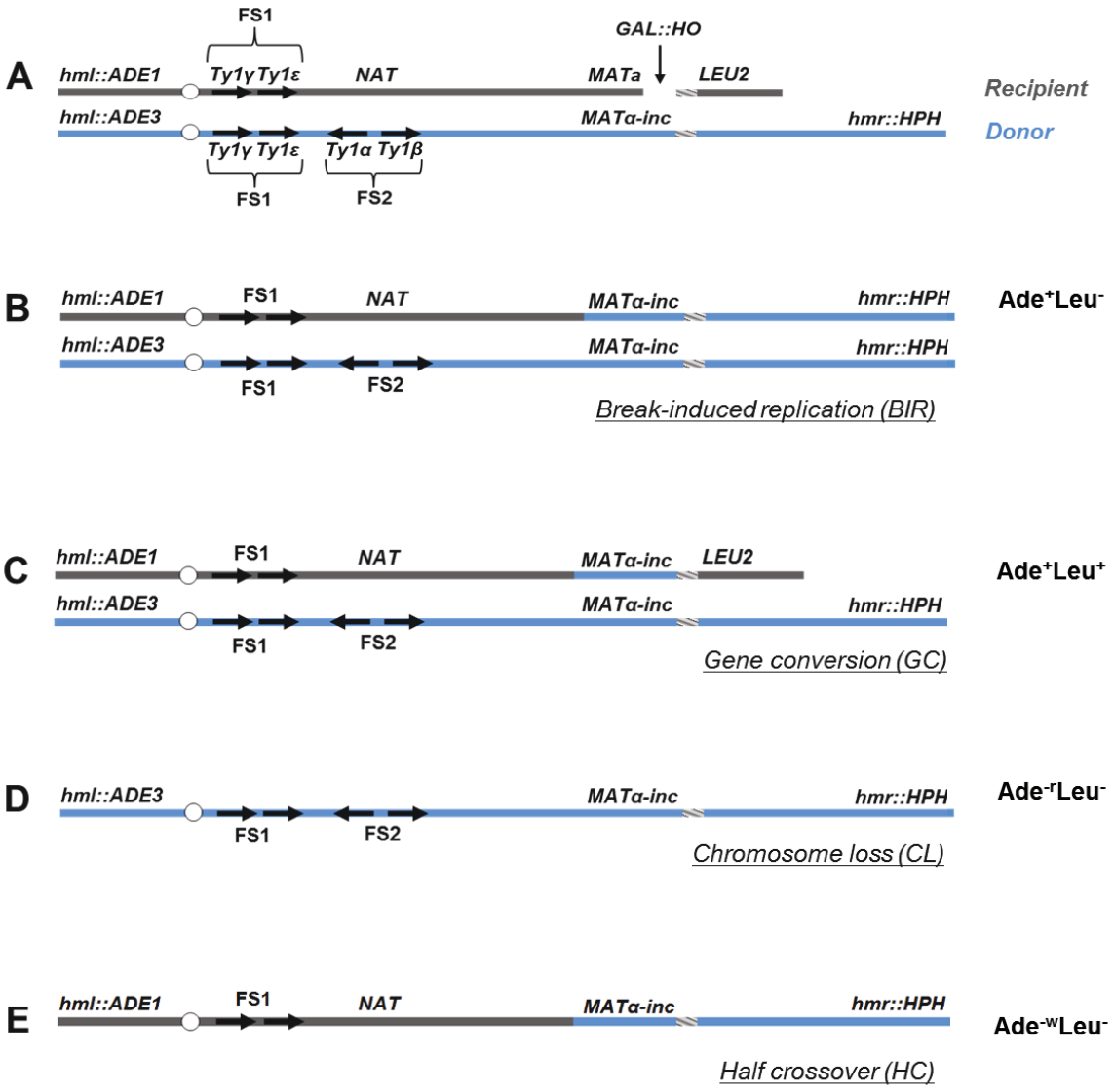

Figure 4.1. Experimental system to study BIR and half crossover formation.

This phenotype is also observed when DSB repair results in GCRs, including translocations and deletions; these events can be distinguished from allelic BIR by Pulse Field Gel Electrophoresis (PFGE; see below). Approximately 14% of the DSB repair outcomes were $Ade^{+}Leu^{+}$, indicating the DSB was repaired by gene conversion (GC) (Fig. 4.1C, Fig. 4.8A). Other colonies had an $Ade^{-r}Leu^{-}$ phenotype (were *ADE1*-deficient and red (as described in [56]) and resulted from failure of the chromosome to repair the DSB leading to chromosome loss (CL) (Fig. 4.1D, Fig. 4.8A). Also, a small number of colonies were $Ade^{-w}Leu^{-}$ (were *ADE3*-deficient and white), which represented HC events resulting from fusion of the *ADE1*-containing segment of the recipient chromosome with the *HPH*-containing segment of the donor chromosome and concurrent loss of the *ADE3* and *LEU2* segments of the donor and recipient chromosomes, respectively (Fig. 4.1E, Fig. 4.8A).

4.2 Reduced processivity of Polδ promotes HC formation

I tested the effect of mutations that impair DNA polymerases on HC formation by plating yeast on a galactose-containing medium [56]. Although each of the Polδ mutations tested here had varying effects on BIR efficiency, they all stimulated HC formation. In particular, *pol3-Y708A,* a mutation that affects the catalytic subunit of Polδ [95], dramatically decreased BIR efficiency, and increased chromosome loss (Fig. 4.4). Also, *pol3-Y708A* increased the number of colonies containing HCs to 17% compared to approximately 5% in wild type (Fig. 4.2; see also Fig. 4.4; note that Fig. 4.2 presents the fraction of colonies that

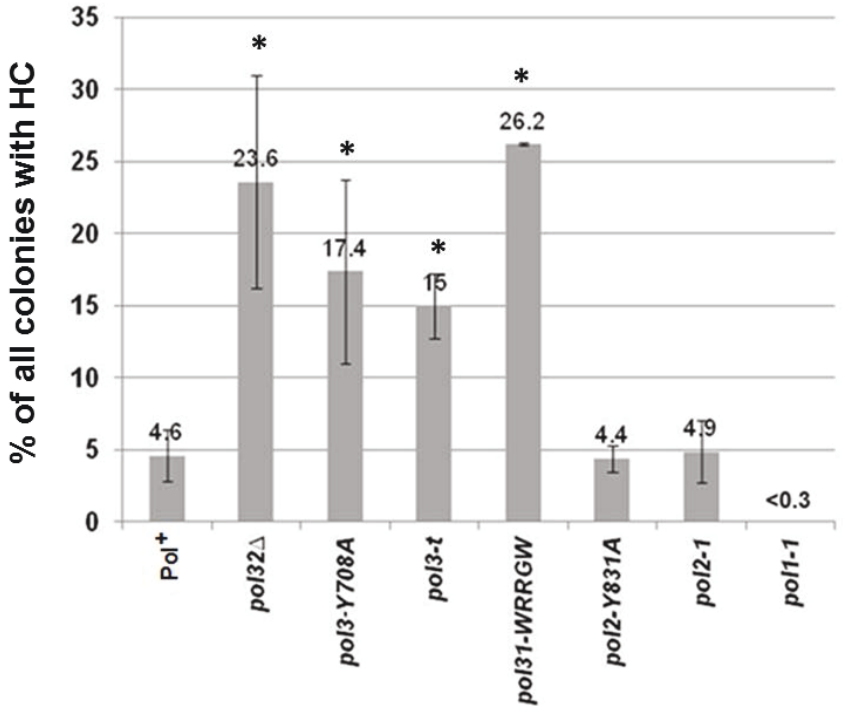

Figure 4.2. Effects of replisome defect on half crossover formation. Effect of mutations impairing DNA polymerases on HC formation. Results of 3 to 14 experiments performed for each strain were used to calculate the average ± SD percent of colonies containing a HC. Asterisks indicate statistically significant increases compared to the Pol$^+$ (wild type) strain. For the number of colonies analyzed, see Materials and Methods section 3.2.6.1. The frequency of HCs in *pol32*Δ was presented previously [12] and the frequencies of HCs in *pol2-Y831A* and *pol2-1* were calculated based on experiments carried out by other members in the lab. Because no HC outcomes were observed in *pol1-1* strains among 454 analyzed colonies, I estimated that the frequency of colonies with HCs was less than 0.3%.

are fully or partially HCs, while Fig. 4.4 shows the fraction of HCs among all DSB repair events). Similarly, the *pol31-WRRGW* mutation, which disrupts the Pol31-Pol32 interaction [96], displayed similar effects and elevated HCs to 26% (Fig. 4.2; Fig. 4.4). These phenotypes were similar to those previously observed in *pol32Δ* and *pol3-ct* mutants [56, 65], suggesting that HCs in these mutants are promoted predominantly by failure to initiate BIR. In strains bearing the *pol3-t* mutation known to compromise the processivity of Polδ during S-phase DNA replication [97, 98], HCs were also elevated, even though these cells frequently successfully completed BIR repair (Fig. 4.2; Fig. 4.4). Therefore, the increase of HCs in *pol3-t* might be explained by interruptions of ongoing BIR rather than by problems in BIR initiation. Thus, an intact Polδ appears to be necessary to prevent HC formation.

In addition, results from our lab demonstrate that mutations impairing Polε show no effect on HCs. No increase was observed in either *pol2-1* [99] mutants with a truncated catalytic subunit or in *pol2-Y831A* mutants [95] with a mutation in the same conserved catalytic motif as *pol3-Y708A* mutants (Fig. 4.2). (Experiments with *pol2-Y831A* and *pol2-1* were conducted by other members in the lab). Conversely, mutations in *pol2-9* showed an increase in HCs. Final conclusions have not been drawn based on these observations because of the inconclusive results I obtained from different sets of experiments. I varied parameters before establishing the fact that HCs could be elevated in *pol2-9* mutants (Fig. 4.3).

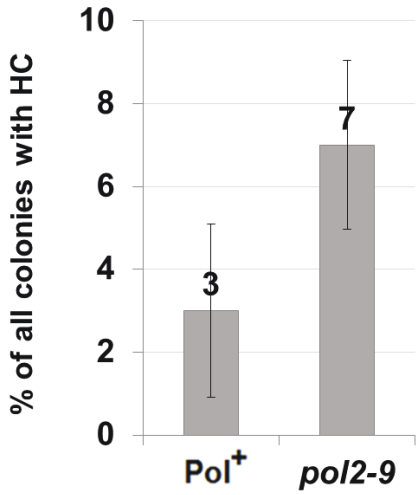

Figure 4.3. Effect of *pol2-9* mutation on half crossover formation. Results of 10 and 16 experiments performed for the Pol^+ (wild type) and *pol2-9* strains respectively were used to calculate the average ± SD percent of colonies containing a HC. For the number of colonies analyzed, see Materials and Methods section 3.2.6.1.

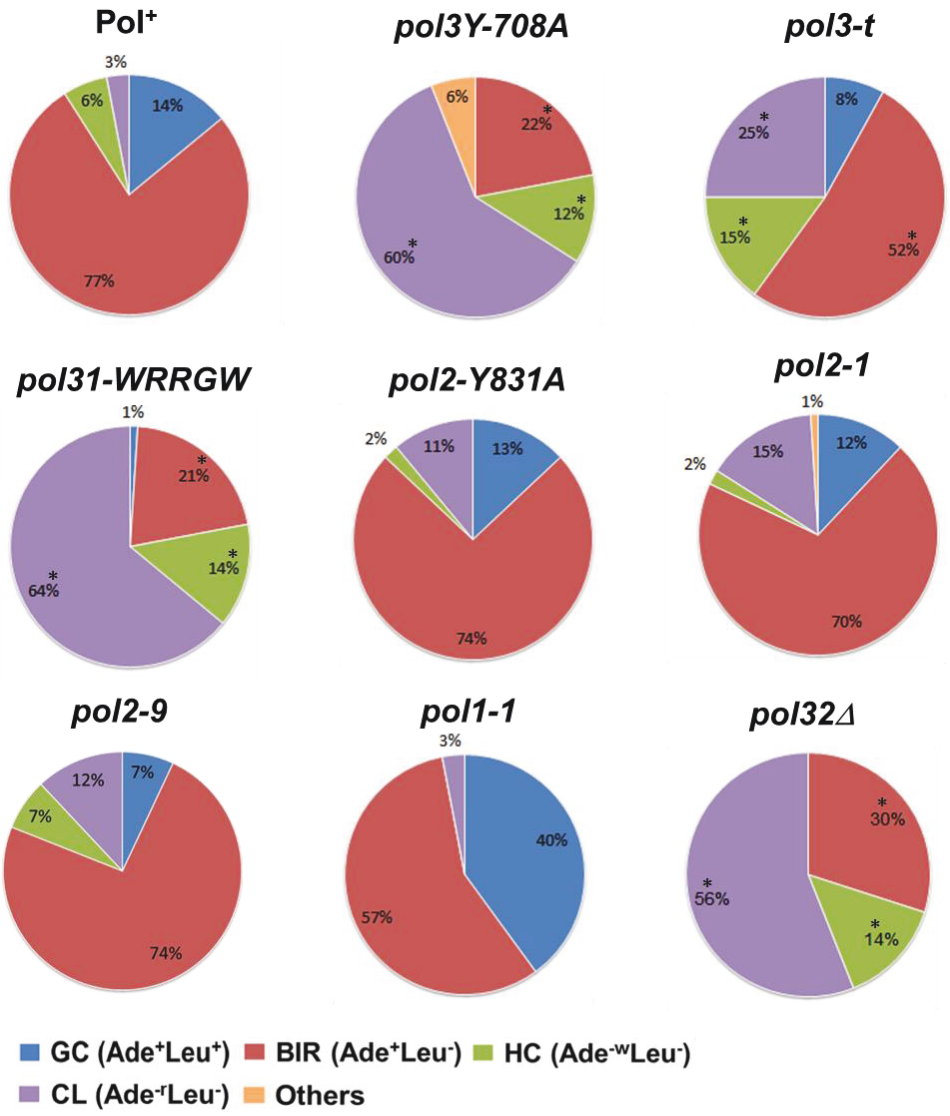

Figure 4.4. The effect of polymerase defects on the distribution of DSB repair outcomes. The fraction (%) of various DSB repair outcomes were determined similarly to [12] following DSB induction in strains containing different mutations affecting Polδ, Polε or Polα. For each strain, the data are based on 3-16 independent experiments. Asterisks indicate a statistically significant change as compared to wild type (Pol^+) cells. Note: While this figure shows the fraction of HCs among all DSB repair events, Fig. 4.2 and 4.3 present the fraction of colonies that are fully or partially HCs.

Gal-plating experiments were conducted to study the effect of *pol2-9* mutation on HC formation and the temperature at which DSBs are induced plays a crucial role in this case since *pol2-9* is a temperature-sensitive strain and optimum growth conditions are at room temperature (RT). In some experiments, upon plating on Gal-medium, the plates were transferred to 30°C for an overnight incubation and then transferred to RT - the 30°C is required for DSB induction. The wild type (Pol^+) plates were not transferred to RT since they grow optimally at 30°C. Results showed elevated HC levels in *pol2-9* with these sets of experiments. However, in other experiments, when the wild type plates were transferred to RT after DSB induction at 30°C, along with the *pol2-9* plates; an increase in HC levels was noted in both wild type and *pol2-9* (Fig. 4.3). Further experiments may be required to summarize the effect of *pol2-9* mutation on HC formation and a conclusive finding would be important because this could explain the potential role of Polε in ongoing BIR synthesis.

Also, interestingly, the *pol1-1* mutation [100], which impairs Polα (a part of the primase complex), decreased HCs to less than 0.3% (Fig. 4.2).

4.3 Sectoring of colonies in *rad9Δ* and *rad24Δ* mutants

Previously, it was demonstrated that the initiation of DNA synthesis during BIR is a very slow process (takes up-to 4 hours) and leads to the establishment of a checkpoint-mediated G2/M cell cycle arrest that prevents mitotic division thus allowing cells to complete ongoing BIR.

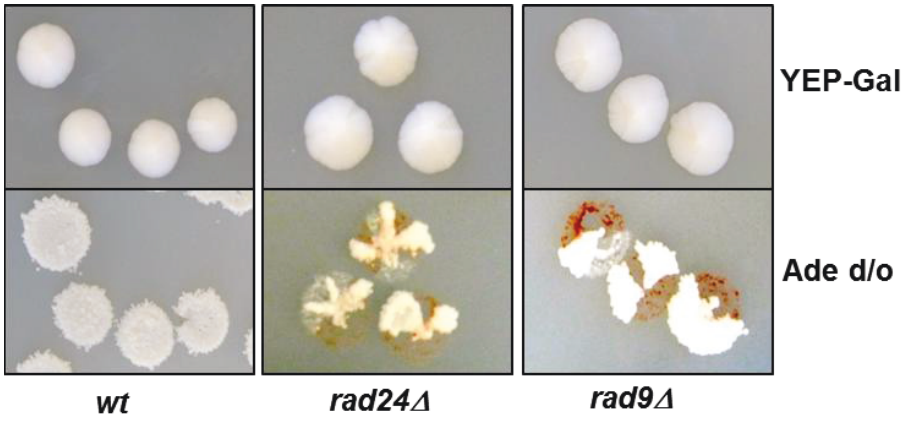

Figure 4.5. DSB repair phenotypes in checkpoint-deficient mutants. Colonies representing DSB repair outcomes in Rad^{+} (wild type; wt), *rad24Δ*, and *rad9Δ* cells are shown here. The morphology of colonies grown on YEP-Gal (top row) and following replica-plating on synthetic complete adenine drop-out medium (Ade d/o, bottom row).

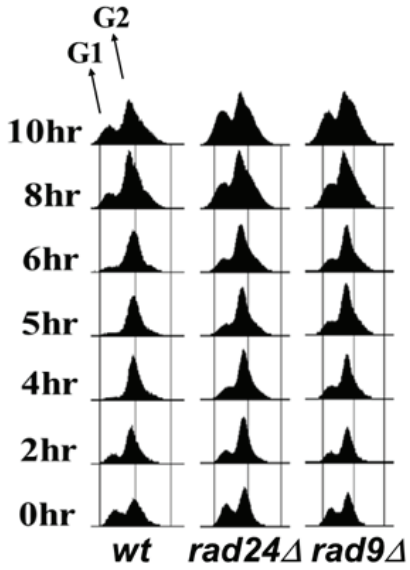

Figure 4.6. FACS analysis to study the cell cycle in checkpoint-deficient mutants. Cell cycle analysis by Flow Cytometery of cells undergoing BIR repair in wt, *rad24Δ*, and *rad9Δ* strains. Positions of peaks corresponding to G1 and G2 phases of the cell cycle are indicated.

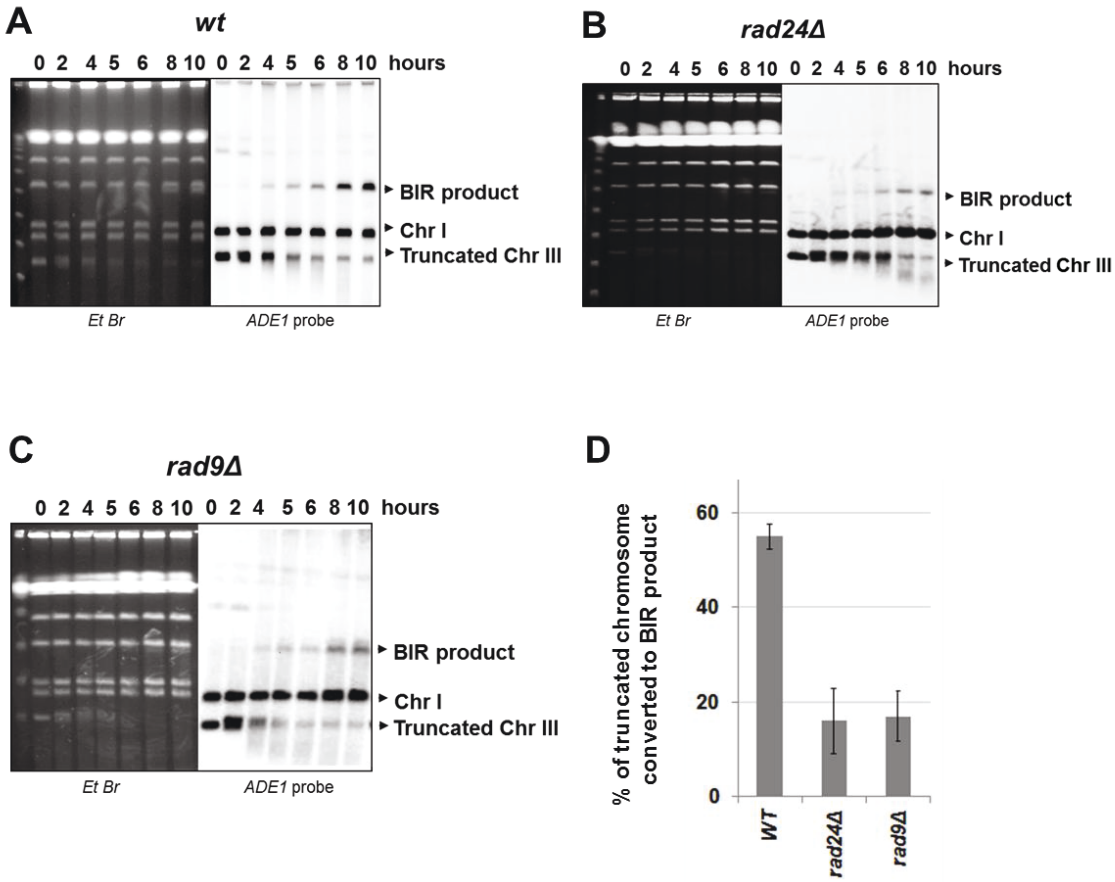

Figure 4.7. Analysis of DSB repair by BIR. BIR kinetics was analyzed by PFGE using cells removed at indicated time points following DSB induction (ethidium bromide-stained gel (left)) followed by Southern hybridization with an *ADE1*-specific probe (right) in wt **(A)**, *rad24Δ* **(B)** and *rad9Δ* **(C). (D)** Quantification of BIR efficiency 10 hours after addition of galactose. Results of 3 experiments performed on each strain were used to calculate average ± SD efficiency of BIR (defined as percent of truncated chromosome converted to BIR product).

Rad9 and Rad24 are two important proteins required for DNA damage response and when the cells of mutants lacking Rad9 or Rad24 were plated on galactose-containing medium to induce a DSB, the resulting colonies showed to contain multiple-sectors (colonies containing ≥2 $Ade^{+}Leu^{-}$ sectors) (Fig. 4.5). The occurrence of multi-sectored colonies most likely resulted from premature onset of mitosis in cells undergoing DSB repair. Consistent with this idea were the results of FACS analyses that confirmed full G2/M arrest in wild type cells between 4 and 8 hours after DSB induction, with only partial arrest observed at these time points in *rad9Δ* and *rad24Δ* mutants (Fig. 4.6).

4.4 Frequency of HC in *rad9Δ* and *rad24Δ* mutants

Given the data that interruptions in BIR due to decreased processivity promote HC formation, I hypothesized that checkpoint deficiency may stimulate HC formation due to an interruption in BIR progression by the premature onset of mitosis. To test this hypothesis, gal-plating experiments were conducted from which I observed that the percentage of colonies with at least one HC sector was extremely high, 71% and 65% among multi-sectored colonies of *rad9Δ* and *rad24Δ* mutants respectively. This was a significant increase as compared to the wild type where the frequency of the colonies with HC was only 4%. In addition, HC sectors comprised approximately 20% of all sectors (events) in multi-sectored colonies (Fig. 4.11). Notably, among simple colonies, no difference in HC frequency was observed between the checkpoint-deficient and wild type strains (Fig. 4.10). I propose that the increase in HCs in checkpoint-deficient

mutants results from premature onset of mitosis that may occur either during the first cell division following DSB induction or during subsequent cell divisions, as further explored in the following sections.

4.5 Efficiency of BIR in *rad9Δ* and *rad24Δ* mutants

Gal-plating experiments were carried out to assess the efficiency of BIR in the checkpoint-deficient mutants. When there is a decrease in BIR and an increase in chromosome loss, cells are said to be BIR deficient. This is justified by the given fact that cells failing to arrest during DSB repair are known to show lower efficiencies of BIR coinciding with a loss of the broken chromatid. In *rad9Δ* and *rad24Δ* mutants, only 28% and 43% respectively were $Ade^{+}Leu^{-}$, compared to the 76% in wild type. Since multi-sectored colonies were exhibited in *rad9Δ* and *rad24Δ* mutants, efficiency of BIR in these colonies was also recorded to be low; with 45% and 46% respectively (Fig. 4.13). The decreased BIR efficiency in checkpoint-deficient mutants was further supported by PFGE analysis of cells undergoing DSB repair over a 10-hour timecourse (performed similarly to [56]), where the amount of BIR repair product was significantly reduced in *rad9Δ* and *rad24Δ* mutants compared to the wild type (Fig. 4.7A-D).

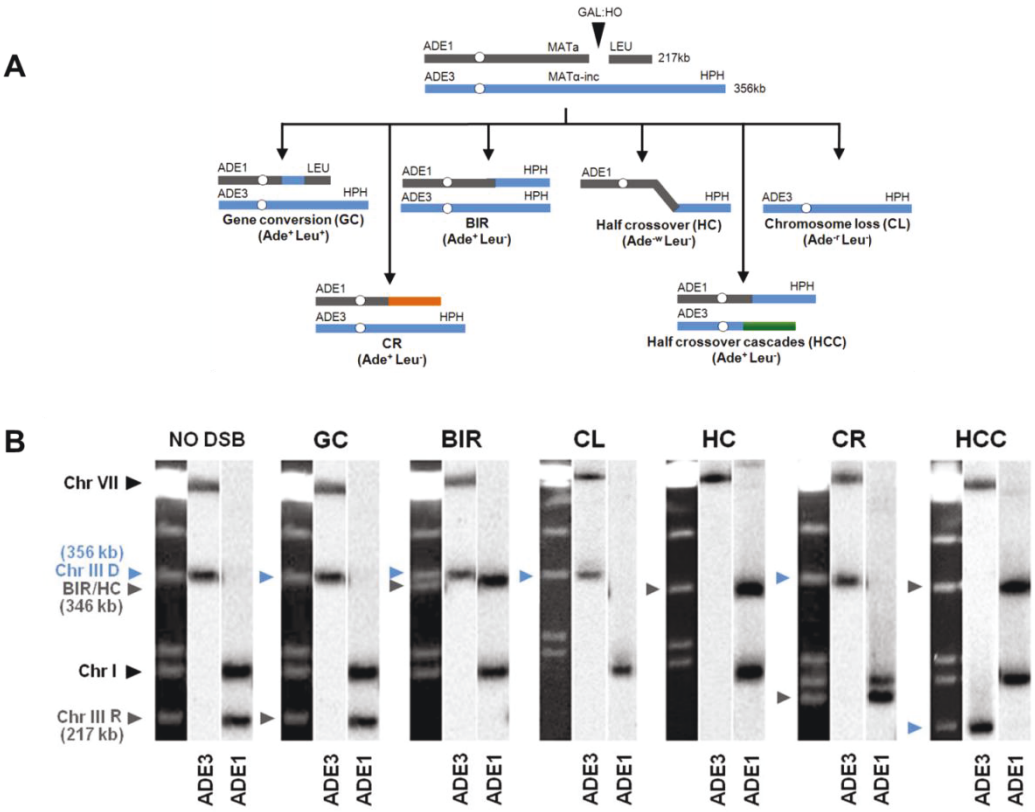

Figure 4.8. Distribution of repair outcomes after DSB. (A) Schematic diagram depicting the following DSB repair outcomes: gene conversion (GC), break-induced replication (BIR), chromosome loss (CL), half crossover (HC), chromosome rearrangements (CRs) resulting from stabilization of the broken recipient chromosome via ectopic recombination or by *de novo* telomere formation, and half crossover cascades (HCC) initiated by HC and resulting from stabilization of the broken donor chromosome. **(B)** PFGE analysis of the DSB repair outcomes listed in **A**. Light bands correspond to chromosomes stained with ethidium bromide, while dark bands correspond to hybridization with *ADE1* (recipient-specific) or *ADE3* (donor-specific) probes marked by grey and blue arrowheads, respectively.

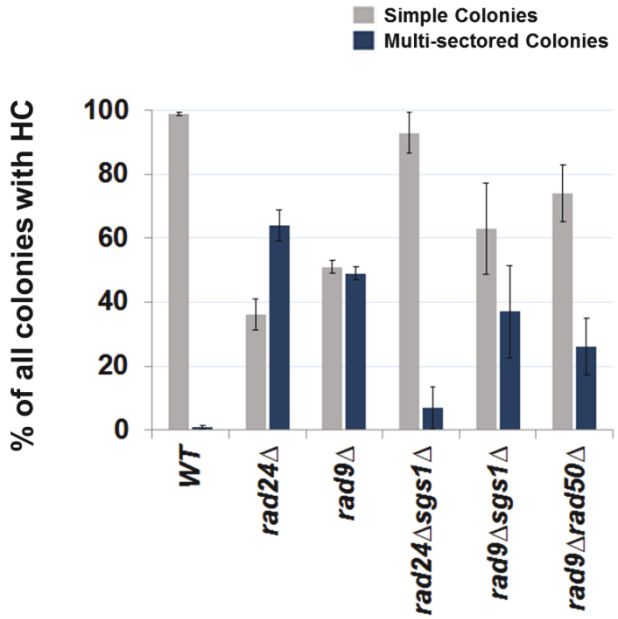

Figure 4.9. Distribution of sectored repair outcomes in checkpoint-deficient mutants. Percentage of simple colonies (containing <2 Ade$^-$ sectors) and multi-sectored colonies (containing ≥2 Ade$^-$ sectors) formed following DSB induction in wt and checkpoint-deficient mutants. Results of 3 to 4 experiments performed for each strain were used to calculate the average ± SD. See Materials and Methods section 3.2.6.1 for the number of colonies analyzed.

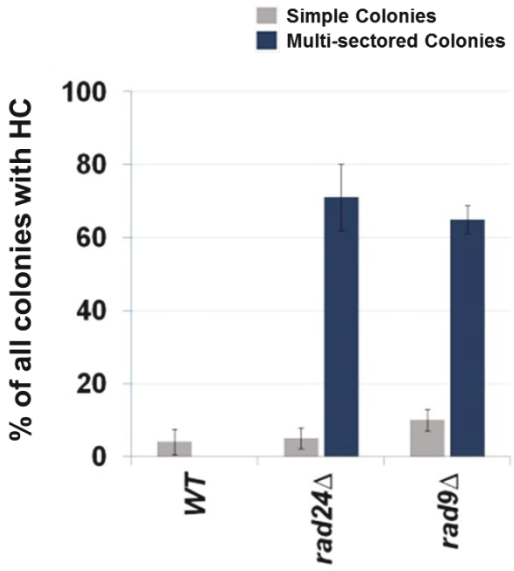

Figure 4.10. Frequency of half crossovers (HC) in checkpoint-deficient mutants with respect to colonies. Percentage of colonies containing HC events in wt and checkpoint-deficient mutants is shown here. Results of 3 to 4 experiments performed for each strain were used to calculate the average ± SD. See Materials and Methods section 3.2.6.1 for the number of colonies analyzed.

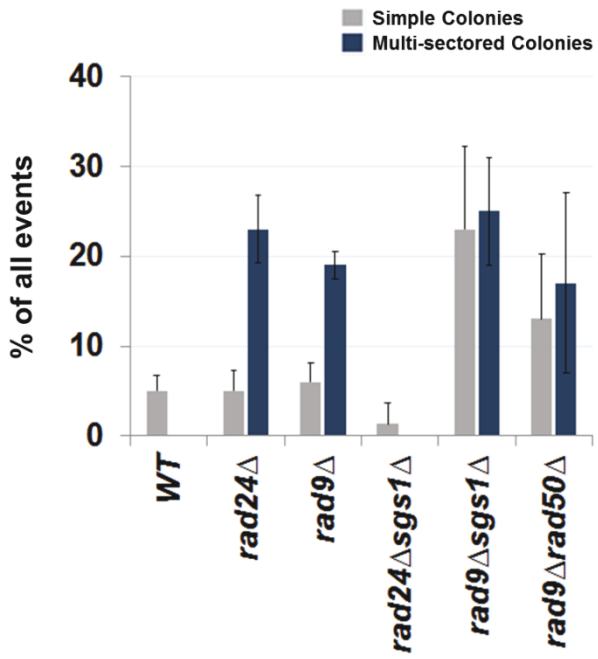

Figure 4.11. Frequency of half crossovers (HC) in checkpoint-deficient mutants with respect to events. Percentage of HC outcomes calculated among all repair events detected in simple and multi-sectored colonies (See Materials and methods for details). Results of 3 to 4 experiments performed for each strain were used to calculate the average ± SD. The number of colonies analyzed were: Pol^{+} (wt) – 1192 colonies and *pol2-9* - 2819 colonies.

4.6 Analysis of DSB repair outcomes in checkpoint-deficient mutants

Genetic analysis of repair outcomes in checkpoint-deficient mutants revealed increased chromosome loss (Fig. 4.8A, 4.12) and a decreased level of $Ade^{+}Leu^{-}$ outcomes, which normally represent BIR (Fig. 4.8A, 4.13). This was consistent with previous results [9] and most likely reflected failed DSB repair in these strains. Based on the decreased efficiency of BIR (as discussed in the previous section (Fig. 4.7A-D)), I hypothesized that a fraction of $Ade^{+}Leu^{-}$ events in checkpoint deficient mutants might in fact represent not BIR, but GCRs resulting from abnormal stabilization of the broken molecules (similar to discussed in [79, 101]). To detect possible GCRs and to characterize their contribution to heterogeneity of the colonies, I employed PFGE to analyze repair outcomes in *rad24Δ* and *rad9Δ* $Ade^{+/-}$ multi-sectored colonies.

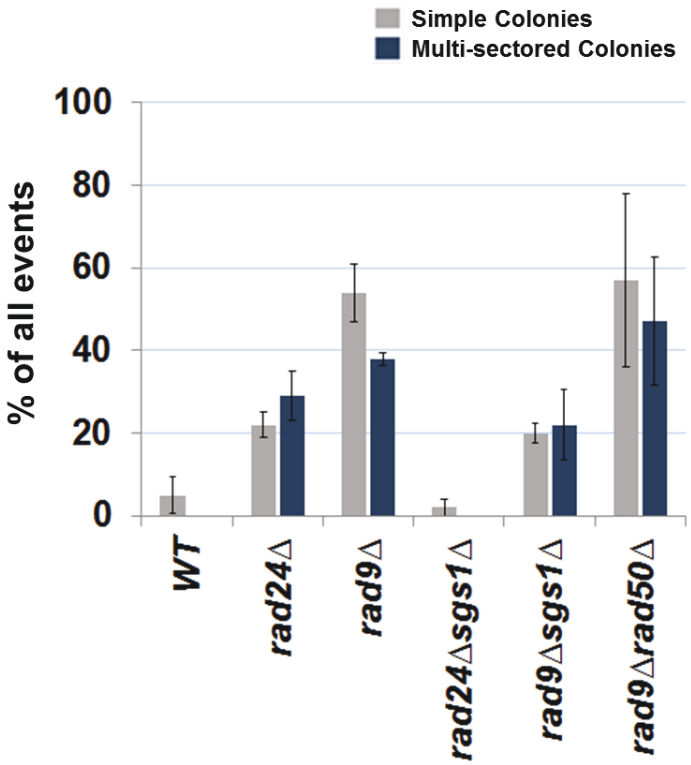

Figure 4.12. Frequency of chromosome losses (CL) in checkpoint-deficient mutants. Percentage of failed repair (CL) outcomes calculated among all repair events detected in simple and multi-sectored colonies (See Materials and Methods for details). Results of 3 to 4 experiments performed for each strain were used to calculate the average ± SD. See Materials and Methods section 3.2.6.1 for the number of colonies analyzed.

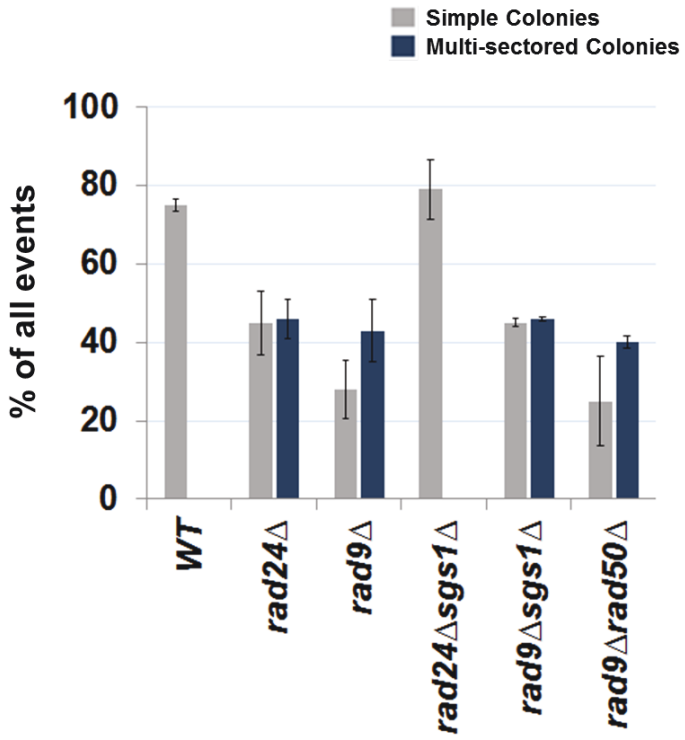

Figure 4.13. Frequency of Ade$^+$Leu$^-$ events in checkpoint-deficient mutants. Percentage of Ade$^+$Leu$^-$ outcomes calculated among all repair events detected in simple and multi-sectored colonies (See Materials and Methods for details). Ade$^+$Leu$^-$ includes BIR*, CR or HCC. Asterisk indicates that BIR could not be distinguished from cases where a HC chromosome segregated in mitosis with an intact donor chromosome (see text for details). Results of 3 to 4 experiments performed for each strain were used to calculate the average ± SD. See Materials and Methods section 3.2.6.1 for the number of colonies analyzed.

4.6.1 Analysis of DSB repair outcomes in checkpoint-deficient mutants with HC-selected colonies

To analyze repair outcomes by PFGE, I focused on 23 individual *rad24Δ* and 11 *rad9Δ* $Ade^{+/-}$ multi-sectored colonies with at least one HC sector (see, for example, colonies in Fig. 4.14A, B). Colonies with HC sectors were considered for analysis because they represented the majority of all multi-sectored colonies in both mutants. All $Ade^{+}Leu^{-}$ sectors as well as a representative number of $Ade^{+}Leu^{+}$ (GC), $Ade^{-w}Leu^{-}$ (HC) and $Ade^{-r}Leu^{-}$ (CL) sectors from each colony were analyzed (see, for example, Fig. 4.14C for PFGE analysis of all sectors from the colony shown in Fig. 4.14A). PFGE analyses of colony sectors with $Ade^{+}Leu^{+}$, $Ade^{-w}Leu^{-}$ and $Ade^{-r}Leu^{-}$ phenotypes confirmed that they resulted from GC, HC, and CL, respectively, as predicted (Fig. 4.14C and see also Fig. 4.8A, B).

PFGE analysis of the $Ade^{+}Leu^{-}$ outcomes from individual colonies revealed three categories of outcomes. In the first group, which comprised 64% and 35% of all $Ade^{+}Leu^{-}$ events in *rad24Δ* (Table 4.1) and *rad9Δ* (Table 4.2), respectively, the chromosome structure was similar to the one observed in true BIR outcomes. However, the high fraction of HC events in the respective colonies makes it highly likely that many of these $Ade^{+}Leu^{-}$ outcomes resulted not from BIR, but from segregation of a HC repair product with an intact copy of the full-length chromosome III (similar to events described in [56, 65]; see Materials and Methods for details).

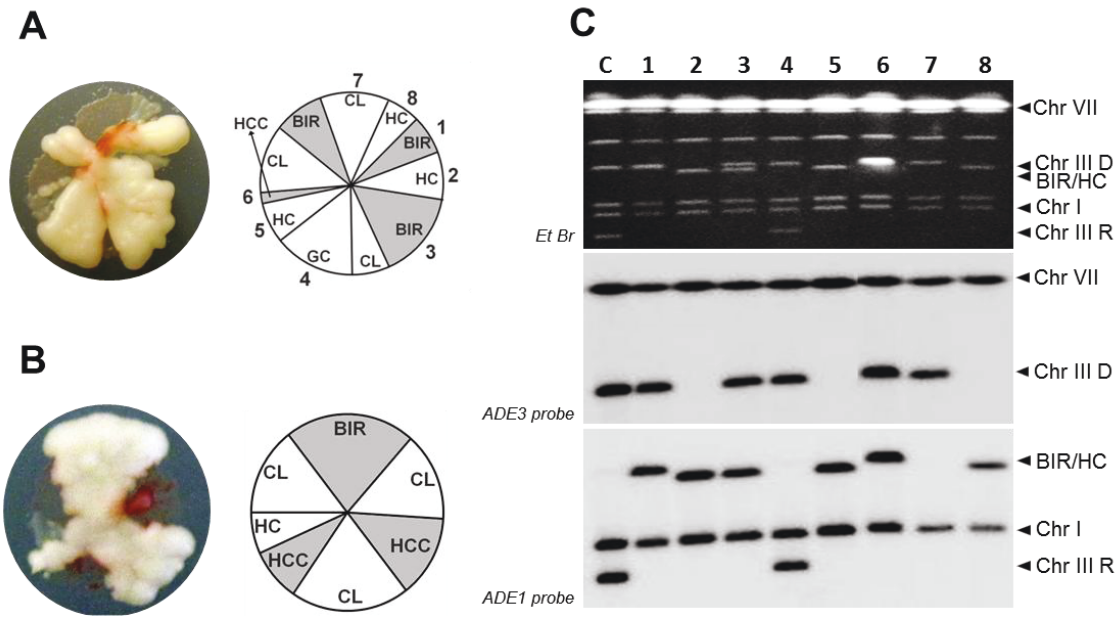

Figure 4.14. Analysis of individual colonies formed by checkpoint-deficient mutants following DSB induction. Analysis performed on colonies containing at least one HC sector. The representative colonies of **(A)** *rad24Δ* and **(B)** *rad9Δ* are shown. Photograph (left) and schematic representation of all sectors (right) are presented. **(C)** PFGE analysis of all sectors from the colony shown in **A**. Lane labeled "C": genomic DNA from *rad24Δ* before DSB induction. Lanes numbered 1-8 represent sectors from the colony in **A**. Top: Ethidium bromide-stained gel; middle and bottom: Southern blot hybridization with *ADE3*- and *ADE1*-specific probes, respectively.

Table 4.1. Analysis of individual colonies in *rad24Δ* by PFGE.

Colony Name	Sectors						Total sectors
	Ade$^+$ Leu$^-$			HC	CL	GC	
	BIR*	CR	HCC				
R24-1	**3**	**0**	**1**	3	3	1	11
R24-2	**1**	**1**	**1**	2	2	0	7
R24-3	**1**	**0**	**1**	1	2	1	6
R24-4	**1**	**0**	**2**	4	0	0	7
R24-5	**1**	**1**	**1**	3	1	1	8
R24-6	**1**	**1**	**2**	2	1	0	7
R24-7	**2**	**1**	**0**	2	1	0	6
R24-8	**2**	**0**	**0**	2	1	0	5
R24-9	**2**	**0**	**1**	2	1	0	6
R24-10	**2**	**0**	**0**	2	0	0	4
R24-11	**1**	**0**	**1**	2	2	0	6
R24-12	**1**	**1**	**1**	2	1	0	6
R24-13	**3**	**0**	**1**	4	2	0	10
R24-14	**2**	**1**	**0**	2	1	0	6
R24-15	**2**	**1**	**1**	2	1	0	7
R24-16	**2**	**0**	**0**	1	1	0	4
R24-17	**4**	**2**	**0**	3	3	0	12
R24-18	**4**	**0**	**0**	1	3	0	8
R24-19	**2**	**0**	**1**	4	1	0	8
R24-20	**4**	**0**	**0**	2	2	0	8
R24-21	**2**	**0**	**1**	2	2	0	7
R24-22	**2**	**1**	**2**	4	0	0	9
R24-23	**2**	**0**	**0**	2	0	0	4
Total Events	**47**	**10**	**17**	**54**	**31**	**3**	**162**

Table 4.1. Analysis of individual colonies in *rad24Δ* by PFGE. Summary of the results of PFGE analysis of all sectors from individual colonies in *rad24Δ* depicting the following DSB repair outcomes: gene conversion (GC), break-induced replication (BIR), chromosome loss (CL), half crossover (HC), chromosome rearrangements (CRs) and half crossover cascades (HCC). Asterisk indicates that BIR could not be distinguished from cases where a HC chromosome segregated in mitosis with an intact donor chromosome (see text for details).

Table 4.2. Analysis of individual colonies in *rad9Δ* by PFGE.

Colony Name	Sectors						Total sectors
	Ade$^+$ Leu$^-$			HC	CL	GC	
	BIR*	CR	HCC				
R9-1	**0**	**0**	**1**	1	1	0	3
R9-2	**1**	**0**	**1**	2	1	0	5
R9-3	**1**	**0**	**0**	1	2	0	4
R9-4	**1**	**0**	**2**	1	2	0	6
R9-5	**2**	**0**	**1**	3	0	0	6
R9-6	**1**	**0**	**2**	1	3	0	7
R9-7	**2**	**1**	**0**	2	1	0	6
R9-8	**0**	**0**	**1**	3	2	0	6
R9-9	**0**	**1**	**1**	1	2	0	5
R9-10	**0**	**1**	**0**	1	1	0	3
R9-11	**0**	**0**	**3**	3	1	0	7
Total Events	**8**	**3**	**12**	**19**	**16**	**0**	**58**

Table 4.2. Analysis of individual colonies in *rad9Δ* by PFGE. Summary of the results of PFGE analysis of all sectors from individual colonies in *rad9Δ* depicting the following DSB repair outcomes: gene conversion (GC), break-induced replication (BIR), chromosome loss (CL), half crossover (HC), chromosome rearrangements (CRs) and half crossover cascades (HCC). Asterisk indicates that BIR could not be distinguished from cases where a HC chromosome segregated in mitosis with an intact donor chromosome (see text for details).

In the second group, $Ade^{+}Leu^{-}$ outcomes were represented by events where DSB repair resulted in formation of GCRs. Thus, approximately 13% of $Ade^{+}Leu^{-}$ from multi-sectored colonies of each of the checkpoint-deficient mutants were chromosomal rearrangements (called CRs), where the broken recipient chromosome was aberrantly stabilized by *de novo* telomere formation or through ectopic recombination between a Ty or delta element in the *MAT***a**-containing chromosome and Ty or delta element located in an ectopic position ((Tables 4.1 and 4.2); similar to previously demonstrated [79]. These CRs carried an unchanged donor chromosome (a 356 kb band that hybridized to the *ADE3*-specific probe) and a recipient band of any size (different from 346 kb) that hybridized to *ADE1* (Fig. 4.8A, 4.8B; CR). The chromosomal structure of one CR event (CR1; Fig. 4.18) was characterized by array-CGH (Table 4.4; see below).

Third, a significant fraction of $Ade^{+}Leu^{-}$ outcomes represented a new type of GCR that contained a single BIR-sized (346 kb) recipient chromosome and a rearranged donor (a band other than 356 kb that hybridized to *ADE3* (Fig. 4.8A, 4.8B; half crossover cascades (HCC), Tables 4.1 and 4.2). I posited that these repair outcomes most likely arose from the rupture of the donor chromosome during HC formation, resulting in an *ADE3*-containing broken fragment that was stabilized by ectopic recombination. The possibility of such HCC events has been previously discussed [56], but never demonstrated. Here I found that 61% and 73% of *rad24Δ* and *rad9Δ* multi-sectored colonies contained at least one $Ade^{+}Leu^{-}$

sector that represented a HCC event (Tables 4.1 and 4.2), the molecular structure of which was further analyzed by array-CGH (see below).

I conclude that premature onset of mitosis resulting from a defective checkpoint leads to aberrant processing of BIR intermediates resulting in frequent HCs and other GCRs. I observed that more than 74% and 91% of all analyzed colonies in *rad24Δ* and *rad9Δ*, respectively contained at least one CR or HCC sector.

4.6.2 Analysis of DSB repair outcomes in checkpoint-deficient mutants with random colonies

In the previous section, colonies with at least one HC sector were selected for PFGE analysis. Here, random (unselected) *rad24Δ* and *rad9Δ* $Ade^{+/-}$ multi-sectored colonies were analyzed. In this case, both HCCs and CR events were frequently observed among $Ade^{+}Leu^{-}$ events obtained from these unselected (random) colonies, but were very rare in the wild type strains (Fig. 4.15A, 4.15B, Table 4.3, and [40, 56]). Importantly, the analysis of strains containing the *pol3-t* mutation, which increased the frequency of HC formation (discussed in the previous section) also revealed DSB-induced HCC outcomes (Fig. 4.17).

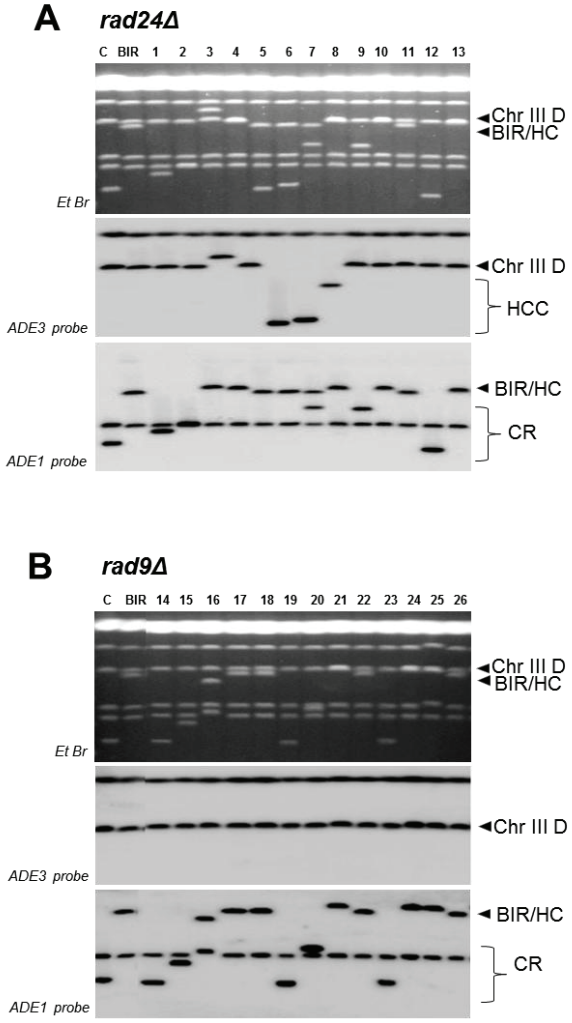

Figure 4.15. Structural analysis of random Ade$^+$Leu$^-$ DSB repair outcomes in *rad24Δ* and *rad9Δ*. PFGE analysis of randomly selected Ade$^+$Leu$^-$ DSB repair events obtained in **(A)** *rad24Δ* and **(B)** *rad9Δ*. On the top of each panel: Ethidium bromide-stained PFGE gel; in the middle and on the bottom: Southern blot analysis of the PFGE gel using *ADE3*- and *ADE1*-specific probes, respectively. Lanes labeled "C": genomic DNA from *rad24Δ* before DSB induction. Lanes labeled "BIR" depict DNA from a BIR outcome. See Fig. 4A and 4B for the structure of BIR, CR, and HCC repair events. For *rad24Δ* (shown in **A**), *rad9Δ* (shown in **B**), lanes 1-13 and lanes 14-26 represent Ade$^+$Leu$^-$ sectors from multi-sectored colonies, respectively.

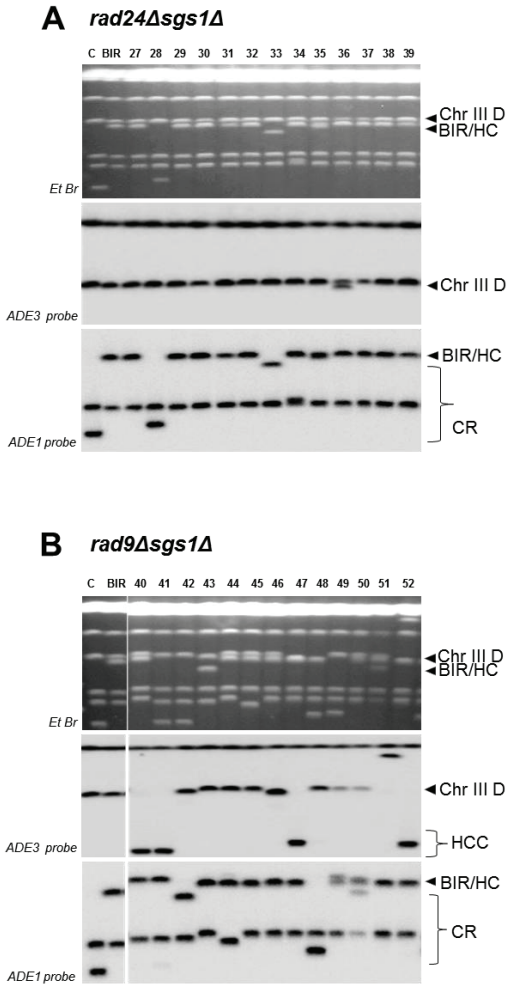

Figure 4.16. Structural analysis of random Ade$^+$Leu$^-$ DSB repair outcomes in *rad24Δsgs1Δ* and *rad9Δsgs1Δ*. PFGE analysis of randomly selected Ade$^+$Leu$^-$ DSB repair events obtained in **(A)** *rad24Δsgs1Δ* and **(B)** *rad9Δsgs1Δ*. On the top of each panel: Ethidium bromide-stained PFGE gel; in the middle and on the bottom: Southern blot analysis of the PFGE gel using *ADE3*- and *ADE1*-specific probes, respectively. Lanes labeled "C": genomic DNA from *rad24Δ* before DSB induction. Lanes labeled "BIR" depict DNA from a BIR outcome. See Fig. 4A and 4B for the structure of BIR, CR, and HCC repair events. For *rad24Δsgs1Δ* (shown in **A**), lanes 27-39 represent Ade$^+$Leu$^-$ sectors from simple colonies. For *rad9Δsgs1Δ* (shown in **B**), lanes 40-52 represent Ade$^+$Leu$^-$ sectors from multi-sectored colonies.

Table 4.3. Distribution of repair events among random Ade$^+$Leu$^-$ outcomes

Relevant genotype	Type of colonies	BIR (or HC*)	CR	HCC
WT	Simple	12 100%	0 0%	0 0%
rad24Δ	Simple	24 80%	4 13%	2 7%
	Multi-sectored	25 47%	16 30%	12 23%
rad9Δ	Simple	7 64%	2 18%	2 18%
	Multi-sectored	23 68%	10 29%	1 3%
rad24Δsgs1Δ	Simple	17 77%	2 9%	3 14%
rad9Δsgs1Δ	Simple	6 38%	2 12%	8 50%
	Multi-sectored	6 20%	8 27%	16 53%

Table 4.3. The distribution of repair events among random Ade$^+$Leu$^-$ outcomes in simple and multi-sectored colonies calculated based on analyses presented in **Figures 4.15 and 4.16**. BIR or HC classes represent Ade$^+$Leu$^-$ outcomes that have chromosome structure similar to BIR, but could also represent instances of HC co-segregation with an intact donor chromosome during mitosis (see text for details).

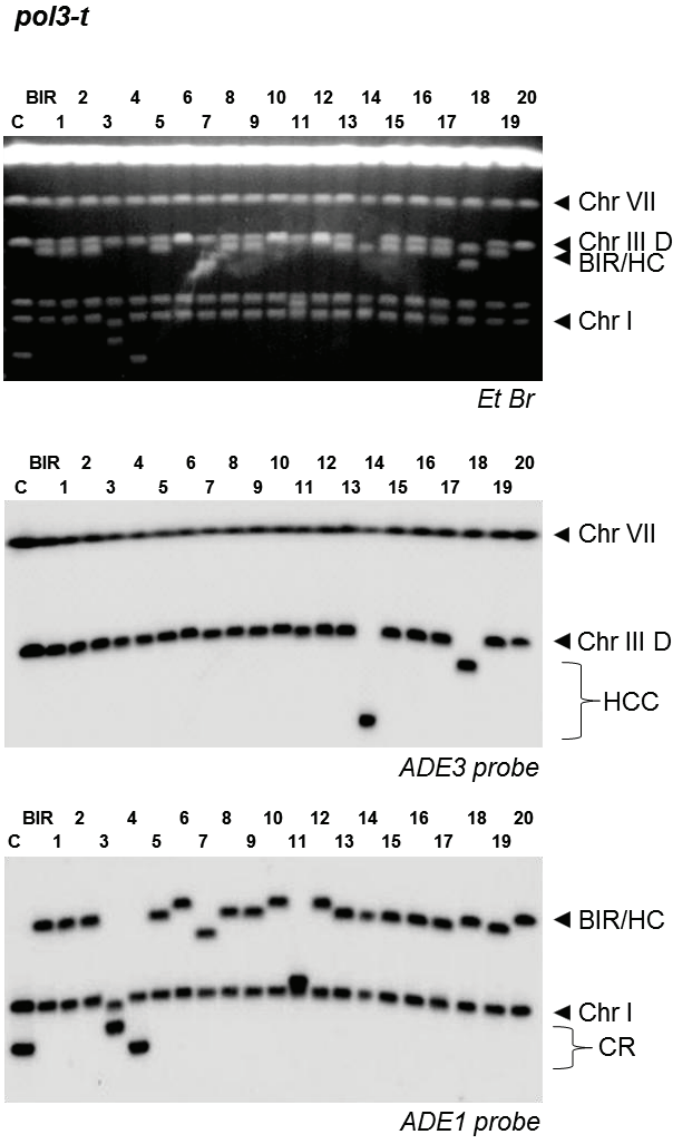

Figure 4.17. Structural analysis of random Ade$^+$Leu$^-$ DSB repair outcomes in *pol3-t* mutants. PFGE analysis of Ade$^+$Leu$^-$ DSB repair events obtained from random multi-sectored colonies in *pol3-t* mutants. Ethidium bromide-stained gel (top), Southern blot analysis of PFGE gel using *ADE3*-specific (middle) and *ADE1*-specific (bottom) probes are shown. Lane labeled “C”: no-DSB control. Lane labeled “BIR”: DNA from a known BIR outcome.

4.7 Analysis of HCCs

As indicated above, the majority of multi-sectored colonies in *rad9Δ* and *rad24Δ* mutants contained at least one HCC event characterized by the presence of a 346 kb band that hybridized to *ADE1*, as well as a second band of varying size (other than 356 kb) that hybridized to an *ADE3*-specific probe and represented a GCR that resulted from breakage and stabilization of the donor chromosome (Fig. 4.8B; HCC). I used comparative genomic hybridization (array-CGH) to further characterize the nature of 12 stabilized donor chromosomes obtained from HCC events identified in *rad24Δ* mutants with the help of our collaborator Dr. Lucas Argueso. (Fig. 4.18) Based on array-CGH, the stabilized donor chromosomes resulting from HCCs were divided into three main classes that accounted for all 12 analyzed outcomes: isochromosomes (Class I), translocations (Class II), and secondary BIR events (Class III) (Table 4.4).

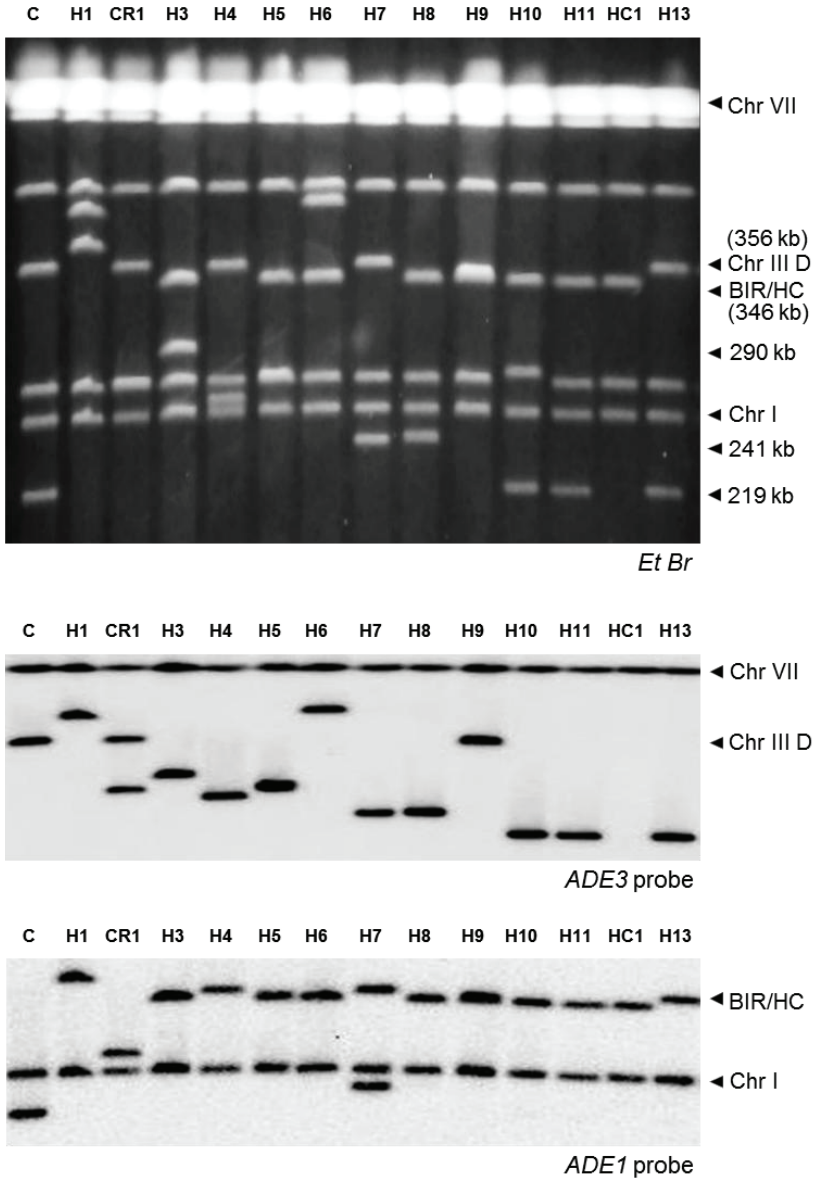

Figure 4.18. Structural analysis of HCC outcomes from *rad24Δ*. PFGE analysis of HCC outcomes (H1, H3–H11, H13), one CR outcome (CR1), and one HC outcome (HC1). Top: Ethidium bromide-stained gel; middle and bottom: Southern blot hybridization with *ADE3*- and *ADE1*-specific probes, respectively.

Table 4.4. The analysis of HCC outcomes in *rad24Δ* cells.

Type of outcome		Class	PFGE Observed Size of Chr III (kb) hybridized to		CGH Results	Predicted Size of Chr III based on CGH and PFGE [ADE3-hybridized (kb)]	Rearrangement type (Chromosome)	Confirmed junctions from Southern Analysis
			ADE1	ADE3				
HCC	**H7**	Ia	356	241 (also with ADE1)	Deletion on **Chr III** between FS1 (150,235) and *MAT* (200,142) Duplication on **Chr III** distal to *YCLCδ1* (0-83,110)	245	Isochromosome (Chr III)	Ty1γ/*YCLCδ1*
	H8	Ia	346	244	Deletion on **Chr III** between FS1 (150,235) and *MAT* (200,142) Duplication on **Chr III** distal to *YCLCδ1* (0-83,110)	245	Isochromosome (Chr III)	Ty1γ/*YCLCδ1*
	H10	Ib	346	219	Deletion on **Chr III** between *YCRCδ6* (124,250) and *MAT* (200,142) Duplication on **Chr III** distal to *YCLWTy1-1* (0-83,110)	219	Isochromosome (Chr III)	*YCRCδ6/YCLWTy1-1*
	H11	Ib	346	219	Deletion on **Chr III** between *YCRCδ6* (124,250) and *MAT* (200,142) Duplication on **Chr III** distal to *YCLWTy1-1* (0-83,110)	219	Isochromosome (Chr III)	*YCRCδ6/YCLWTy1-1*
	H12	Ib	346	219	Deletion on **Chr III** between *YCRCδ6* (124,250) and *MAT* (200,142) Duplication on **Chr III** distal to *YCLWTy1-1* (0-83,110)	219	Isochromosome (Chr III)	ND
	H13	Ib	356	219	Deletion on **Chr III** between *YCRCδ6* (124,250) and *MAT* (200,142) Duplication on **Chr III** distal to *YCLWTy1-1* (0-83,110)	219	Isochromosome (Chr III)	*YCRCδ6/YCLWTy1-1*
	H4	Ic	356	263	Deletion on **Chr III** between FS2 (169,419) and *MAT* (200,142) Duplication on **Chr III** distal to *YCLWTy1-1* (0-83,917)	277	Isochromosome (Chr III)	ND
	H5	Ic	346	278	Deletion on **Chr III** between FS2 (169,419) and *MAT* (200,142) Duplication on **Chr III** distal to *YCLWTy1-1* (0-83,917)	277	Isochromosome (Chr III)	ND
	H3	II	346	297	Deletion on **Chr III** between FS1 (150,235) and *MAT* (200,142) Duplication on **Chr V** distal to *YERCδ16* (436,156)	296	Translocation (Chr III - Chr V)	Ty1γ/*delta*
	H9	IIIa	346	348	Duplication on **Chr III** from *MAT* upto the telomeric end (200,142-308,302)	346	Secondary BIR (Chr III)	ND
	H6	IIIb	346	415	Duplication on **Chr III** between FS1 and FS2 (145,816-168,576) and from *MAT* upto the telomeric end (200,142-308,302)	> 375	BFB-mediated Secondary BIR (Chr III)	ND
	H1	IIIb	374	406	Triplication on **Chr III** between FS1 and FS2 (131,046-169,419) and a duplication from *MAT* upto the telomeric end (200,142-308,302)	> 375	BFB-mediated Secondary BIR (Chr III)	ND
CR	**CR1**	CR	275	356	Deletion on **Chr III** between FS2 (169,419) and *MAT* (200,142) Duplication on **Chr III** distal to *LEU* (83,917)	NA	CR	NA

* BFB = Breakage-fusion-bridge cycle.

4.7.1 Characterization of Class I HCC outcomes

Class I rearrangements included 8 of the 12 HCC events analyzed by array-CGH (Fig. 4.18, Table 4.4). Each of these events had in common a deletion of sequences in the right arm of chromosome III and a duplication of sequences from the opposite chromosome arm (Fig. 4.19, 4.21; Table 4.4), thus forming an isochromosome. (Class I is subdivided into Class Ia, Ib, and Ic depending on the point of recombination; see Table 4.4 for details). I propose that the formation of these outcomes was initiated by invasion of the broken recipient into the full donor chromosome III, which led to the formation of an HC represented by a 346 kb band hybridized to *ADE1*-specific probe (Fig. 4.20, 4.22). The resulting broken *ADE3*-containing fragment was then resected and subsequently repaired by non-allelic homologous recombination between a Ty or delta element located in the right arm of chromosome III and a Ty or delta element located in the left arm of chromosome III.

4.7.1.1 Characterization of Class Ia HCC outcomes (H7 and H8)

In the case of Class Ia outcomes (H7 and H8), the recombination occurred between the Ty1γ element in FS1 and a delta element *YCLCδ1* (Fig. 4.18, Table 4.4, Fig. 4.20). The predicted size of such an isochromosome (calculated based on [77, 102], and also based on the data from SGD) was approximately 245 kb (Fig. 4.18), which was consistent with the size of the *ADE3*-hybridizing band observed by PFGE analysis. Our proposed molecular structure was further

Figure 4.19. Structural analysis of HCC outcomes H7 and H8 (Class Ia). The schematic diagram of HCC outcomes H7 and H8 (Class Ia) based on the results of array-CGH analysis is shown here. Array-CGH analysis shows a deletion (red) in Chr. III (between FS1 (Ty1γ; 150235 bp position) and *MAT* (200142 bp position)) and a duplication (blue) of sequences in the same Chr. III (located centromere-distal to *YCLCδ1* (83055 bp position)). Underlined numbers in the schematic diagram (1 and 4) indicate the positions of hybridization probes used for Southern analysis. The positions of *Eco*O109I (E) and *Eci*I (Ec) restriction sites are indicated. The Southern blot shows H7 and H8 digested with *Eco*O109I and hybridized to Probe 1 and Probe 4. As expected, the size of the DNA fragment corresponding to the HCC junction (H) was approximately 8 kb. Similarly, an 8 kb HCC junction (H) fragment was detected when H7 and H8 were digested with *Eci*I and hybridized to Probe 1 and Probe 4. **P**: the positions of bands corresponding to the original (unrearranged) chromosomes.

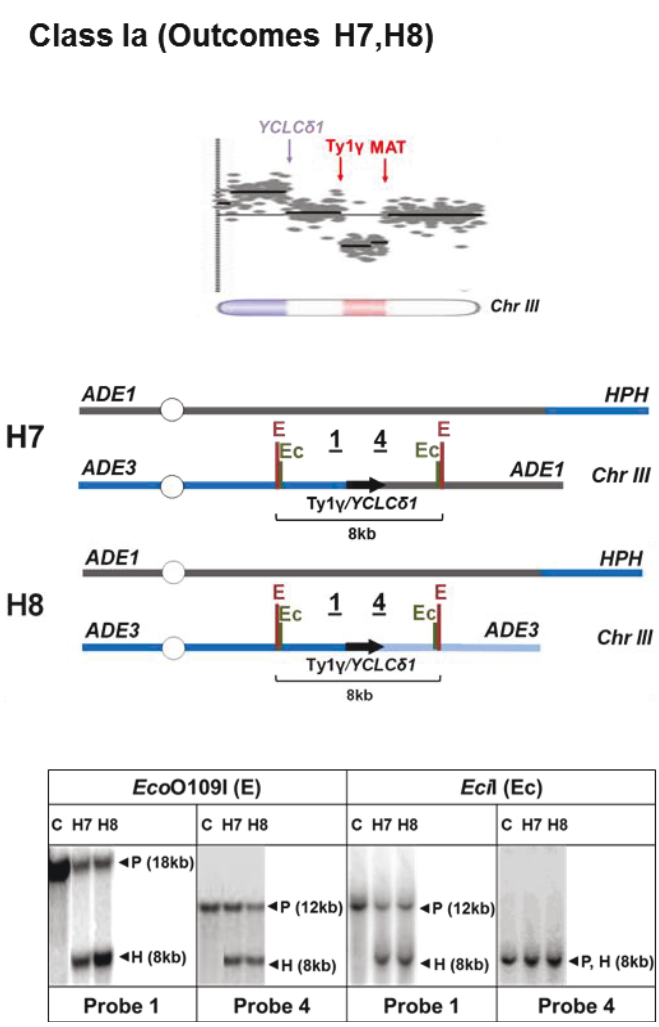

Figure 4.19. Structural analysis of HCC outcomes H7 and H8 (Class Ia).

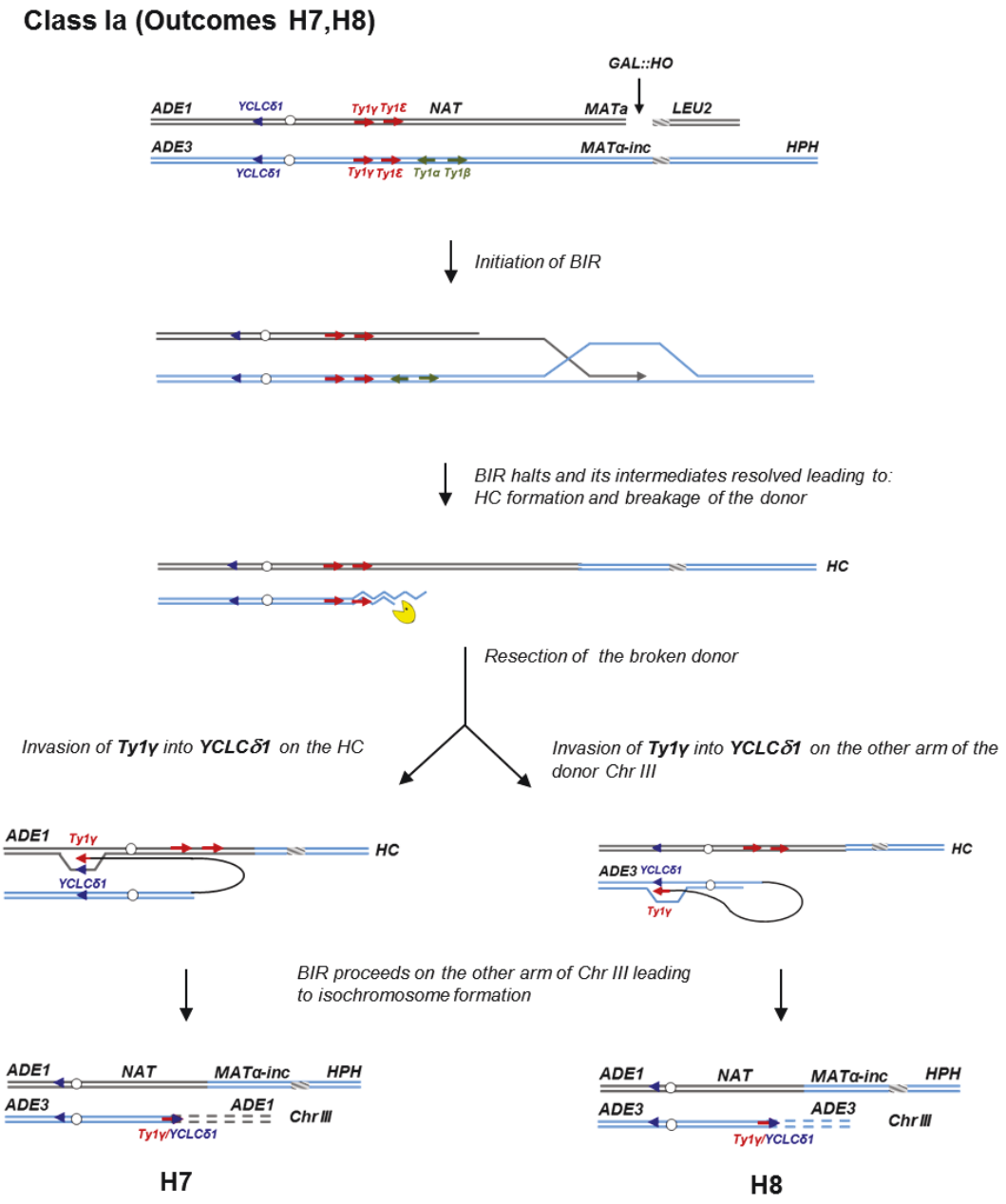

Figure 4.20. Molecular mechanism explaining the formation of H7 and H8. The schematic model shows the molecular mechanism that explains the formation of H7 and H8 (Class Ia). See text for details.

confirmed through a detailed Southern analysis using the restriction enzymes *Eco*O1091 and *Eci*I and Probe 1 (FS1-specific) and Probe 4 (specific to the region of chromosome III located centromere-distal to *YCLCδ1* (Fig. 4.19, Fig. 4.20 (also see Materials and Methods)).

4.7.1.2 Characterization of Class Ib HCC outcomes (H10, H11, H12 and H13)

In the case of Class Ib outcomes (H10, H11, H12 and H13), recombination occurred between delta elements *YCRCδ6* and *YCLWTy1-1* [77], which corresponds to *YCLWδ15 in SGD.* The predicted size of such an isochromosome was approximately 219 kb (Fig. 4.18), which was consistent with the size of the *ADE3*-hybridizing band observed by PFGE analysis (Table 4.4). The structures of H10, H11, and H13 were further confirmed by Southern analysis using the restriction enzymes *Eci*I and *Psh*AI and also Probe 4 and Probe 5 (specific to region of chromosome III located centromere proximal to *YCRCδ6*) (Fig. 4.21, Fig. 4.22 (also see Materials and Methods)).

Figure 4.21. Structural analysis of HCC outcomes H10, H11 and H13 (Class Ib). The schematic diagram of HCC outcomes H10, H11 and H13 (Class Ib) based on the results of array-CGH analysis is shown here. Array-CGH analysis shows a deletion (red) in Chr. III (between *YCRCδ6*; 124250 bp position) and *MAT* (200142 bp position)) and a duplication (blue) of sequences in the same Chr. III (located centromere-distal to *YCLWTy1-1*, which corresponds to *YCLWδ15* in SGD (83110 bp position)). Underlined numbers in the schematic diagram (4 and 5) indicate the positions of probes used for Southern hybridization. The positions of *Eci*I (Ec) and *Psh*AI (Ps) restriction sites are indicated. As expected from the maps, the size of the DNA fragment corresponding to the HCC junction (H) was approximately 8 kb following digestion with *EciI* and 11 kb following digestion with *Psh*AI.

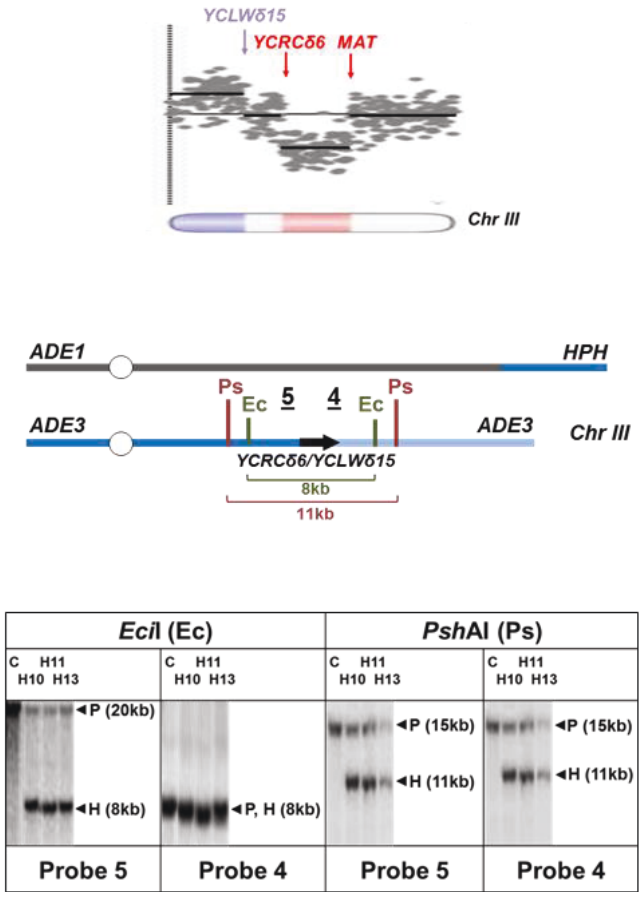

Figure 4.21. Structural analysis of HCC outcomes H10, H11 and H13 (Class Ib).

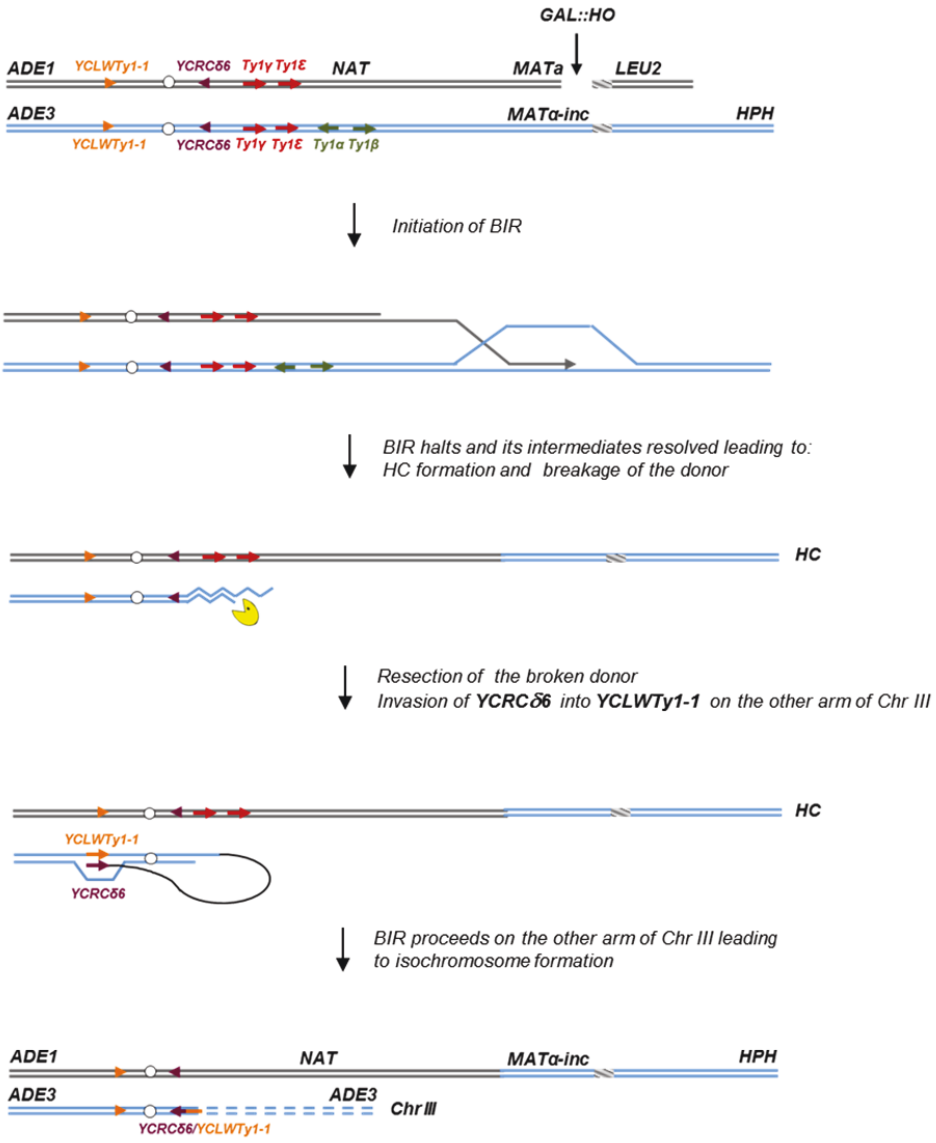

Figure 4.22. Molecular mechanism explaining the formation of H10, H11 and H13. The schematic model shows the molecular mechanism that explains the formation of H10, H11 and H13 (Class IIb). See text for details.

4.7.1.3 Characterization of Class Ic HCC outcomes (H4 and H5)

I proposed that the formation of H4 and H5 was initiated by invasion of the broken *MAT***a** chromosome into the full copy of *MAT*α-inc-containing chromosome III, which led to the formation of an HC. The only difference was that in the case of H5, the invasion occurred centromere-distal to FS2, thus leading to the formation of HC represented by a 346 kb band while in the case of H4, the invasion occurred centromere-proximal to FS2 which resulted in the formation of a 356 kb HC band (Fig. 4.18; Fig. 4.23). The broken *ADE3*-containing fragment resulted from HC formation was then resected, leading to the deletion of sequences between *FS2* and *MAT*α-inc, and was later stabilized by recombination between Ty1α (FS2) and a delta element of *YCLWTy1-1*, which corresponds to *YCLW*δ*15* in SGD (83110 bp position) in the left arm of chromosome III. The predicted size of such a translocation is 277 kb, which is consistent with the size of the band that hybridized to the *ADE3*-specific probe in H5 (Fig. 4.18, Table 4.4). The reduced size of *ADE3*-hybridized bands observed in H4 (263 kb) might result from recombination between delta elements of Ty1α of FS2 and *YCLWTy1-1* in such a way that it resulted in deletion of Ty1 at the junction.

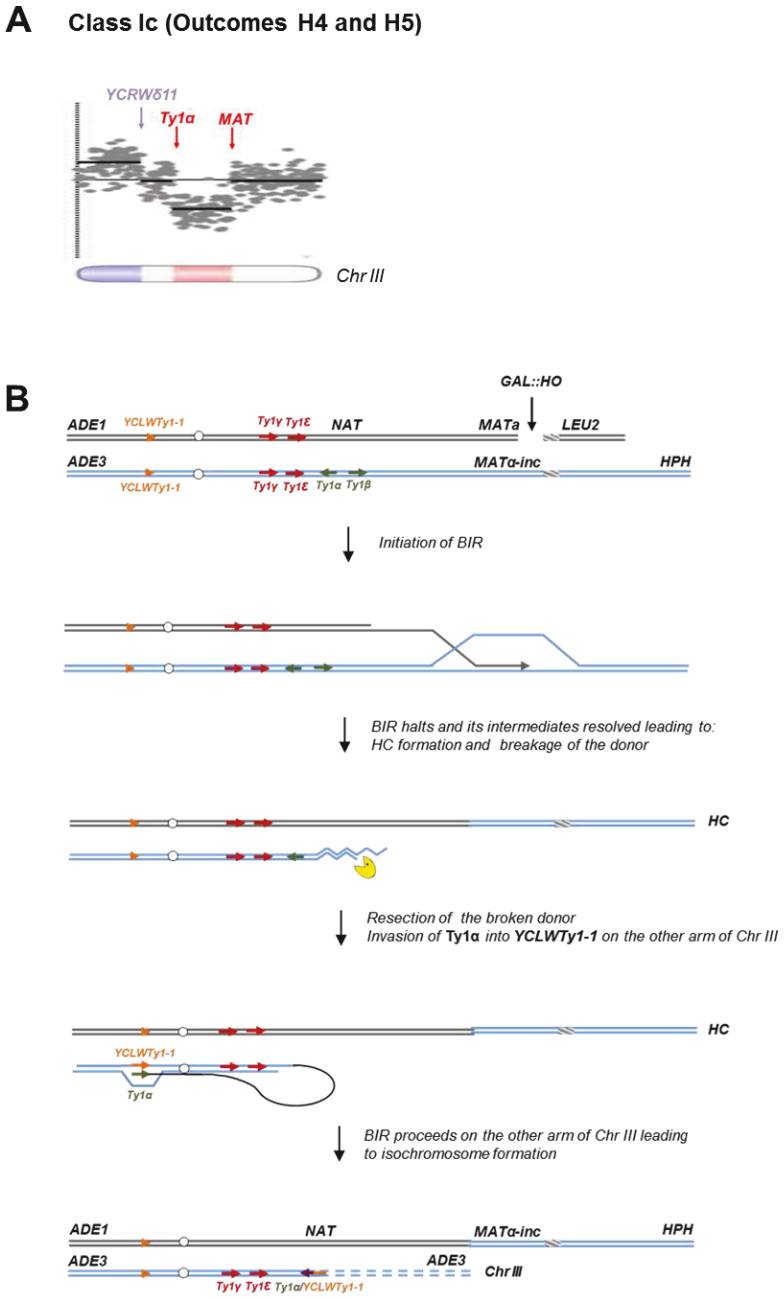

Figure 4.23. Structural analysis of HCC outcomes H4 and H5. **(A)** Array-CGH analysis of HCC outcomes H4 and H5 (Class Ic) shows a deletion (red) in Chr III (between FS2; 169419 bp position) and *MAT*; and a duplication (blue) of Chr III sequences located centromere-distal to *YCLWTy1-1*, which corresponds to *YCLWδ15* in SGD (83110 bp position). **(B)** Molecular mechanism explaining the formation of H4 and H5.

4.7.2 Characterization of Class II HCC outcomes

Class II included only one of the 12 HCC outcomes, outcome H3. H3 was determined to result from a deletion in chromosome III between positions of FS1 (a tandem repeat of Ty1 elements) and *MAT,* and a duplication of all sequences located on chromosome V distal to a solo delta element *YERCdelta16* (Fig. 4.24, 4.25 and Table 4.4). I propose that the formation of H3 was initiated by invasion of the broken *MAT***a** chromosome into the full copy of *MAT*α-inc-containing chromosome III, which led to the formation of an HC represented by a 346 kb band that hybridized to the *ADE1*-specific probe (Fig. 4.18, Fig. 4.24, 4.25). The resulting broken *ADE3*-containing fragment was then resected, leading to the deletion of sequences between *FS1* and *MAT*, and was later stabilized by recombination between Ty1γ (FS1) and a delta element located close to *YERCdelta16* on chromosome V. The predicted size of such a translocation is 296 kb, which is consistent with the size of the band that hybridized to the *ADE3*-specific probe (Fig. 4.18, Table 4.4).

The proposed molecular structure was further confirmed through a detailed Southern analysis using the restriction enzymes *Psy*I and *Ppu*MI combined with Probe 1 (FS1-specific) and Probe 2 (specific to the region of chromosome V located centromere-distal to *YERCdelta16*; Fig. 4.24).

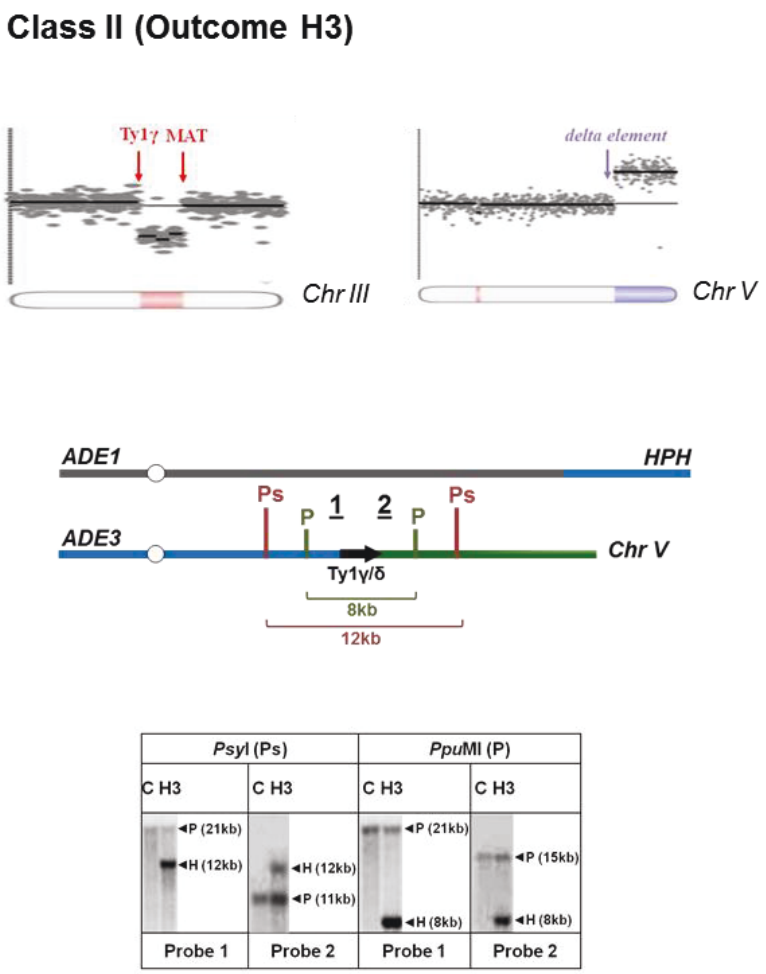

Figure 4.24. Structural analysis of HCC outcome H3 (Class II). Array-CGH analysis of HCC outcome H3 (Class II) shows a deletion (red) in Chr III (between FS1 (Ty1γ; 149482 bp position) and *MAT*; and a duplication (blue) of sequences in Chr V (located centromere-distal to a delta element located close to *YERCδ16* (435946 bp position)). Underlined numbers (1 and 2) indicate the positions of probes used for Southern hybridization. The positions of *Psy*I (Ps) and *Ppu*MI (P) restriction sites are indicated. The Southern blot of H3 genomic DNA digested with *Psy*I and hybridized to Probes 1 and 2 shows a 12-kb-long DNA fragment at the HCC junction. Also, an 8 kb DNA fragment was obtained when H3 was digested with *Ppu*MI and hybridized with Probe 1 and Probe 2.

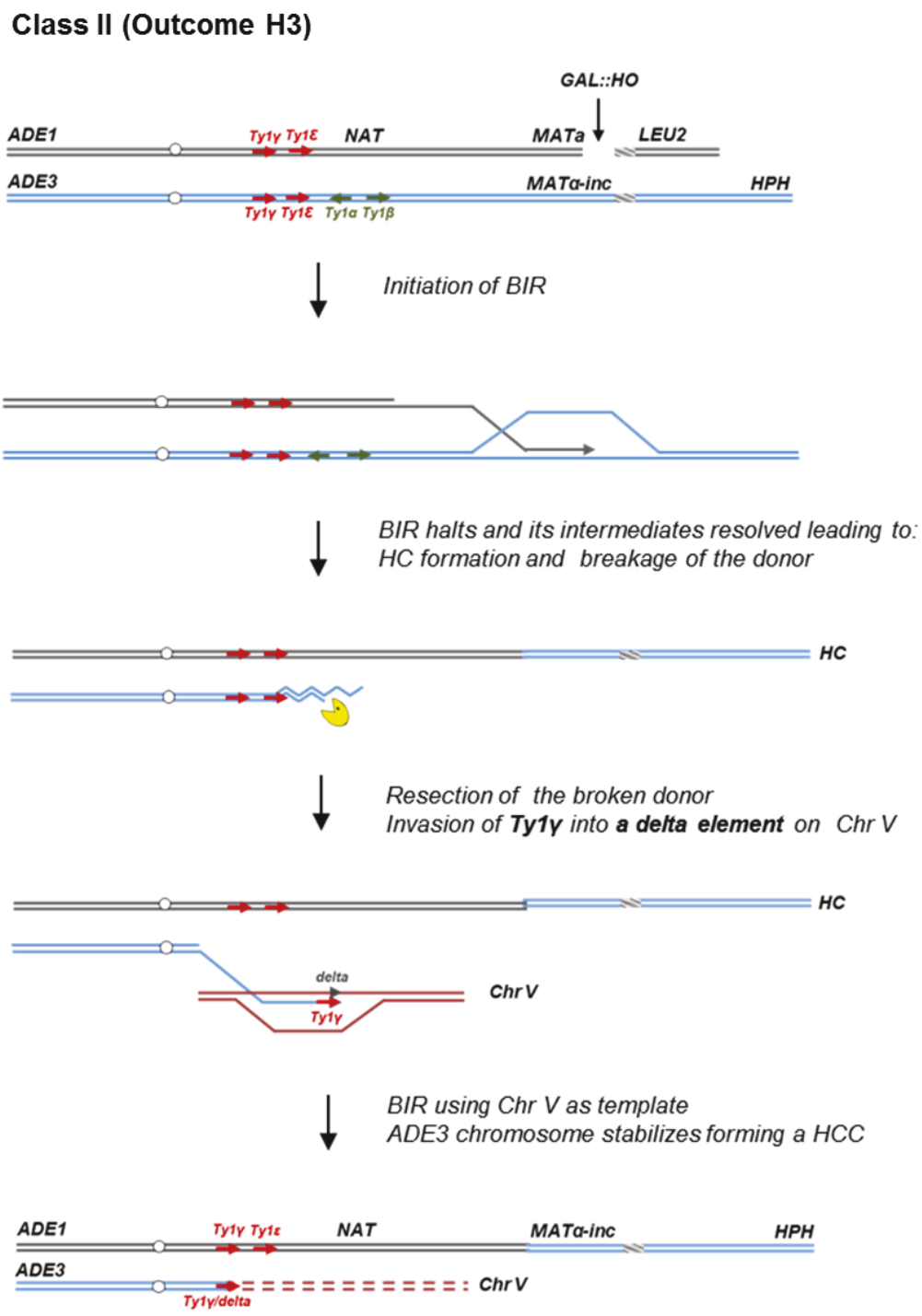

Figure 4.25. Molecular mechanism explaining the formation of H3. The schematic model shows the molecular mechanism that explains the formation of H3 (Class II). See text for details.

Notably, the orientation of the delta elements within Ty1γ and *YERCdelta16* is not consistent with the generation of a monocentric translocation; therefore, I propose that recombination occurred between Ty1γ and an un-annotated delta element located close to *YERCdelta16* but in the opposite orientation. This recombination between chromosome III and V could proceed by BIR or by a half crossover event. In the latter case, it would continue the cascade of genomic instability.

4.7.3 Characterization of Class III HCC outcomes

Class III rearrangements included 3 of the 12 analyzed HCC outcomes and were further divided into IIIa and IIIb.

4.7.3.1 Characterization of Class IIIa HCC outcome (H9)

Class IIIa was represented by the outcome H9. Array-CGH analysis of this outcome indicated a duplication of chromosome III sequences from *MAT* through the telomere indicative of BIR repair; however, PFGE analysis revealed that both *ADE1* and *ADE3*-hybridizing chromosomes were equal in size (346 kb long). I hypothesized that, similar to other HCC events, the formation of H9 was initiated by HC, which led to the formation of an *ADE3*-containing broken fragment. This broken donor fragment was stabilized through invasion into the HC product centromere proximal to *NAT* followed by BIR that copied the right arm of HC (Fig. 4.26). Therefore, I named this outcome a “secondary BIR event”.

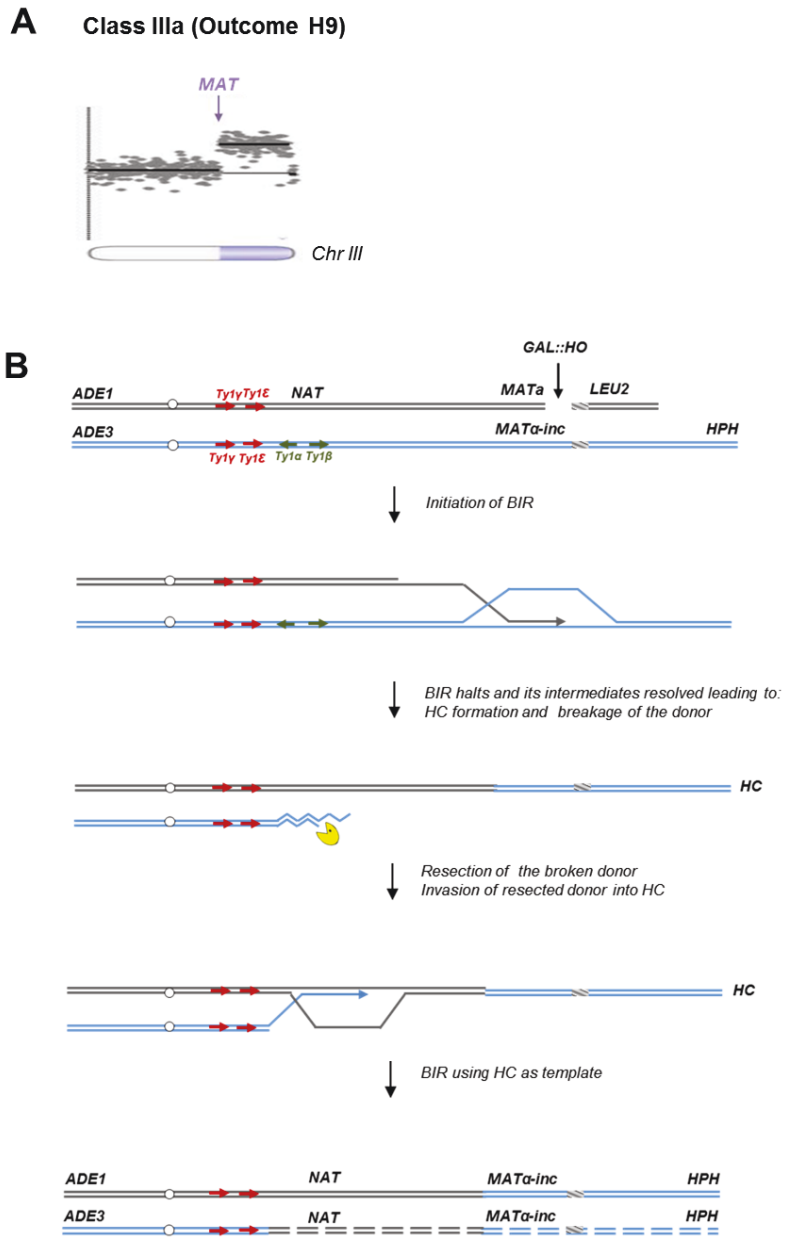

Figure 4.26. Structural analysis of HCC outcome H9 (Class IIIa). **(A)** Array-CGH analysis of HCC outcome H9 (Class IIIa) shows duplication (blue) of Chr III from *MAT* through the telomeric end. **(B)** Molecular mechanism explaining the formation of H9.

Importantly, 8 of 24 HCCs that were originally identified by PFGE showed a pattern similar to H9 (both *ADE1*- and *ADE3*-hybridizing bands were approximately 346 kb; data not shown), which suggests that all of them most likely represented secondary BIR events, even though only H9 was analyzed by array-CGH. Therefore, it appears that secondary BIR events are relatively common among BIR outcomes in checkpoint-deficient mutants.

4.7.3.2 Characterization of Class IIIb HCC outcome (H6)

Array-CGH analysis of the HCC outcome H6 (Class IIIb) demonstrated a duplication of chromosome III sequences from *MAT* to the telomere, which was similar to all normal BIR. In addition, duplication between FS1 and FS2 was observed. However, the PFGE analysis detected a change in the donor chromosome, which became longer than the BIR product (415 kb) (Fig. 4.18, Table 4.4). Due to the change in the donor chromosome, it was placed in the HCC category, and I propose that it was also formed by a cascade of events. Similar to classes I and II, its formation was also triggered by a breakage in the donor chromosome resulting from the formation of a HC. Further, I propose that the broken donor chromosome was stabilized through breakage-fusion bridge cycle (similar to [16, 38 and 103]), where simultaneous breakage of two donor sister chromatids resulted in the formation in the inverted dicentric dimer, which initiated a BFB cycle, followed by stabilization of a broken fragment by BIR using HC as a template.

4.7.3.3 Characterization of Class IIIb HCC outcome (H1)

Array-CGH analysis of the HCC outcome H1 (Class IIIb) demonstrated a duplication of chromosome III sequences from *MAT* to the telomere, which was similar to all normal BIR. In addition, a triplication between FS1 and FS2 was observed. The PFGE analysis detected a change in the donor chromosome, which became longer than the BIR product (407 kb) (Fig. 4.18, Table 4.4), and the change of the size of the recipient chromosome, which became 374 kb long. I propose that H1 represents a complex event, and several steps contributed to its formation. Specifically, similar to H6, the formation of H1 was triggered by a breakage in the donor chromosome resulting from the formation of a HC. Also, the donor likely stabilized via a BFB cycle. In addition, it is possible that a BFB cycle or a template switching event contributed to the formation of the original HC, which resulted in its increased size (374kb).

Overall, I conclude that frequent interruptions during BIR repair in checkpoint-deficient mutants leads to frequent breakage of the donor chromosome that results in further cascades of DNA instabilities.

4.8 Effect of DSB resection on distribution of repair outcomes in checkpoint-deficient mutants

It has been demonstrated that the absence of Rad9 increases the rate of resection at a DSB, which could contribute to the increased frequency of chromosome loss and GCRs I observed in *rad9Δ* mutants [104, 105]. Therefore, I

tested to see if *sgs1Δ* and *rad50Δ* (known to decrease the efficiency of DSB resection) [42, 44 and 106] affected the distribution of repair outcomes in *rad9Δ* and *rad24Δ*.

I observed that the deletion of *SGS1*, which is required for long-range 5'-strand resection, in *rad24Δ*, dramatically reduced the frequency of chromosome loss, HCs, and virtually eliminated all multi-sectored colonies (Fig. 4.9, 4.11, 4.12 and 4.13). The majority of colonies formed in *rad24Δsgs1Δ* were fully $Ade^{+}Leu^{-}$, and their PFGE analysis indicated that they contained normal BIR events (Fig. 4.13; Fig. 4.16A, Table 4.3), even though they can also represent secondary BIR events. Deletion of *SGS1* in *rad9Δ* also affected the distribution of repair outcomes. Compared to *rad9Δ* alone, the frequency of chromosome loss was decreased, while HCs were increased in the double mutant, along with an increase in HCC events (Fig. 4.11, 4.12 and 4.13; Fig. 4.16B, Table 4.3). In addition, I observed that deletion of *RAD50*, which is involved in end processing near the DSB site [44], did not affect the distribution of repair outcomes in *rad9Δ* or *rad24Δ* (Fig. 4.11, 4.12 and 4.13). Overall, my data suggest that deletion of *Sgs1*, responsible for long-range resection of DSB ends significantly affects the distribution of repair outcomes in the absence of a functional checkpoint response.

CHAPTER 5. DISCUSSION

5.1 Decreased quality of BIR DNA synthesis promotes HC formation

BIR is a critical mechanism to repair broken chromosomes. Normally, BIR is initiated by a DSB produced in such a way that only one end of the broken molecule is available for repair (Fig. 5.1A). It thus initiates with a single invasion into a homologous template (Fig. 5.1B) followed by initiation of DNA synthesis (Fig. 5.1C) that proceeds to the telomere (Fig. 5.1D). Increased HC formation and chromosome loss was previously demonstrated in *pol32Δ* and *pol3-ct* mutants during BIR repair where strand invasion was successful, but DNA synthesis could not be (or was poorly) initiated [56, 65]. Likewise, here I report a similar phenotype in strains containing other mutations in Polδ, *pol3-Y708A* (a mutation affecting the catalytic subunit of Polδ) [95] and *pol31-WRRGW* (a mutation in the Pol31 subunit of Polδ) [96]. For each of these cases, I propose that HC formation results from resolution of HJ structures that persist when BIR DNA synthesis is not initiated (Fig. 5.1B, 5.1L).

I demonstrate that BIR interrupted at various stages of its progression, for example during replication, also stimulates HCs. This most likely occurs in *pol3-t* mutants because the processivity of Polδ is compromised (Fig. 5.1C, 5.1L).

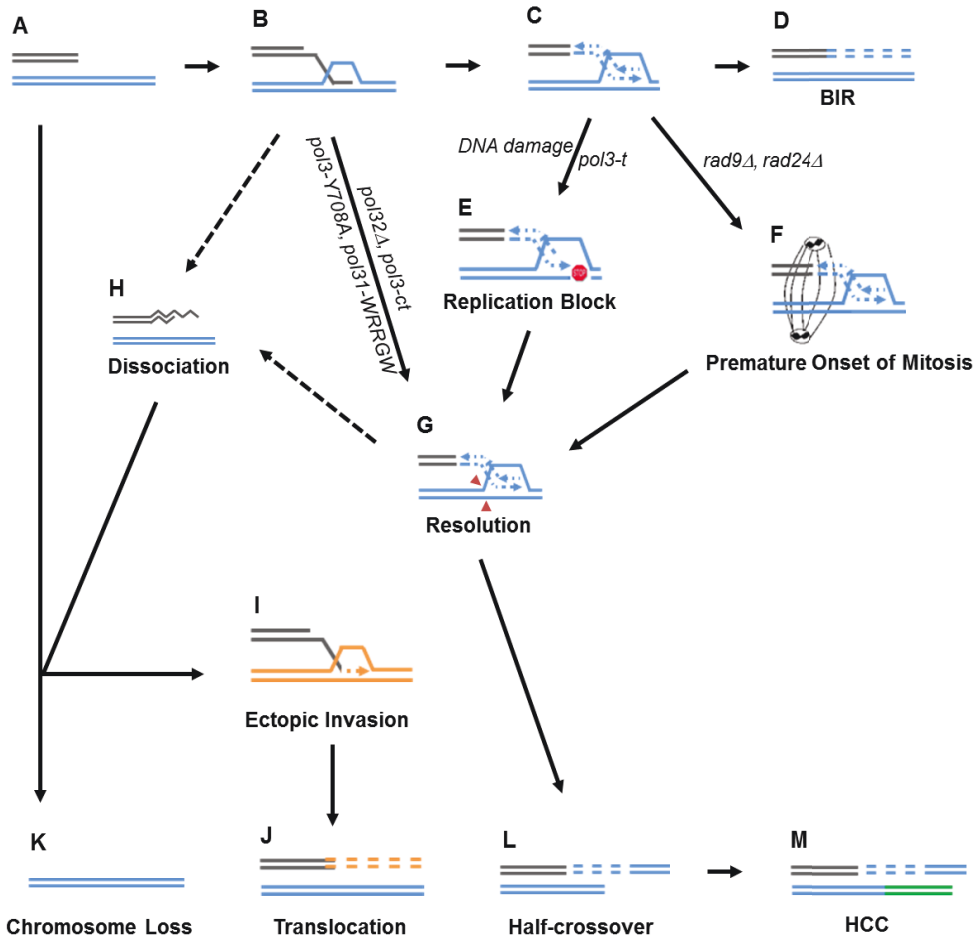

Figure 5.1. Model for BIR-induced genetic instabilities. (A) One-ended DSB. **(B)** Invasion of 3'-ssDNA end into a homologous chromosome. **(C)** Unidirectional DNA synthesis **(D)** BIR product **(E)** A pause during BIR replication (indicated by the red "stop" symbol) promotes resolution of the Holliday junction **(G)** and leads to formation of half crossovers **(L)**. **(F)** Premature onset of mitosis during BIR. **(H)** Dissociation of a newly synthesized strand from its template during BIR can lead to its invasion at ectopic position **(I)** resulting in translocation **(J)**. **(K)** Chromosome loss. **(M)** Half crossover cascade (HCC).

Similarly, results from another recent study (Marenda Wilson and Gregory Ira, personal communication) demonstrate that the deletion of *PIF1*, which encodes a DNA helicase specifically required for DNA synthesis during BIR [89], also leads to more frequent HCs. We speculate that in these mutants, DNA synthesis is successfully initiated but proceeds with frequent stops, thereby promoting HC formation. Regardless of the mechanism that leads to paused replication, these data support my hypothesis that interruptions in DNA replication during BIR induce HCs. Interestingly, some mutations affecting Polε that were investigated so far did not promote HCs; while *pol2-9* shows an increase in HCs. Although the role of Polε has not been completely understood, it was proposed that Polε showed limited participation in BIR [32]. However, only further studies can help in drawing conclusions to this theory. Curiously, the mutation in Polα (*pol1-1*) led to decreased HCs compared to wild type, which may indicate that *pol1-1* delays accumulation of BIR intermediates that are resolved to produce HCs.

It was previously demonstrated that successful completion of BIR replication requires checkpoint machinery to maintain cell cycle arrest until repair is completed [40]. Consistently, here I observed that the premature onset of mitosis in checkpoint-deficient cells undergoing BIR repair led to an increased frequency of HCs (Fig. 5.1F, 5.1L). Formation of HC molecules could result from a signal from the cell to resolve the HJ structure as previously discussed, but mechanical rupture of BIR intermediates initiated by chromosomal segregation is also a possibility. In checkpoint-deficient mutants, I also frequently observed

chromosome loss and translocations, which I propose result from strand dissociation that can be stimulated by HJ resolution (Fig. 5.1G, 5.1H). 5'-to-3' DNA resection following dissociation may lead to chromosome loss (Fig. 5.1K) or to ectopic strand invasion at positions of DNA repeats (Fig. 5.1I) resulting in translocations (Fig. 5.1J). Alternatively, elevated chromosome loss and translocations may result from increased 5'-to-3' resection of DSB ends prior to strand invasion (Fig. 5.1A, 5.1K) or following unwinding of a D-loop (Fig. 5.1B)

5.2 Half crossovers initiate cascades of genetic instability

An important outcome of this study is the discovery of HC-induced cascades (HCC). The existence of HCCs has been previously hypothesized [56], but, until now, had not been demonstrated. HCCs represent DSB repair outcomes that contain a HC product along with a rearranged donor chromosome (Fig. 5.1M). I propose that HCCs are initiated by a single HC that leads to breakage of the donor chromosome (Fig. 5.2A). The new DSB in the donor molecule undergoes 5' to 3' resection (Fig. 5.2C), and the resulting 3' DNA end invades a homologous DNA molecule at an ectopic position (Fig. 5.2E) in the newly formed HC (Fig. 5.2F), or in the sister chromatid (Fig. 5.2G). This initiates recombination and can stabilize the broken donor chromosome if repair proceeds through BIR; conversely, this intermediate may also stabilize through HC formation, thereby continuing the cascade of genetic instability.

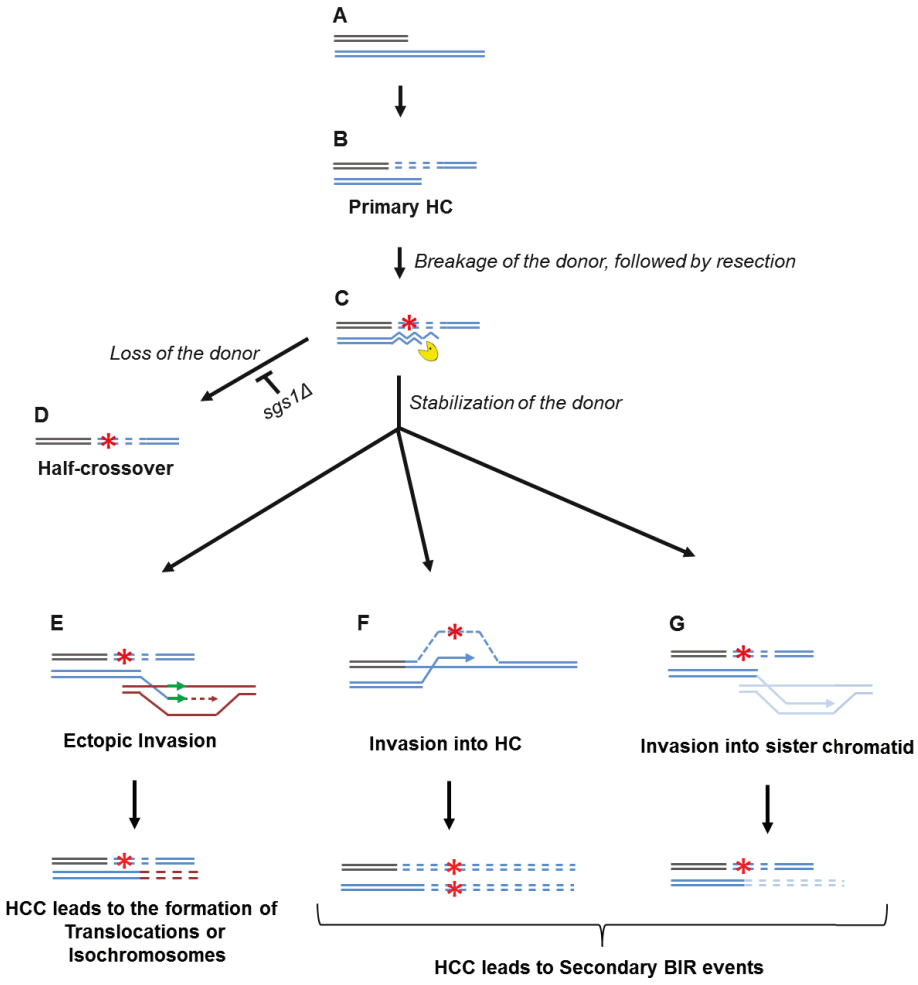

Figure 5.2. Model of half crossover cascades (HCC). (A) One-ended DSB. **(B)** Formation of half crossover (HC) leading to breakage of the donor chromosome. **(C)** Resection of the broken donor chromosome. (**D)** HC associated with the loss of a donor chromosome. **(E)** Stabilization of the donor chromosome by invasion at ectopic chromosomal location leads to formation of a translocation or of an isochromosome. **(F)** Stabilization of the donor chromosome by invasion into the initial HC followed by BIR (secondary BIR event). **(G)** Stabilization of the broken donor by strand invasion into sister chromatid followed by BIR (secondary BIR event). Red stars represent mutagenic errors during DNA synthesis leading to HC formation. Secondary BIR in **(F)** may lead to formation of homozygous mutations (see the text for details).

Even when the donor fragment successfully stabilizes through BIR, if an ectopic site such as a Ty or delta element is used for recombination, translocations will occur (Fig. 5.2E; see also Figs. 4.20-4.25).

In our system, repair of the broken donor chromosome often proceeded by BIR using the recently formed HC (Fig. 5.2F) or the sister chromatid (Fig. 5.2G) as a template. I termed these events “secondary BIR”. Among all HCC events analyzed by PFGE, approximately half showed a pattern suggestive of HCC resulting in invasion of the broken donor into the initial HC, even though only one of these cases was analyzed by array-CGH (case H9; Fig. 4.26). Additionally, 15% of the HCCs analyzed by CGH could be explained by secondary BIR associated with complex rearrangements (cases H1 and H6). It should be noted that all identified secondary BIR events were initiated by strand invasion that occurred centromere distal to FS2 which resulted in a change in the size of the donor and therefore allowed the detection of these events. It remains possible; however, that many additional secondary BIR events are initiated by strand invasion between *FS2* and *MAT*. This is expected to result in chromosome structures and phenotypes indistinguishable from classic BIR.

Therefore, I propose that the actual frequency of secondary BIR events maybe higher than currently estimated. This is significant because secondary BIR events could be more deleterious than classic BIR events. For example, I speculate that secondary BIR may result in homozygous mutations that result

when a mutation occurs during DNA synthesis associated with HC formation (Fig. 5.2F) and is then copied during the repair of the broken donor using the initial HC as a template. Homozygous mutations could be more deleterious than heterozygous ones (reported in association with classic BIR [76]) because they can lead to the manifestation of recessive phenotypes including those leading to cancer.

A significant finding was the formation of multi-sectored colonies consisting of broad genotypic variations by checkpoint-deficient mutants. More than 70% of the multi-sectored colonies contained at least one sector with chromosomal rearrangements of recipient or donor chromosomes, with HCC being a major class of these rearrangements. In addition, I observed that the efficiency of DSB end resection most likely affected the frequency of HCC events, as deletion of *SGS1*, which is known to reduce long-range DSB resection, led to a significant increase in HCC frequency in *rad9Δ* mutants. Possibly, reduced resection stabilizes the broken donor chromosome, thus giving it more chances to repair by invading a homologous template (Fig. 5.2E-G). Interestingly, in *rad24Δsgs1Δ,* the multiple sectoring of colonies was completely eliminated, and the majority of outcomes were indistinguishable from normal BIR. I propose that these events are likely to be secondary HCC resulting from secondary BIR.

In addition to being frequently observed when BIR is induced in checkpoint-defective mutants, HCCs occurred in cases of compromised BIR in polymerase-

deficient mutants (*pol3-t*) and when BIR proceeds in the presence of MMS (Cynthia Sakofsky and Anna Malkova, manuscript in preparation). HCCs were also observed in BIR-defective *pif1Δ* mutants (Marenda Wilson and Gregory Ira, personal communication). Overall, I propose that ongoing cycles of genetic instability are a ubiquitous outcome of HC formation.

5.3 HC-induced cascades: potential for promoting genetic instability in humans

We propose that HCs and HCCs may be a mechanism for genetic destabilization leading to various diseases in humans. In particular, I propose HCCs to be a mechanism capable of producing non-reciprocal translocations (NRTs) that have been described in mammalian tumor cells. NRT is a pathway of telomere acquisition by broken chromosomes that results in the donor molecule losing genetic information, including its telomere, and becoming unstable [94]. This destabilization of the donor makes NRTs especially devastating because the events are self-perpetuating and result in cascades of genomic destabilization, including chromosome loss and multiple rearrangements. I propose that the cycles of NRTs can be explained by initiation of BIR followed by its interruption leading to HCCs in tumor cells. Importantly, I suggest that initiation of HCC can be facilitated by checkpoint deficiency, which is frequent in cancer cells [107, 108]. In addition, my data suggest that cycles of HCCs could also contribute to clonal evolution leading to clonal variations in pre-cancerous cells.

5.4 Future Directions

The importance of Polε in ongoing BIR synthesis has not been completely understood, yet. From this study, it can be observed that experiments related to mutations in Polε show biased results. While mutations *pol2-Y831A* and *pol2-1* seem to have negligible effects on HC formation, *pol2-9* may seem to exacerbate the frequency of HCs. Although many experiments were conducted to analyze the frequency of HCs in *pol2-9* mutants, I have not made conclusive declarations because of the increase in HCs observed in the wild type controls. Further experiments with careful consideration of temperature conditions may help draw conclusions to my observation. In addition, conducting time-course experiments for analyzing DSB repair by BIR in different Polε mutants may aid in understanding the role Polε might be playing in ongoing BIR synthesis.

The results obtained in this study demonstrate a plausible mechanism for HCC events in *rad24Δ* cells where I show that the broken donor could be stabilized by three different mechanisms (Fig. 5.2E, F, and G). Secondary HCC resulting from secondary BIR events are shown to occur frequently in *rad24Δ.* Moreover, I propose that these events that are indistinguishable from normal BIR seem to be common in *rad24Δsgs1Δ* but this is a hypothesis and the occurrence of these events has not been proven. Further investigation involving the analysis of $Ade^{+}Leu^{-}$ events in *rad24Δsgs1Δ* by array-CGH analysis could throw more light on these secondary BIR events and also on the importance of end-resection in DSB repair.

LIST OF REFERENCES

LIST OF REFERENCES

1. McClintock B., (1941). The Stability of Broken Ends of Chromosomes in Zea Mays.Genetics, Vol. 26, No. 2. (March 1941), pp. 234-282
2. Kuzminov, A. (1995). Collapse and repair of replication forks in Escherichia coli. Mol Microbiol 16, 373-384.
3. Aguilera A., R.R., ed. (2007). Molecular Genetics of Recombination, 1st edn (Springer).
4. Clancy, S. (2008) DNA damage & repair: mechanisms for maintaining DNA integrity. Nature Education 1(1)
5. Nickoloff, J.A., Chen, E.Y., and Heffron, F. (1986). A 24-base-pair DNA sequence from the MAT locus stimulates intergenic recombination in yeast. Proceedings of the National Academy of Sciences of the United States of America 83, 7831-7835.
6. Jensen, R.E., and Herskowitz, I. (1984). Directionality and regulation of cassette substitution in yeast. Cold Spring Harb Symp Quant Biol 49, 97-104
7. Daley, J.M., Palmbos, P.L., Wu, D., and Wilson, T.E. (2005). Nonhomologous end joining in yeast. Annual Review of Genetics 39, 431-451.

8. Li Li, Carine Robert and Feyruz V. Rassool (2011). The Role of Error-Prone Alternative Non-Homologous End-Joining in Genomic Instability in Cancer, DNA Repair and Human Health, Dr. Sonya Vengrova (Ed.), ISBN: 978-953-307-612-6, InTech, DOI: 10.5772/24262.
9. Ma, J.L., Kim, E.M., Haber, J.E., and Lee, S.E. (2003). Yeast Mre11 and Rad1 proteins define a Ku-independent mechanism to repair double-strand breaks lacking overlapping end sequences. Mol Cell Biol 23, 8820-8828.
10. McVey M, Lee SE (2008) MMEJ repair of double-strand breaks (director's cut): deleted sequences and alternative endings. Trends Genet 24: 529-538.
11. Kadyk, L.C., and Hartwell, L.H. (1992). Sister Chromatids Are Preferred Over Homologs as Substrates for Recombinational Repair in Saccharomyces cerevisiae. Genetics 132, 387-402.
12. Larocque JR, Jasin M (2010) Mechanisms of recombination between diverged sequences in wild-type and BLM-deficient mouse and human cells. Mol Cell Biol 30: 1887-1897.
13. Resnick MA, Martin P (1976) The repair of double-strand breaks in the nuclear DNA of Saccharomyces cerevisiae and its genetic control. Mol Gen Genet 143: 119-129.
14. Orr-Weaver, T.L., Szostak, J.W., and Rothstein, R.J. (1981). Yeast transformation: a model system for the study of recombination. Proceedings of the National Academy of Sciences of the United States of America 78, 6354-6358.

15. Szostak, J.W., Orr-Weaver, T.L., Rothstein, R.J., and Stahl, F.W. (1983). The double-strand-break repair model for recombination. Cell 33, 25-35.
16. Paques F, Haber JE (1999) Multiple pathways of recombination induced by double-strand breaks in Saccharomyces cerevisiae. Microbiol Mol Biol Rev 63: 349-404.
17. Ira, G., Malkova, A., Liberi, G., Foiani, M., and Haber, J.E. (2003). Srs2 and Sgs1-Top3 suppress crossovers during double-strand break repair in yeast. Cell 115, 401-411.
18. Fishman-Lobell J, Haber JE (1992) Removal of nonhomologous DNA ends in double-strand break recombination: the role of the yeast ultraviolet repair gene RAD1. Science 258: 480-484.
19. Lin FL, Sperle K, Sternberg N. (1984) Model for homologous recombination during transfer of DNA into mouse L cells: role for DNA ends in the recombination process. Mol Cell Biol. 1984 Jun; 4(6):1020–1034.
20. Ivanov, E.L., and Haber, J.E. (1995). RAD1 and RAD10, but not other excision repair genes, are required for double-strand break-induced recombination in Saccharomyces cerevisiae. Mol Cell Biol 15, 2245-2251.
21. Wu, X., Wu, C., and Haber, J.E. (1997). Rules of Donor Preference in Saccharomyces Mating-Type Gene Switching Revealed by a Competition Assay Involving Two Types of Recombination. Genetics 147, 399-407.
22. Mosig, G. (1998). Recombination and recombination-dependent DNA replication in bacteriophage T4. Annual Review of Genetics 32,379-413.

23. Asai, T., Bates, D.B., and Kogoma, T. (1994). DNA replication triggered by double-stranded breaks in E. coli: Dependence on homologous recombination functions. Cell 78, 1051-1061.
24. Malkova, A., Ivanov, E.L., and Haber, J.E. (1996a). Double-strand break repair in the absence of RAD51 in yeast: a possible role for break-induced DNA replication. Proc Natl Acad Sci U S A 93, 7131-7136.
25. Bosco, G., and Haber, J.E. (1998). Chromosome break-induced DNA replication leads to nonreciprocal translocations and telomere capture. Genetics 150, 1037-1047.
26. Paques F, Haber JE (1999) Multiple pathways of recombination induced by double-strand breaks in Saccharomyces cerevisiae. Microbiol Mol Biol Rev 63: 349-404.
27. Davis, A.P., and Symington, L.S. (2004). RAD51-dependent break-induced replication in yeast. Mol Cell Biol 24, 2344-2351.
28. Lydeard JR, L.-M.Z., Sheu YJ, Stillman B, Burgers PM, Haber JE. (2010). Break-induced replication requires all essential DNA replication factors except those specific for pre-RC assembly. Genes Dev 24, 1133-1144.
29. Malkova A, Haber JE (2012) Mutations arising during repair of chromosome breaks. Annu Rev Genet 46: 455-473.
30. Dunn, B., Szauter, P., Pardue, M.L., and Szostak, J.W. (1984). Transfer of yeast telomeres to linear plasmids by recombination. Cell 39, 191-201.

31. Vollrath D, Davis RW, Connelly C, Hieter P (1988) Physical mapping of large DNA by chromosome fragmentation. Proc Natl Acad Sci U S A 85: 6027-6031.
32. Lydeard, J.R., Jain, S., Yamaguchi, M., and Haber, J.E. (2007). Break-induced replication and telomerase-independent telomere maintenance require Pol32. Nature 448, 820-823.
33. Kuzminov, A. (1999). Recombinational repair of DNA damage in Escherichia coli and bacteriophage lambda. Microbiol Mol Biol Rev 63, 751-813, table of contents.
34. Seigneur M, Bidnenko V, Ehrlich SD, Michel B (1998) RuvAB acts at arrested replication forks. Cell 95: 419-430.
35. Malkova A, Ira G (2013) Break-induced replication: functions and molecular mechanism. Curr Opin Genet Dev. 23: 271-279.
36. Jain S, Sugawara N, Lydeard J, Vaze M, Tanguy Le Gac N, et al. (2009) A recombination execution checkpoint regulates the choice of homologous recombination pathway during DNA double-strand break repair. Genes Dev 23: 291-303.
37. McMurray MA, Gottschling DE (2003) An age-induced switch to a hyper-recombinational state. Science 301: 1908-1911
38. Llorente B, Smith CE, Symington LS (2008) Break-induced replication: what is it and what is it for? Cell Cycle 7: 859-864.
39. Sakofsky CJ, Ayyar S, Malkova A (2012) Break-Induced Replication and Genome Stability. Biomolecules 2: 483-504.

40. Malkova A, Naylor ML, Yamaguchi M, Ira G, Haber JE (2005) *RAD51*-dependent break-induced replication differs in kinetics and checkpoint responses from *RAD51*-mediated gene conversion. Mol Cell Biol 25: 933-944.
41. Ira, G., Pellicioli, A., Balijja, A., Wang, X., Fiorani, S., Carotenuto, W., Liberi, G., Bressan, D., Wan, L., Hollingsworth, N.M., et al. (2004). DNA end resection, homologous recombination and DNA damage checkpoint activation require CDK1. Nature 431, 1011-1017.
42. Mimitou, E.P., and Symington, L.S. (2008). Sae2, Exo1 and Sgs1 collaborate in DNA double-strand break processing. Nature 455, 770-774.
43. Kaye, J.A., Melo, J.A., Cheung, S.K., Vaze, M.B., Haber, J.E., and Toczyski, D.P. (2004). DNA breaks promote genomic instability by impeding proper chromosome segregation. Curr Biol 14, 2096-2106.
44. Zhu, Z., Chung, W.H., Shim, E.Y., Lee, S.E., and Ira, G. (2008). Sgs1 helicase and two nucleases Dna2 and Exo1 resect DNA double-strand break ends. Cell 134, 981-994.
45. Foster SS, Balestrini A, Petrini JH (2011) Functional interplay of the Mre11 nuclease and Ku in the response to replication-associated DNA damage. Mol Cell Biol 31: 4379-4389.
46. Krogh, B.O., and Symington, L.S. (2004). Recombination proteins in yeast. Annu Rev Genet 38, 233-271.
47. Sung, P. (1997). Yeast Rad55 and Rad57 proteins form a heterodimer that functions with replication protein A to promote DNA strand exchange by Rad51 recombinase. Genes & Development 11, 1111-1121.

48. Mortensen, U.H., Bendixen, C., Sunjevaric, I., and Rothstein, R. (1996). DNA strand annealing is promoted by the yeast Rad52 protein. Proceedings of the National Academy of Sciences of the United States of America 93, 10729-10734.
49. Petukhova, G., Stratton, S., and Sung, P. (1998). Catalysis of homologous DNA pairing by yeast Rad51 and Rad54 proteins. Nature 393, 91-94.
50. Solinger, J.A., and Heyer, W.-D. (2001). Rad54 protein stimulates the postsynaptic phase of Rad51 protein-mediated DNA strand exchange. Proceedings of the National Academy of Sciences of the United States of America 98, 8447-8453.
51. Shinohara, M., Shita-Yamaguchi, E., Buerstedde, J.M., Shinagawa, H., Ogawa, H., and Shinohara, A. (1997). Characterization of the Roles of the Saccharomyces cerevisiae RAD54 Gene and a Homologue of RAD54, RDH54/TID1, in Mitosis and Meiosis. Genetics 147, 1545-1556.
52. Holmes, A.M., and Haber, J.E. (1999). Double-strand break repair in yeast requires both leading and lagging strand DNA polymerases. Cell 96, 415-424.
53. Wang, X., Ira, G., Tercero, J.A., Holmes, A.M., Diffley, J.F., and Haber, J.E. (2004). Role of DNA replication proteins in double-strand break-induced recombination in Saccharomyces cerevisiae. Mol Cell Biol 24, 6891-6899.
54. Hicks, W.M., Kim, M., and Haber, J.E. (2010). Increased Mutagenesis and Unique Mutation Signature Associated with Mitotic Gene Conversion. Science 329, 82-85.

55. Ira, G., Satory, D., and Haber, J.E. (2006). Conservative inheritance of newly synthesized DNA in double-strand break-induced gene conversion. Mol Cell Biol 26, 9424-9429.
56. Deem A, Barker K, Vanhulle K, Downing B, Vayl A, et al. (2008) Defective break-induced replication leads to half-crossovers in *Saccharomyces cerevisiae*. Genetics 179: 1845-1860.
57. Malkova, A., Signon, L., Schaefer, C.B., Naylor, M.L., Theis, J.F., Newlon, C.S., and Haber, J.E. (2001). RAD51-independent break-induced replication to repair a broken chromosome depends on a distant enhancer site. Genes Dev 15, 1055-1060.
58. Santocanale, C., and Diffley, J.F.X. (1998). A Mec1- and Rad53-dependent checkpoint controls late-firing origins of DNA replication. Nature 395, 615-618.
59. Putnam, C.D., Jaehnig, E.J., and Kolodner, R.D. (2009). Perspectives on the DNA damage and replication checkpoint responses in Saccharomyces cerevisiae. DNA Repair (Amst) 8, 974-982.
60. Tyson JJ, Csikasz-Nagy A, Novak B (2002) The dynamics of cell cycle regulation. BioEssays 24: 1095-1109.
61. Harrison, J.C., and Haber, J.E. (2006). Surviving the Breakup: The DNA Damage Checkpoint. Annual Review of Genetics 40, 209-235.

62. Paciotti, V., Clerici, M., Lucchini, G., and Longhese, M.P. (2000). The checkpoint protein Ddc2, functionally related to S. pombe Rad26, interacts with Mec1 and is regulated by Mec1-dependent phosphorylation in budding yeast. Genes & Development 14, 2046-2059.

63. Lisby, M., Barlow, J.H., Burgess, R.C., and Rothstein, R. (2004). Choreography of the DNA Damage Response: Spatiotemporal Relationships among Checkpoint and Repair Proteins. Cell 118, 699-713.

64. Melo, J.A., Cohen, J., and Toczyski, D.P. (2001). Two checkpoint complexes are independently recruited to sites of DNA damage in vivo. Genes & Development 15, 2809-2821.

65. Smith CE, Lam AF, Symington LS (2009) Aberrant double-strand break repair resulting in half crossovers in mutants defective for Rad51 or the DNA polymerase delta complex. Mol Cell Biol 29: 1432-1441.

66. Sun, Z., Hsiao, J., Fay, D.S., and Stern, D.F. (1998). Rad53 FHA Domain Associated with Phosphorylated Rad9 in the DNA Damage Checkpoint. Science 281, 272-274.

67. Agarwal, R., Tang, Z., Yu, H., and Cohen-Fix, O. (2003). Two Distinct Pathways for Inhibiting Pds1 Ubiquitination in Response to DNA Damage. Journal of Biological Chemistry 278, 45027-45033.

68. Chen, S.-h., Smolka, M.B., and Zhou, H. (2007). Mechanism of Dun1 Activation by Rad53 Phosphorylation in Saccharomyces cerevisiae. Journal of Biological Chemistry 282, 986-995.

69. Hebert ML, Wells RD (2005) Roles of double-strand breaks, nicks, and gaps in stimulating deletions of CTG.CAG repeats by intramolecular DNA repair. J Mol Biol 353: 961-979.
70. Manthey GM, Bailis AM (2010) Rad51 inhibits translocation formation by non-conservative homologous recombination in Saccharomyces cerevisiae. PLoS One 5: e11889.
71. Symington LS, Gautier J (2011) Double-strand break end resection and repair pathway choice. Annu Rev Genet 45: 247-271.
72. Hackett JA, Greider CW (2003) End resection initiates genomic instability in the absence of telomerase. Mol Cell Biol 23: 8450-8461.
73. Moore JK, Haber JE (1996) Cell cycle and genetic requirements of two pathways of nonhomologous end-joining repair of double-strand breaks in Saccharomyces cerevisiae. Mol Cell Biol 16: 2164-2173.
74. Bosco G, Haber JE (1998) Chromosome break-induced DNA replication leads to nonreciprocal translocations and telomere capture. Genetics 150: 1037-1047.
75. Chan JE, Kolodner RD (2011) A genetic and structural study of genome rearrangements mediated by high copy repeat Ty1 elements. PLoS Genet 7: e1002089.
76. Deem A, Keszthelyi A, Blackgrove T, Vayl A, Coffey B, et al. (2011) Break-induced replication is highly inaccurate. PLoS Biol 9: e1000594.

77. Hoang ML, Tan FJ, Lai DC, Celniker SE, Hoskins RA, et al. (2010) Competitive repair by naturally dispersed repetitive DNA during non-allelic homologous recombination. PLoS Genet 6: e1001228.
78. Morrow DM, Connelly C, Hieter P (1997) "Break copy" duplication: a model for chromosome fragment formation in *Saccharomyces cerevisiae*. Genetics 147: 371-382.
79. Vanhulle K, Lemoine FJ, Narayanan V, Downing B, Hull K, et al. (2007) Inverted DNA repeats channel repair of distant double-strand breaks into chromatid fusions and chromosomal rearrangements. Mol Cell Biol 27: 2601-2614.
80. Pardo B, Aguilera A (2012) Complex chromosomal rearrangements mediated by break-induced replication involve structure-selective endonucleases. PLoS Genet 8: e1002979.
81. Hastings PJ, Ira G, Lupski JR (2009) A microhomology-mediated break-induced replication model for the origin of human copy number variation. PLoS Genet 5: e1000327.
82. Hastings PJ, Lupski JR, Rosenberg SM, Ira G (2009) Mechanisms of change in gene copy number. Nat Rev Genet 10: 551-564.
83. Payen C, Koszul R, Dujon B, Fischer G (2008) Segmental duplications arise from Pol32-dependent repair of broken forks through two alternative replication-based mechanisms. PLoS Genet 4: e1000175.

84. Haber JE, Hearn M (1985) Rad52-independent mitotic gene conversion in *Saccharomyces cerevisiae* frequently results in chromosomal loss. Genetics 111: 7-22.

85. Coic E, Feldman T, Landman AS, Haber JE (2008) Mechanisms of Rad52-independent spontaneous and UV-induced mitotic recombination in *Saccharomyces cerevisiae.* Genetics 179: 199-211.

86. Malkova A, Ivanov EL, Haber JE (1996) Double-strand break repair in the absence of *RAD51* in yeast: a possible role for break-induced DNA replication. Proc Natl Acad Sci U S A 93: 7131-7136.

87. Argueso JL, Westmoreland J, Mieczkowski PA, Gawel M, Petes TD, et al. (2008) Double-strand breaks associated with repetitive DNA can reshape the genome. Proc Natl Acad Sci U S A 105: 11845-11850.

88. Wach, A., Brachat, A., Pohlmann, R., and Philippsen, P. (1994). New heterologous modules for classical or PCR-based gene disruptions in Saccharomyces cerevisiae. Yeast 10, 1793-1808.

89. Chung, W.H., Zhu, Z., Papusha, A., Malkova, A., and Ira, G. (2010). Defective resection at DNA double-strand breaks leads to de novo telomere formation and enhances gene targeting. PLoS Genet 6, e1000948.

90. Guthrie, C., and Fink, G.R. (1991). Guide to Yeast Genetics and Molecular Biology. (San Diego: Academic Press).

91. Joseph Sambrook and David W. Russell. Cold Spring Harb Protoc 2006; doi:10.1101/pdb.prot3235

92. Paulovich, A.G., and Hartwell, L.H. (1995). A checkpoint regulates the rate of progression through S phase in S. cerevisiae in Response to DNA damage. Cell 82, 841-847.

93. Zhang H, Zeidler AF, Song W, Puccia CM, Malc E, et al. (2013) Gene copy-number variation in haploid and diploid strains of the yeast Saccharomyces cerevisiae. Genetics 193: 785-801.

94. Sabatier L, Ricoul M, Pottier G, Murnane JP (2005) The loss of a single telomere can result in instability of multiple chromosomes in a human tumor cell line. Mol Cancer Res 3: 139-150.

95. Pavlov YI, Shcherbakova PV, Kunkel TA (2001) *In vivo* consequences of putative active site mutations in yeast DNA polymerases alpha, epsilon, delta, and zeta. Genetics 159: 47-64.

96. Baranovskiy AG, Babayeva ND, Liston VG, Rogozin IB, Koonin EV, et al. (2008) X-ray structure of the complex of regulatory subunits of human DNA polymerase delta. Cell Cycle 7: 3026-3036.

97. Gordenin DA, Malkova AL, Peterzen A, Kulikov VN, Pavlov YI, et al. (1992) Transposon Tn5 excision in yeast: influence of DNA polymerases alpha, delta, and epsilon and repair genes. Proc Natl Acad Sci U S A 89: 3785-3789.

98. Kokoska RJ, Stefanovic L, Tran HT, Resnick MA, Gordenin DA, et al. (1998) Destabilization of yeast micro- and minisatellite DNA sequences by mutations affecting a nuclease involved in Okazaki fragment processing (rad27) and DNA polymerase delta (*pol3-t*). Mol Cell Biol 18: 2779-2788.

99. Morrison A, Araki H, Clark AB, Hamatake RK, Sugino A (1990) A third essential DNA polymerase in *S. cerevisiae.* Cell 62: 1143-1151.

100. Pizzagalli A, Valsasnini P, Plevani P, Lucchini G (1988) DNA polymerase I gene of *Saccharomyces cerevisiae*: nucleotide sequence, mapping of a temperature-sensitive mutation, and protein homology with other DNA polymerases. Proc Natl Acad Sci U S A 85: 3772-3776.

101. Downing B, Morgan R, VanHulle K, Deem A, Malkova A (2008) Large inverted repeats in the vicinity of a single double-strand break strongly affect repair in yeast diploids lacking Rad51. Mutat Res 645: 9-18.

102. Lemoine FJ, Degtyareva NP, Lobachev K, Petes TD (2005) Chromosomal translocations in yeast induced by low levels of DNA polymerase a model for chromosome fragile sites. Cell 120: 587-598.

103. San Filippo J, Sung P, Klein H (2008) Mechanism of eukaryotic homologous recombination. Annual review of biochemistry 77: 229-257.

104. Lazzaro F, Sapountzi V, Granata M, Pellicioli A, Vaze M, et al. (2008) Histone methyltransferase Dot1 and Rad9 inhibit single-stranded DNA accumulation at DSBs and uncapped telomeres. EMBO J 27: 1502-1512.

105. Chen X, Cui D, Papusha A, Zhang X, Chu CD, et al. (2012) The Fun30 nucleosome remodeller promotes resection of DNA double-strand break ends. Nature 489: 576-580.

106. Gravel S, Chapman JR, Magill C, Jackson SP (2008) DNA helicases Sgs1 and BLM promote DNA double-strand break resection. Genes Dev 22: 2767-2772.

107. Negrini S, Gorgoulis VG, Halazonetis TD (2010) Genomic instability--an evolving hallmark of cancer. Nature reviews Molecular cell biology 11: 220-228.

108. Halazonetis TD, Gorgoulis VG, Bartek J (2008) An oncogene-induced DNA damage model for cancer development. Science 319: 1352-1355.

APPENDICES

Appendix A Sectoring of colonies in checkpoint-deficient mutants

Sectoring of colonies was observed in the checkpoint-deficient mutants *rad24Δ* and *rad9Δ* when compared to the wild type which can be observed as on the Ade d/o replica-plate (Figures A 1 - A 3).

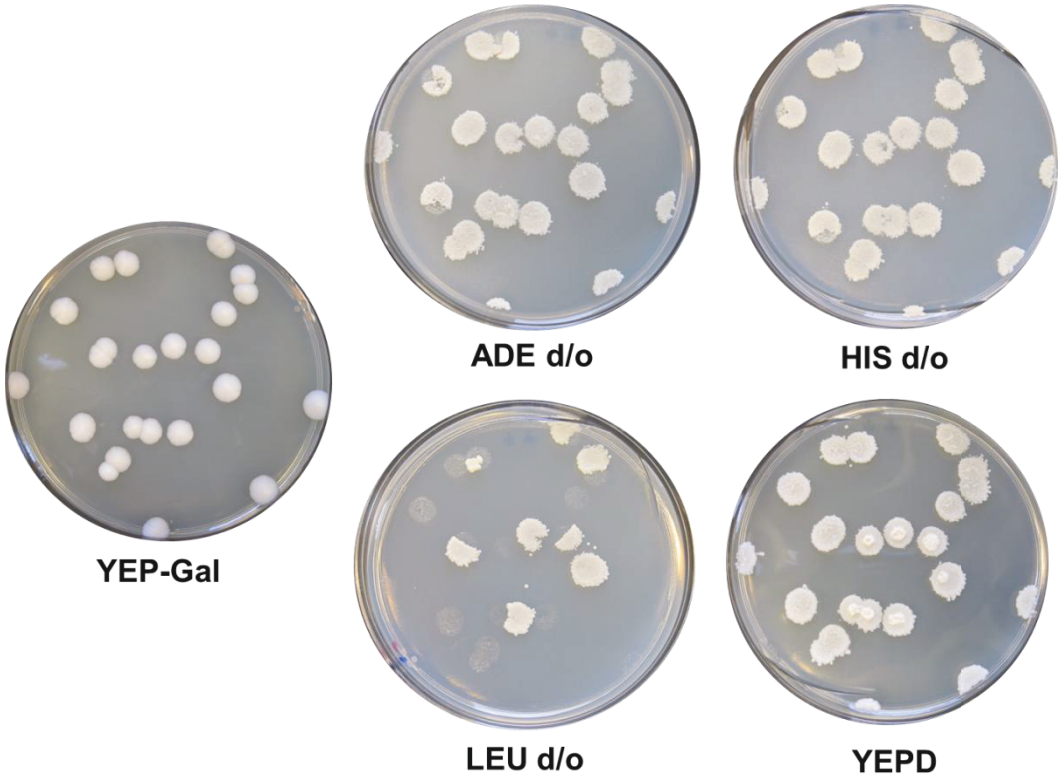

Figure A 1. Simple colonies in the wild type. Colonies grown on YEP-GAL replica-plated onto different drop-out media (Ade d/o, His d/o and Leu d/o help determine the repair outcomes obtained after DSB induction. Refer to Section 4.3 and Figure 4.5 for related information.

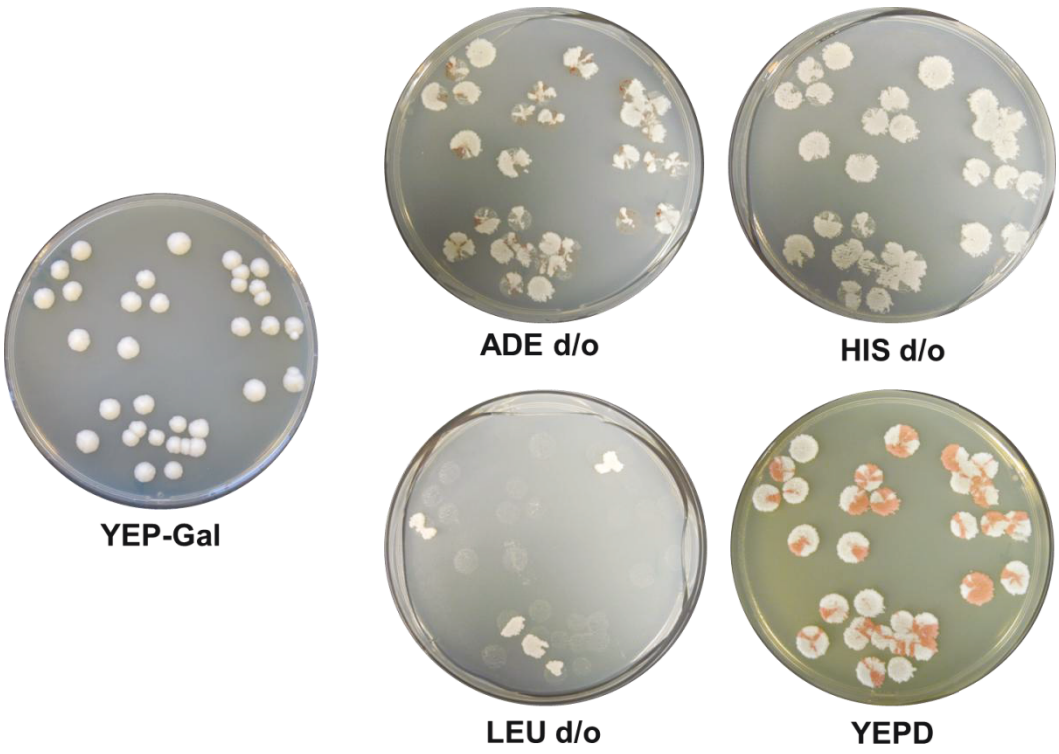

Figure A 2. Sectored colonies in *rad24Δ*. Colonies grown on YEP-GAL replica-plated onto different drop-out media (Ade d/o, His d/o and Leu d/o help determine the repair outcomes in the sectors obtained after DSB induction. Refer to Section 4.3 and Figure 4.5 for related information.

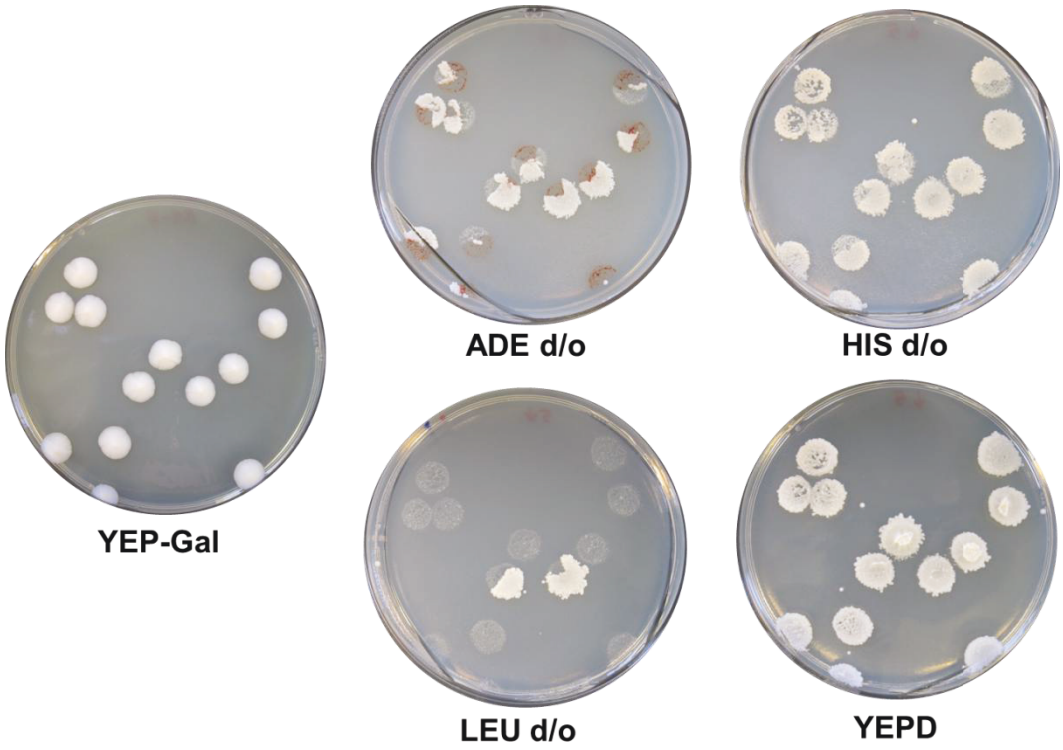

Figure A 3. Sectored colonies in *rad9Δ*. Colonies grown on YEP-GAL replica-plated onto different drop-out media (Ade d/o, His d/o and Leu d/o help determine the repair outcomes in the sectors obtained after DSB induction. Refer to Section 4.3 and Figure 4.5 for related information.

Appendix B Analysis of individual colonies in checkpoint-deficient mutants

The following pictures of individual colonies and sectors from the checkpoint-deficient mutants *rad24Δ* and *rad9Δ* are examples of colonies considered for this analysis elaborated in section 4.6.1 and tables 4.1 and 4.2.

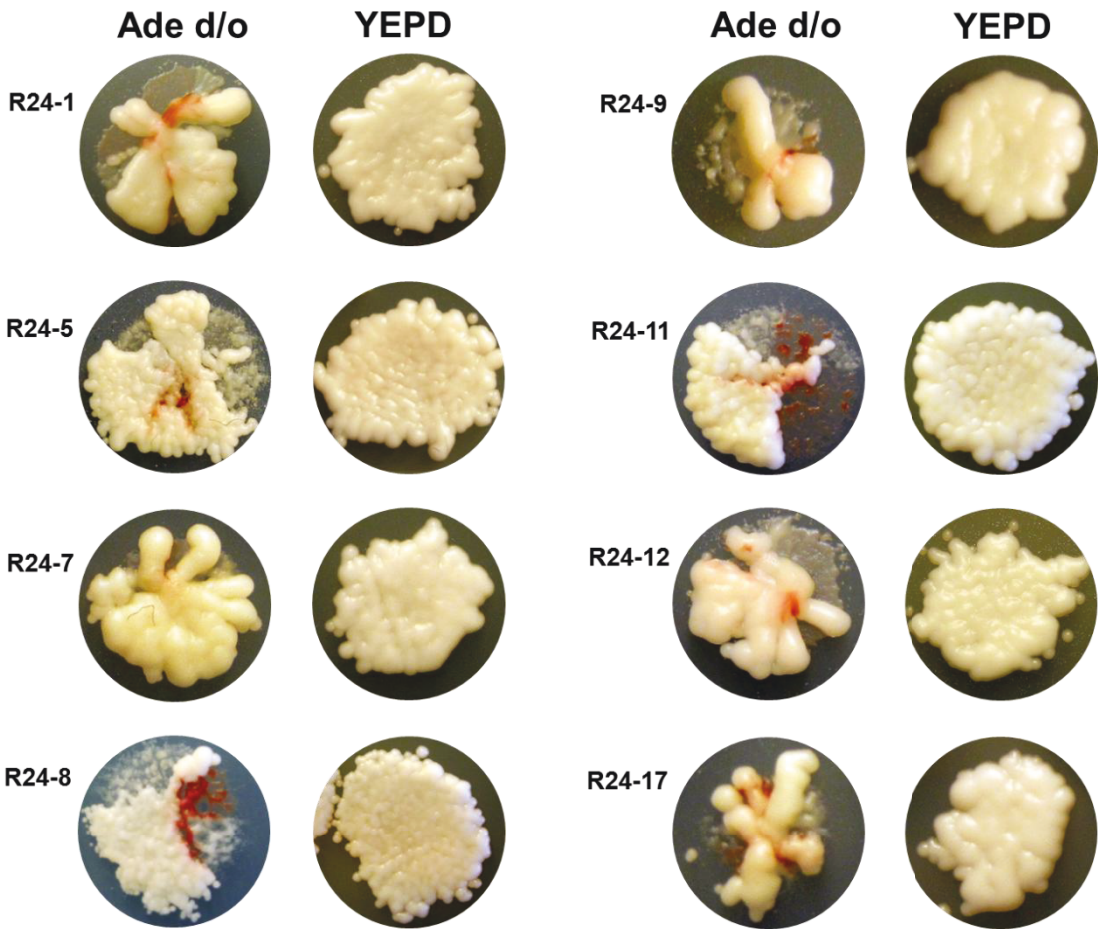

Figure A 4. Analysis of individual colonies in *rad24Δ*. Some of the colonies considered for analysis of repair outcomes in individual colonies and sectors are shown here. Cells from HC and CL sectors were streaked from corresponding cells growing on YEPD. The names of sectors correspond to the names in Table 4.1. Also refer to section 4.6.1 for more information.

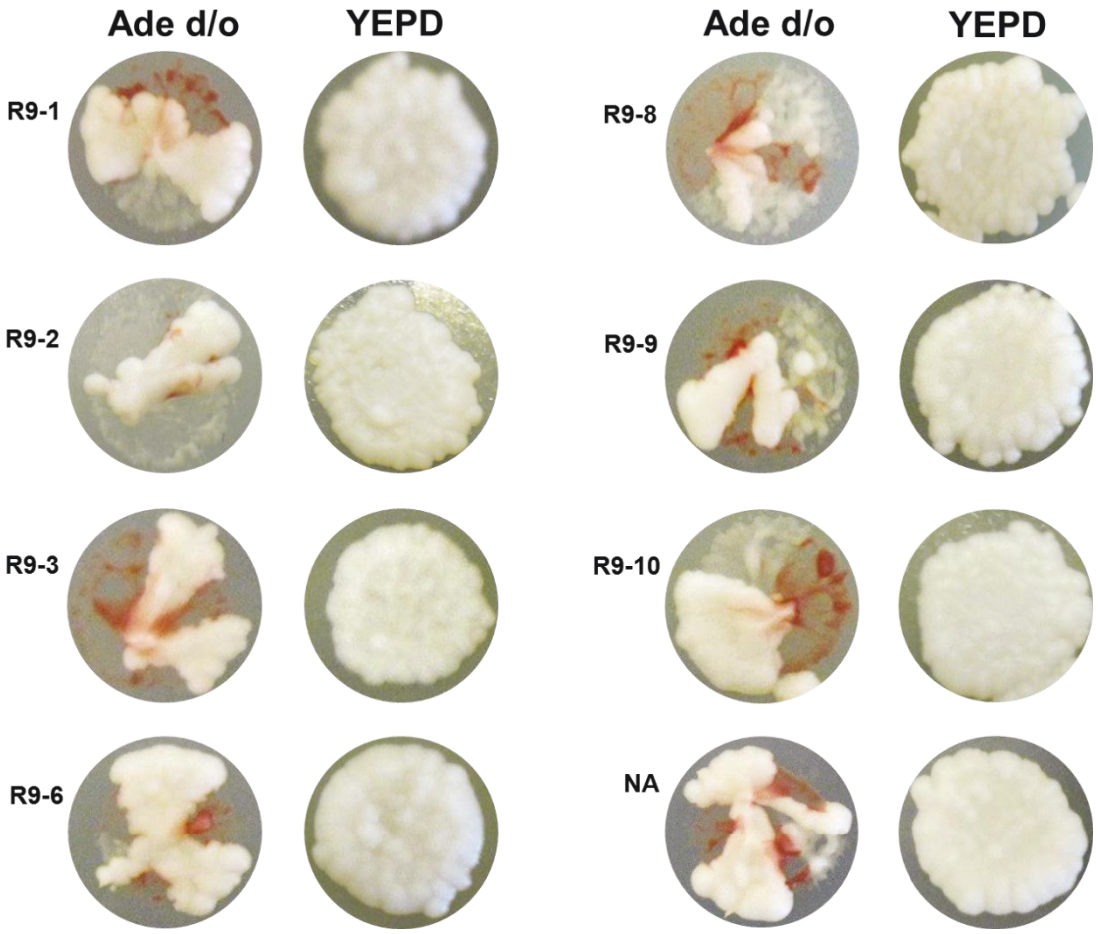

Figure A 5. Analysis of individual colonies in *rad9Δ*. Some of the colonies considered for analysis of repair outcomes in individual colonies and sectors are shown here. Cells from HC and CL sectors were streaked from corresponding cells growing on YEPD. The names of sectors correspond to the names in Table 4.2. Also refer to section 4.6.1 for more information. NA refers to an example colony that was not analyzed.

Appendix C Array-CGH analysis of HCC events from *rad24Δ* cells

Detailed information of all the breakpoints and coordinates as analyzed by array-CGH with CNV regions identified using GenePix 6.0 and Nexus Copy Number software is provided in the following table and pictures for all the samples described in Table 4.4.

Table A 1. Copy Number Variation software calls

Sample	Chromosome Region	Software Call	Length	Probes in region	Probe Median LOG2 R/G
H1	chr5:513,803-518,112	CN Loss	4310	6	-0.394
H1	chr7:1,064,194-1,068,582	High Copy Gain	4389	5	0.612
H1	chr7:1,071,688-1,074,109	CN Loss	2422	3	-0.433
H1	chr7:1,074,109-1,090,944	CN Gain	16836	6	0.254
H1	chr8:212,322-213,069	CN Gain	748	11	0.490
H1	chr11:359,057-362,961	CN Loss	3905	5	-0.447
H1	chr16:858,918-865,189	CN Loss	6272	8	-0.351
H1	chr2:801,392-813,136	High Copy Gain	11745	5	0.819
H1	chr3:131,046-150,235	CN Gain	19190	24	0.239
H1	chr3:150,235-169,419	High Copy Gain	19185	24	1.506
H1	chr3:200,142-308,302	High Copy Gain	108161	139	1.079
H2	chr14:0-784,328	High Copy Gain	784329	965	0.751
H2	chr1:81,319-92,323	CN Loss	11005	15	-0.395
H2	chr3:0-83,917	CN Gain	83918	98	0.525
H2	chr3:169,419-200,142	CN Loss	30724	38	-0.885
H3	chr5:126,914-136,512	CN Loss	9599	12	-0.289
H3	chr5:436,156-576,869	High Copy Gain	140714	156	1.042
H3	chr8:212,322-213,069	CN Gain	748	11	0.447
H3	chr11:359,057-363,651	CN Loss	4595	6	-0.408
H3	chr16:858,918-865,189	CN Loss	6272	8	-0.347
H3	chr16:939,166-948,060	CN Loss	8895	5	-0.280
H3	chr1:65,159-68,606	CN Loss	3448	5	-0.501
H3	chr3:150,235-170,245	CN Loss	20011	25	-0.962
H3	chr3:170,245-183,967	Homozygous Copy Loss	13723	17	-1.067
H3	chr3:183,967-200,142	CN Loss	16176	20	-0.891
H4	chr7:905,421-908,521	High Copy Gain	3101	4	1.249
H4	chr8:212,419-213,069	CN Gain	651	10	0.481
H4	chr16:858,918-864,578	CN Loss	5661	7	-0.355
H4	chr3:0-17,692	CN Gain	17693	12	0.390

Table A 1. Copy Number Variation software calls (continued)

H4	chr3:17,692-83,110	High Copy Gain	65419	85	0.725
H4	chr3:169,419-175,346	CN Loss	5928	8	-0.914
H4	chr3:175,346-183,967	Homozygous Copy Loss	8622	10	-1.089
H4	chr3:183,967-202,102	CN Loss	18136	21	-0.867
H5	chr3:0-83,110	CN Gain	83111	97	0.477
H5	chr3:169,419-200,142	CN Loss	30724	38	-0.848
H6	chr3:145,816-168,576	High Copy Gain	22761	27	0.845
H6	chr3:200,142-306,694	High Copy Gain	106553	137	0.952
H7	chr8:0-13,097	CN Loss	13098	3	-0.604
H7	chr8:212,322-213,069	CN Gain	748	11	0.468
H7	chr11:359,057-362,961	CN Loss	3905	5	-0.506
H7	chr16:858,918-864,578	CN Loss	5661	7	-0.384
H7	chr3:0-12,384	CN Gain	12385	9	0.540
H7	chr3:12,384-83,110	High Copy Gain	70727	88	0.799
H7	chr3:150,235-175,346	CN Loss	25112	32	-0.968
H7	chr3:175,346-183,967	Homozygous Copy Loss	8622	10	-1.123
H7	chr3:183,967-200,142	CN Loss	16176	20	-0.911
H8	chr7:905,421-908,521	High Copy Gain	3101	4	1.169
H8	chr8:212,419-212,679	High Copy Gain	261	4	0.973
H8	chr16:858,918-864,578	CN Loss	5661	7	-0.345
H8	chr3:0-17,692	CN Gain	17693	12	0.374
H8	chr3:17,692-83,110	High Copy Gain	65419	85	0.762
H8	chr3:150,235-185,269	Homozygous Copy Loss	35035	44	-1.013
H8	chr3:185,269-202,102	CN Loss	16834	19	-0.891
H9	chr7:1,064,194-1,068,582	CN Gain	4389	5	0.599
H9	chr8:212,419-213,069	CN Gain	651	10	0.436
H9	chr16:858,918-864,578	CN Loss	5661	7	-0.382
H9	chr16:939,166-948,060	CN Loss	8895	5	-0.336
H9	chr2:801,392-813,136	High Copy Gain	11745	5	0.945
H9	chr3:200,142-308,302	High Copy Gain	108161	139	1.075
H10	chr7:905,421-908,521	High Copy Gain	3101	4	1.221
H10	chr8:212,419-212,679	High Copy Gain	261	4	1.190

Table A 1. Copy Number Variation software calls (continued)

H10	chr16:858,918-864,578	CN Loss	5661	7	-0.502
H10	chr16:939,166-948,060	CN Loss	8895	5	-0.296
H10	chr3:0-17,692	CN Gain	17693	12	0.387
H10	chr3:17,692-83,110	High Copy Gain	65419	85	0.868
H10	chr3:124,250-170,245	CN Loss	45996	58	-0.910
H10	chr3:170,245-185,269	Homozygous Copy Loss	15025	19	-1.028
H10	chr3:185,269-200,142	CN Loss	14874	18	-0.892
H11	chr7:905,421-908,521	High Copy Gain	3101	4	1.265
H11	chr8:0-13,097	CN Loss	13098	4	-0.971
H11	chr8:212,419-212,679	High Copy Gain	261	4	1.158
H11	chr16:858,918-864,578	CN Loss	5661	7	-0.455
H11	chr16:939,166-948,060	CN Loss	8895	5	-0.315
H11	chr3:0-17,692	CN Gain	17693	12	0.382
H11	chr3:17,692-83,110	High Copy Gain	65419	85	0.815
H11	chr3:124,250-175,346	CN Loss	51097	65	-0.917
H11	chr3:175,346-185,269	Homozygous Copy Loss	9924	12	-1.110
H11	chr3:185,269-202,102	CN Loss	16834	19	-0.845
H12	chr3:0-83,110	CN Gain	83111	97	0.552
H12	chr3:124,250-200,142	CN Loss	75893	95	-0.921
H13	chr7:0-6,839	Homozygous Copy Loss	6840	3	-1.321
H13	chr10:0-25,679	Homozygous Copy Loss	25680	4	-1.020
H13	chr3:18,553-83,110	High Copy Gain	64558	84	0.620
H13	chr3:124,250-157,453	CN Loss	33204	43	-0.901
H13	chr3:157,453-167,850	Homozygous Copy Loss	10398	13	-1.288
H13	chr3:167,850-202,102	CN Loss	34253	41	-0.840

H1

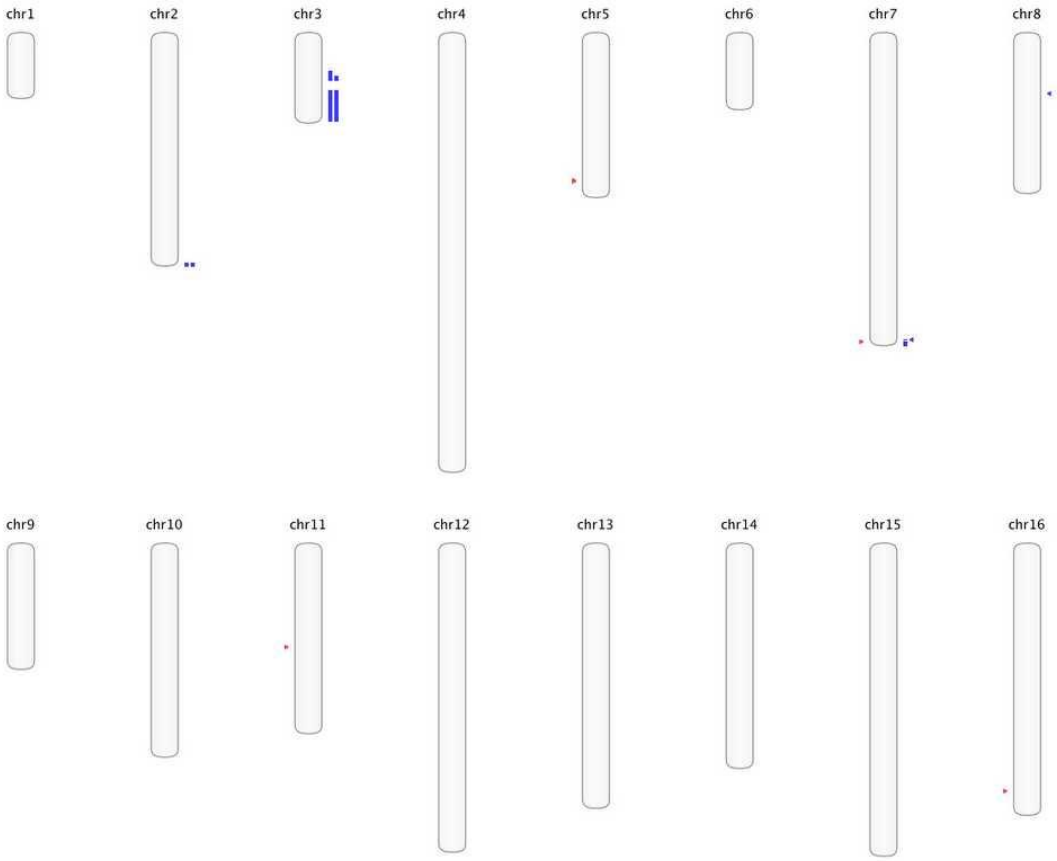

Figure A 6. H1 overview. Array-CGH overview for H1 showing small CNVs in all chromosomes where blue specks on the right side of the chromosome represent copy number gains and red specks on the left side of the chromosome represent copy number losses.

H1

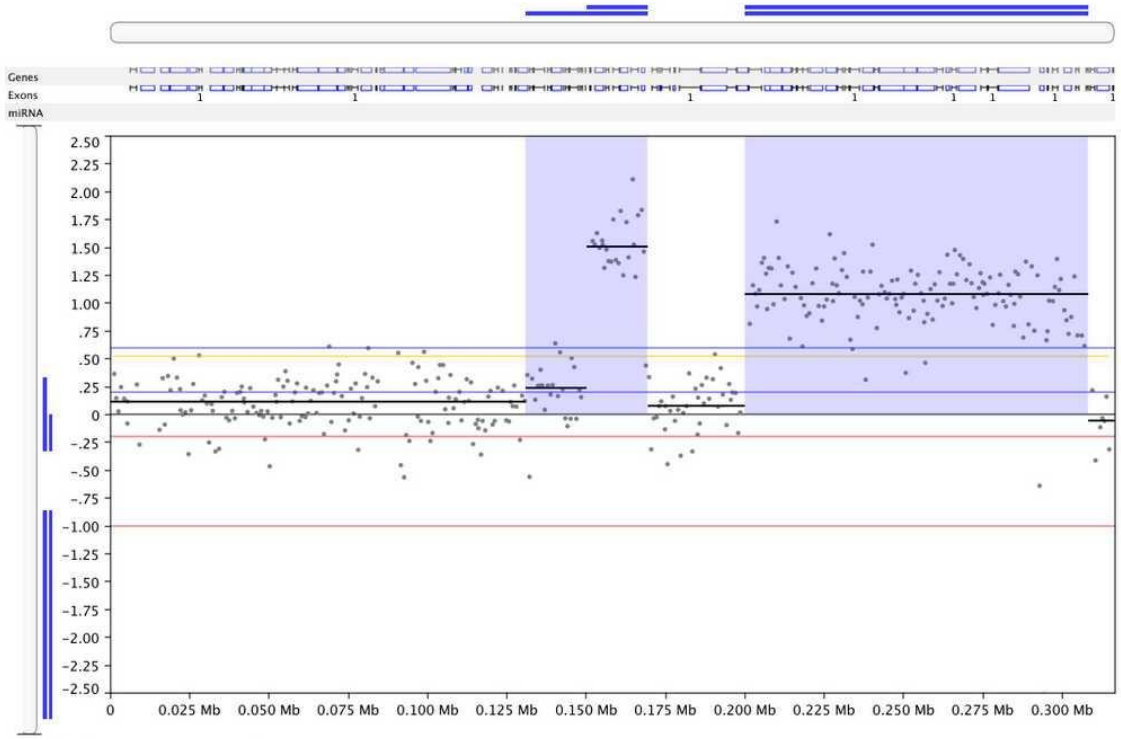

Figure A 7. Chromosome III in H1. Array-CGH profile of Chromosome III in H1 showing copy number gains (blue) with respect to LOG2 ratio for all probes in the region.

H2

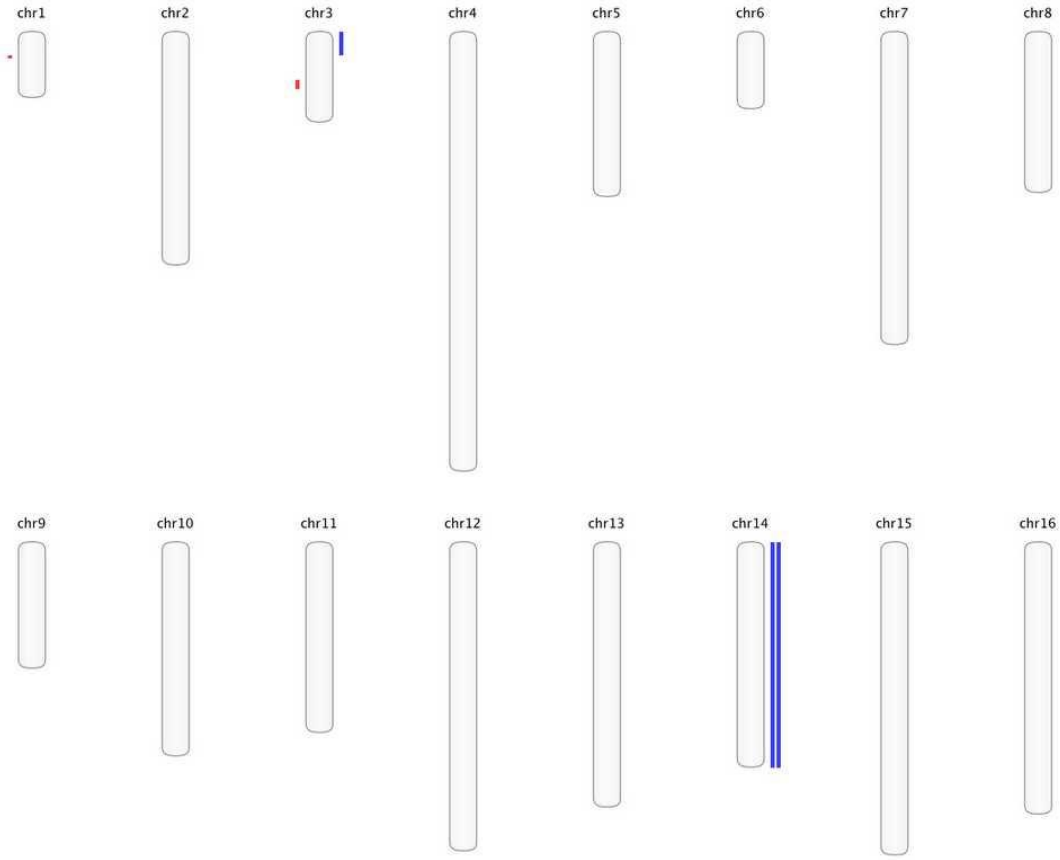

Figure A 8. H2 overview. Array-CGH overview for H2 showing small CNVs in all chromosomes where blue specks on the right side of the chromosome represent copy number gains and red specks on the left side of the chromosome represent copy number losses.

H2

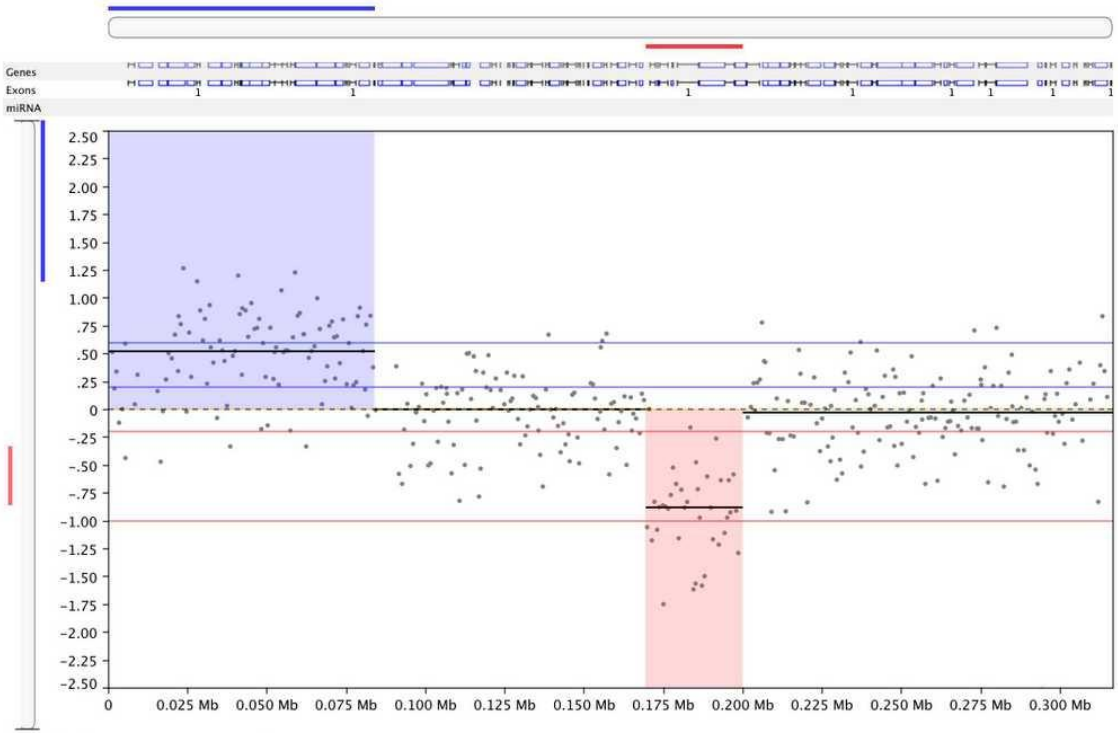

Figure A 9. Chromosome III in H2. Array-CGH profile of Chromosome III in H2 showing copy number gains (blue) and copy number losses (red) with respect to LOG2 ratio for all probes in the region.

H3

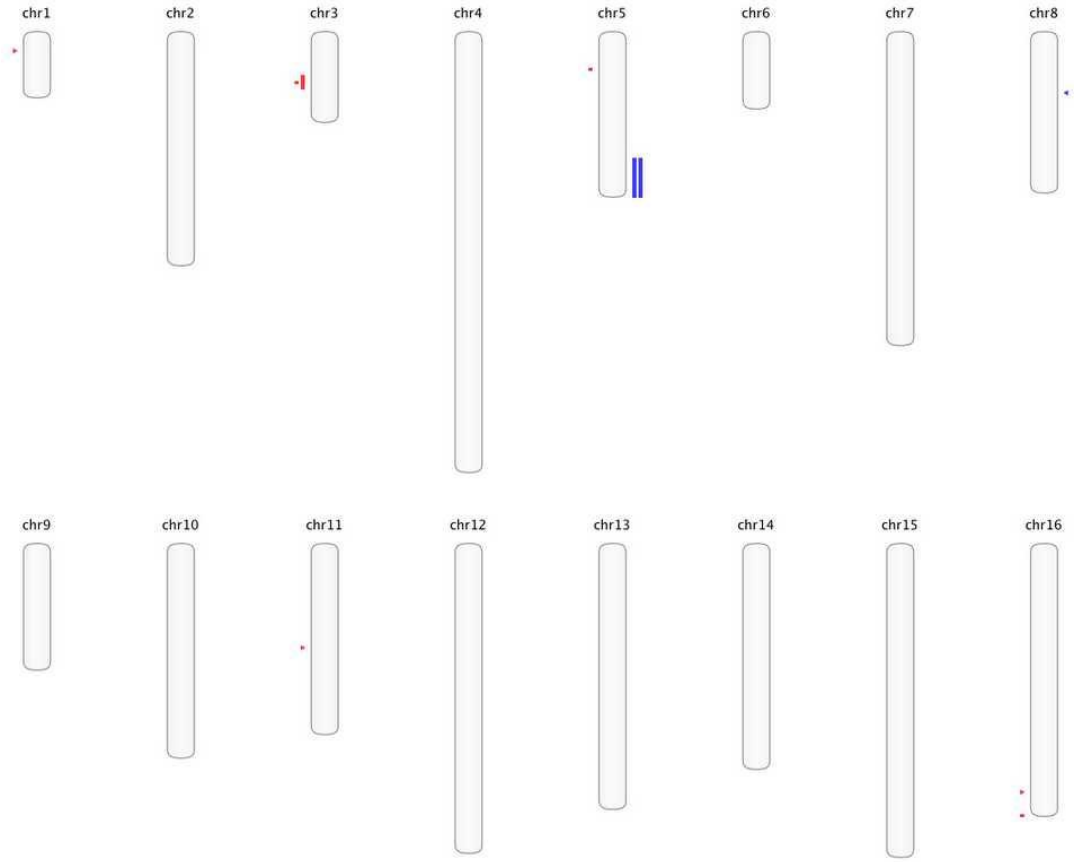

Figure A 10. H3 overview. Array-CGH overview for H3 showing small CNVs in all chromosomes where blue specks on the right side of the chromosome represent copy number gains and red specks on the left side of the chromosome represent copy number losses.

H3

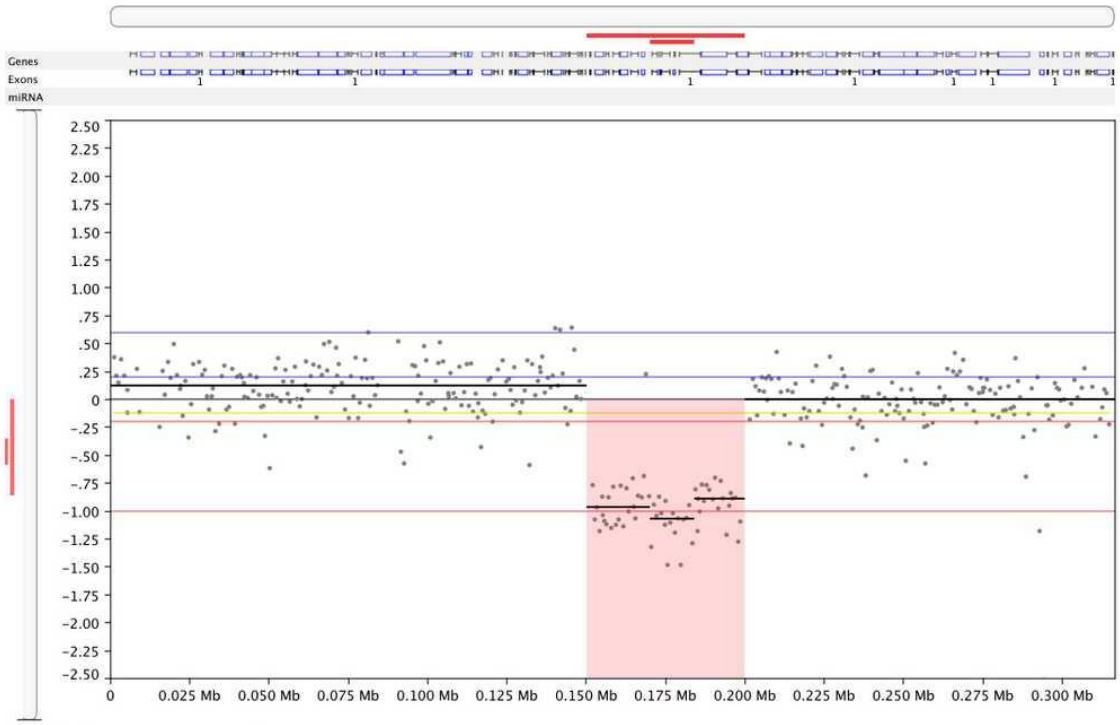

Figure A 11. Chromosome III in H3. Array-CGH profile of Chromosome III in H3 showing a copy number loss (red) with respect to LOG2 ratio for all probes in the region.

H3

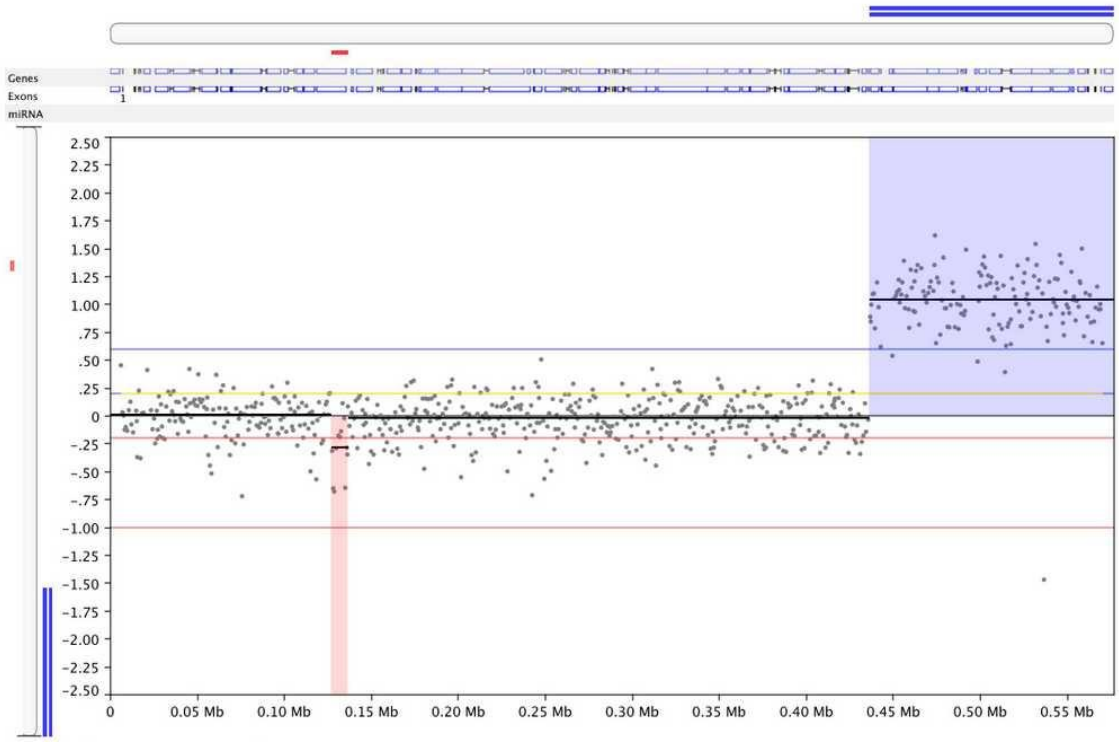

Figure A 12. Chromosome V in H3. Array-CGH profile of Chromosome V in H3 showing copy number gains (blue) and copy number losses (red) with respect to LOG2 ratio for all probes in the region.

H4

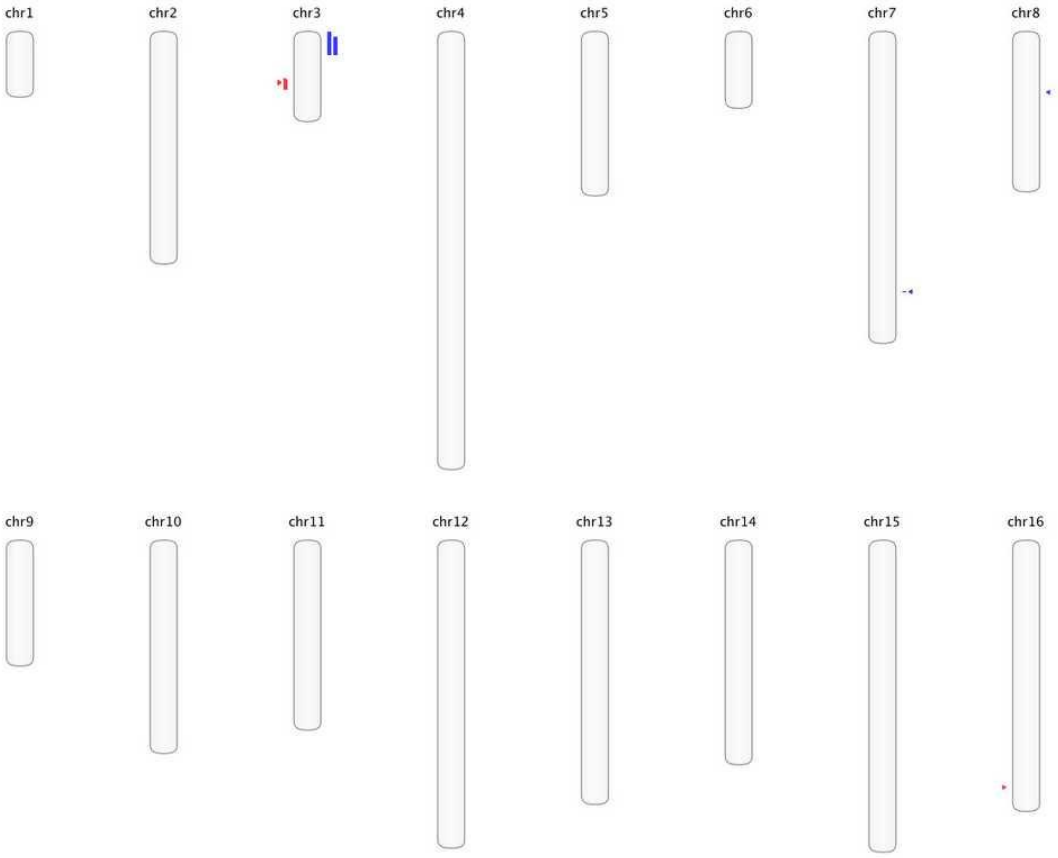

Figure A 13. H4 overview. Array-CGH overview for H4 showing small CNVs in all chromosomes where blue specks on the right side of the chromosome represent copy number gains and red specks on the left side of the chromosome represent copy number losses.

H4

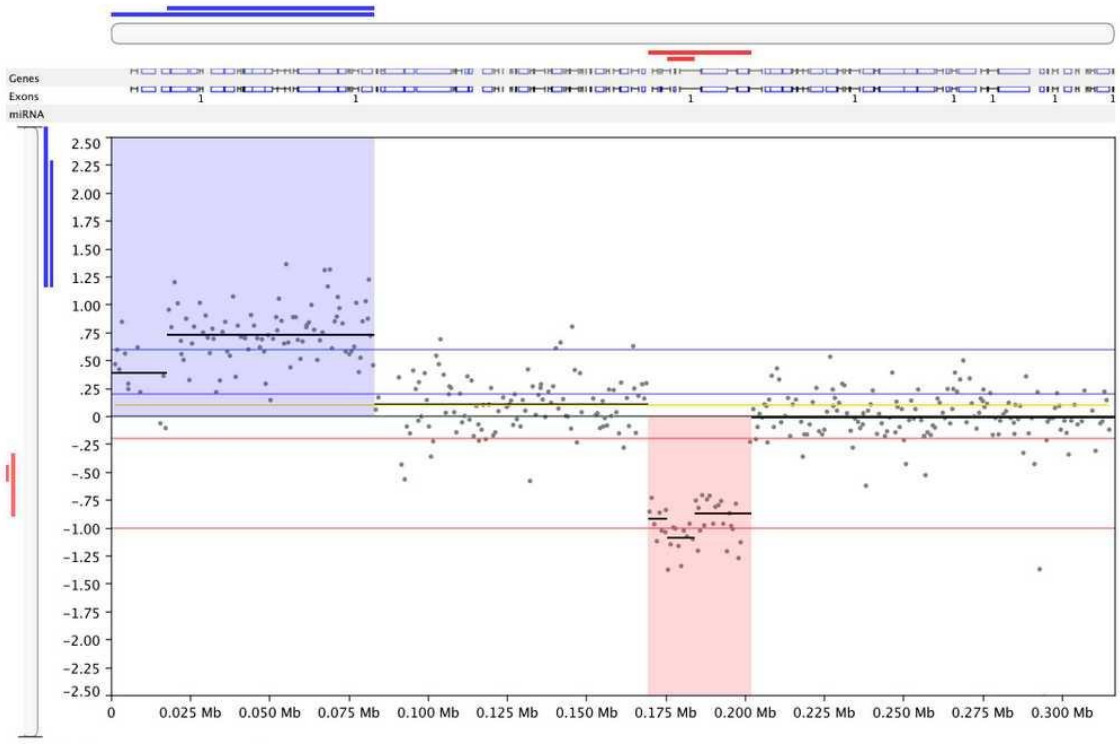

Figure A 14. Chromosome III in H4. Array-CGH profile of Chromosome III in H4 showing copy number gains (blue) and copy number losses (red) with respect to LOG2 ratio for all probes in the region.

H5

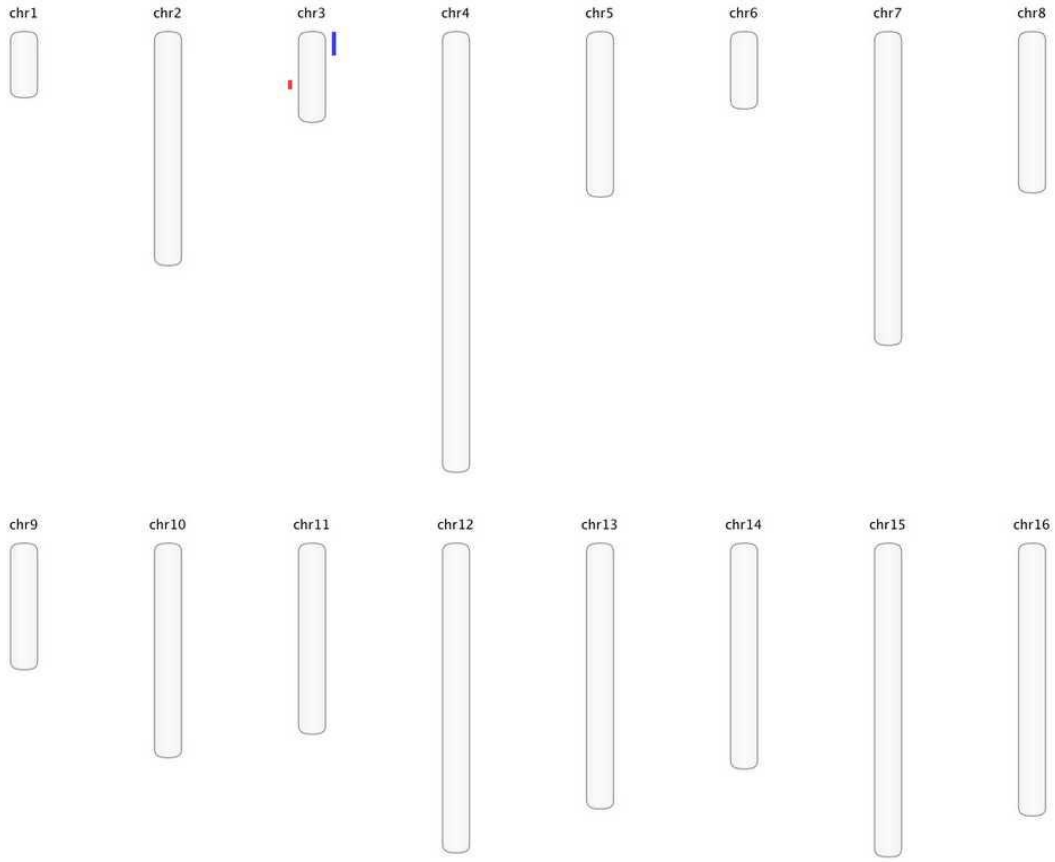

Figure A 15. H5 overview. Array-CGH overview for H5 showing small CNVs in all chromosomes where blue specks on the right side of the chromosome represent copy number gains and red specks on the left side of the chromosome represent copy number losses.

H5

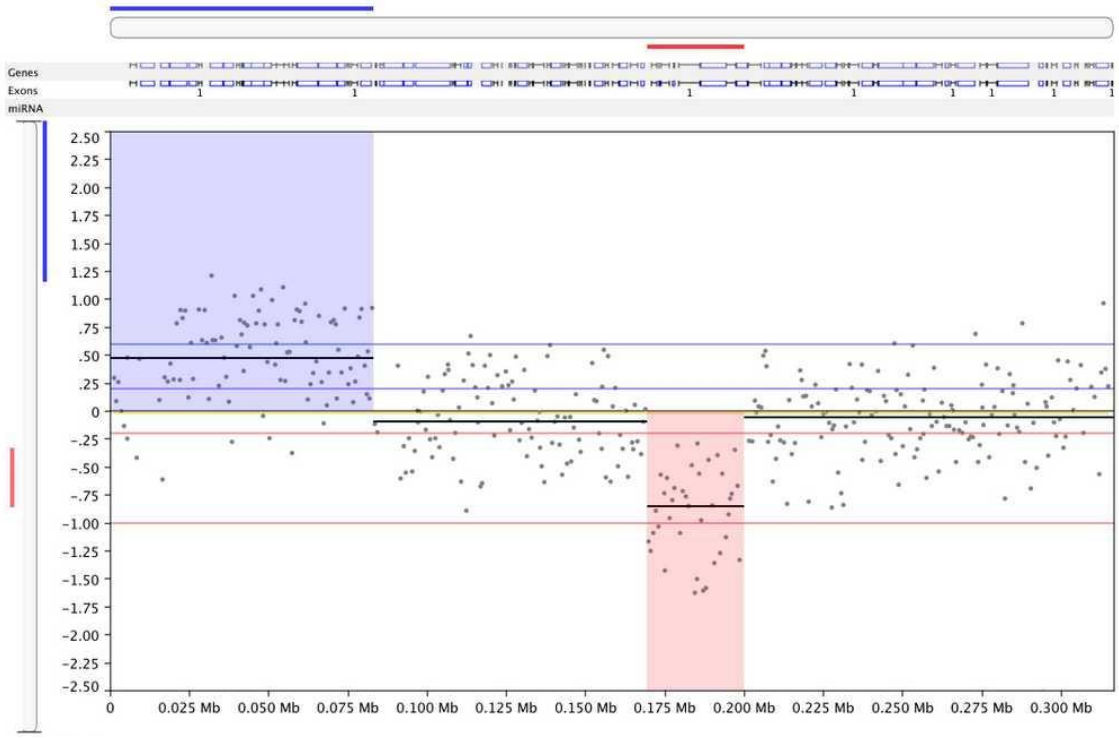

Figure A 16. Chromosome III in H5. Array-CGH profile of Chromosome III in H5 showing copy number gains (blue) and copy number losses (red) with respect to LOG2 ratio for all probes in the region.

H6

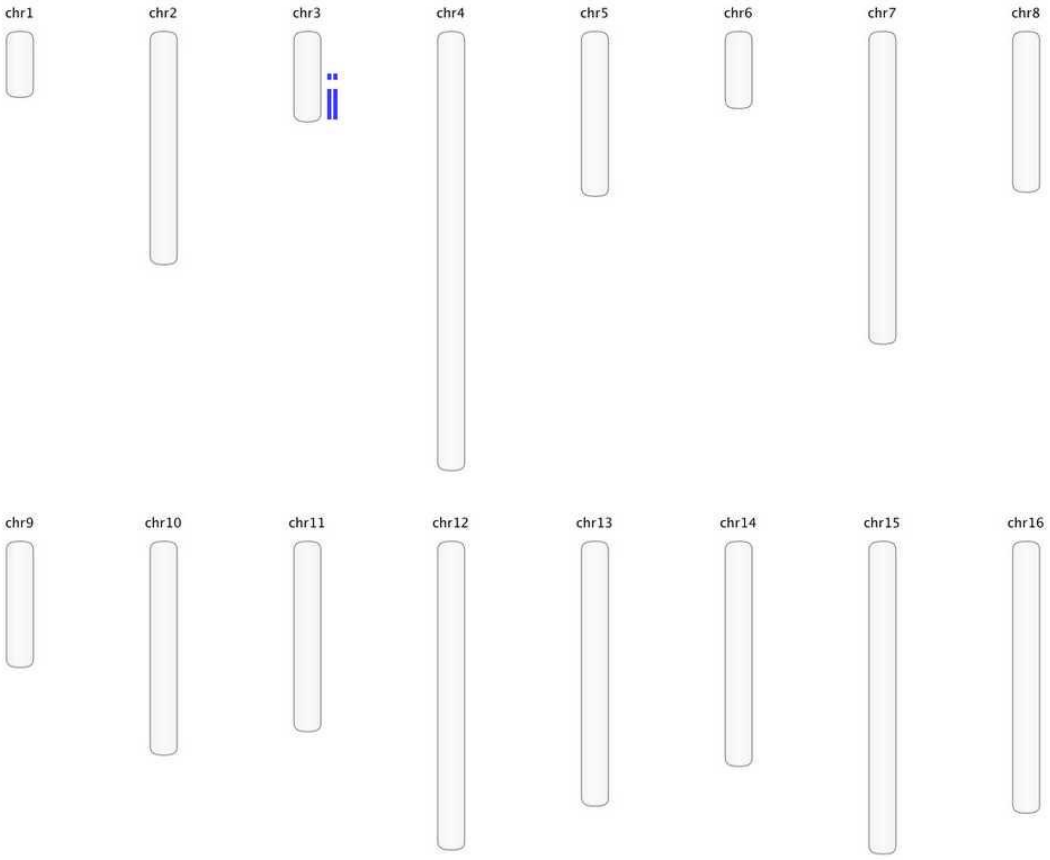

Figure A 17. H6 overview. Array-CGH overview for H6 showing small CNVs in all chromosomes where blue specks on the right side of the chromosome represent copy number gains and red specks on the left side of the chromosome represent copy number losses.

H6

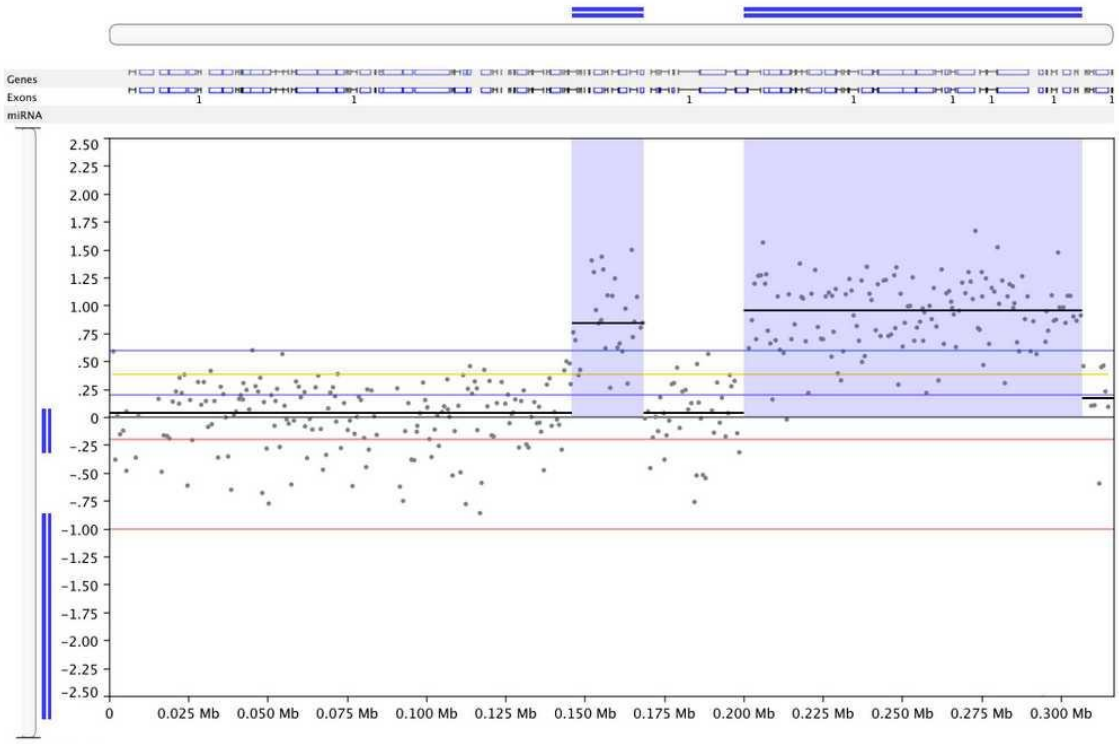

Figure A 18. Chromosome III in H6. Array-CGH profile of Chromosome III in H6 showing copy number gains (blue) with respect to LOG2 ratio for all probes in the region.

H7

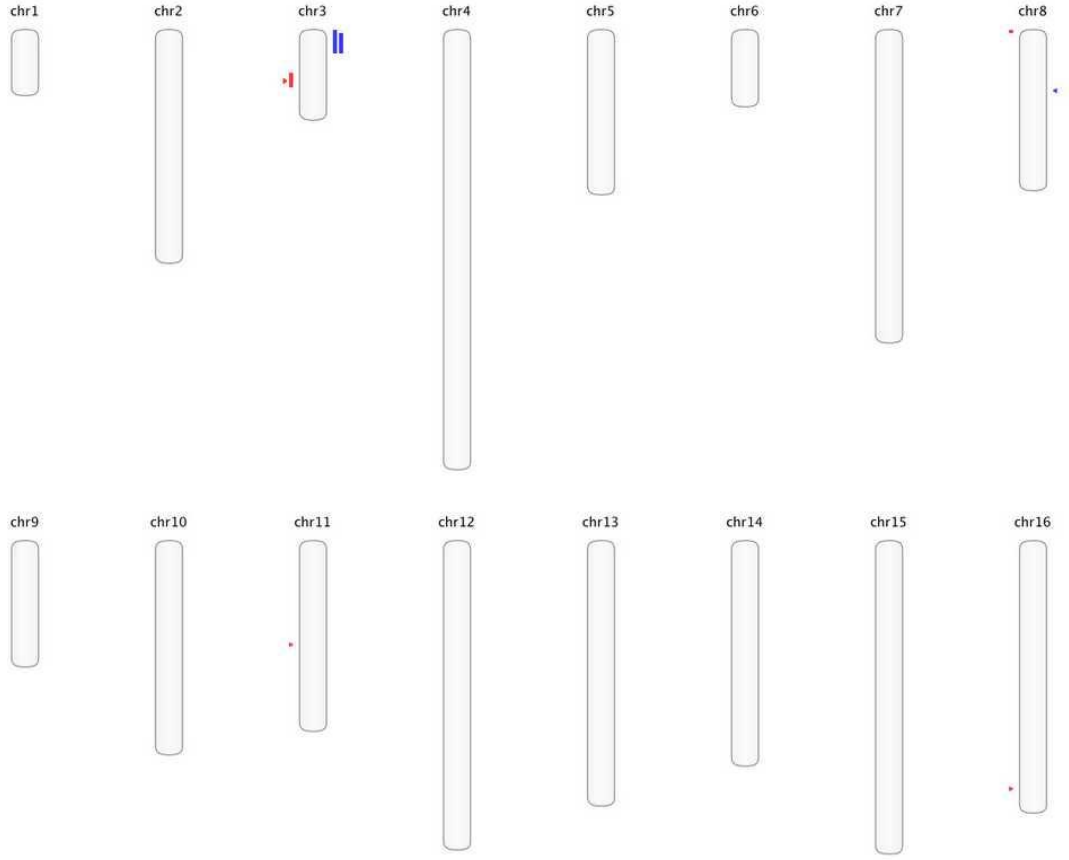

Figure A 19. H7 overview. Array-CGH overview for H7 showing small CNVs in all chromosomes where blue specks on the right side of the chromosome represent copy number gains and red specks on the left side of the chromosome represent copy number losses.

H7

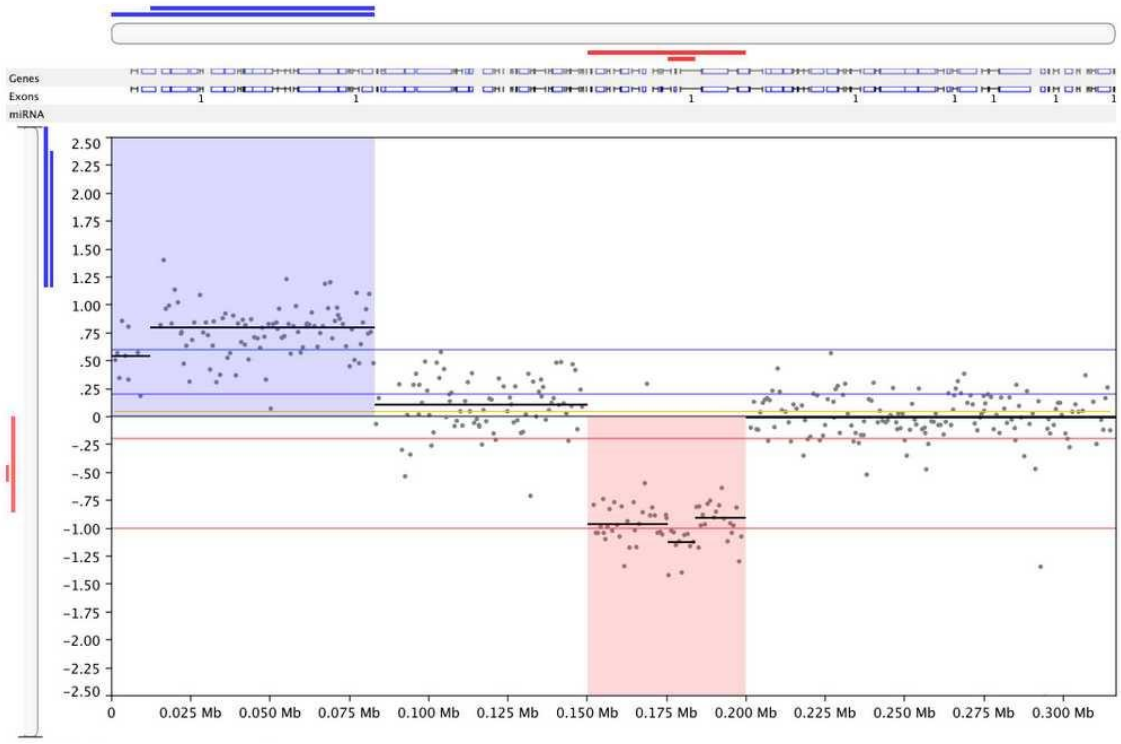

Figure A 20. Chromosome III in H7. Array-CGH profile of Chromosome III in H7 showing copy number gains (blue) and copy number losses (red) with respect to LOG2 ratio for all probes in the region.

H8

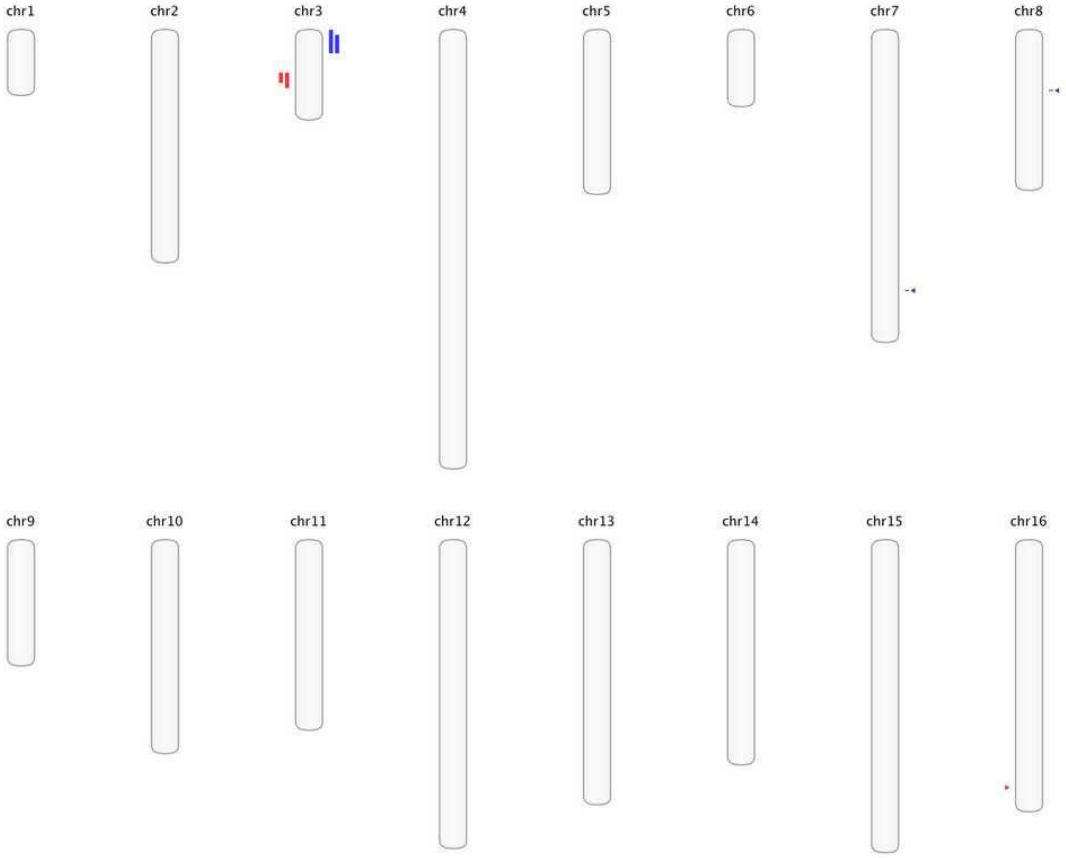

Figure A 21. H8 overview. Array-CGH overview for H8 showing small CNVs in all chromosomes where blue specks on the right side of the chromosome represent copy number gains and red specks on the left side of the chromosome represent copy number losses.

H8

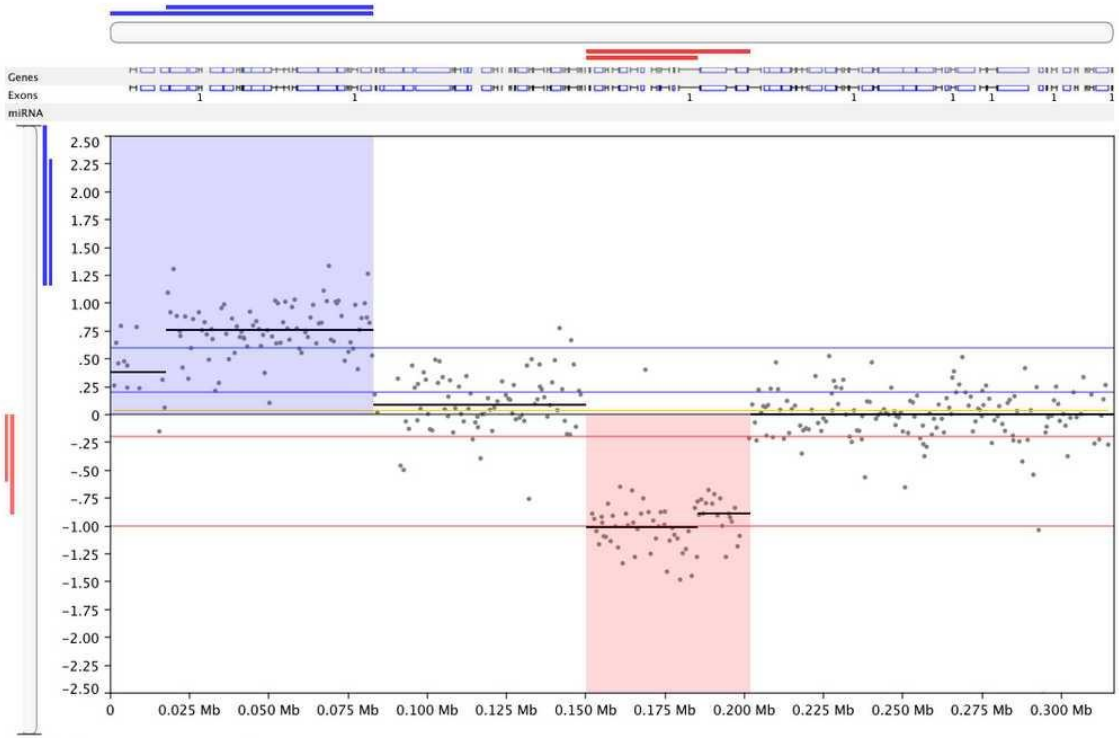

Figure A 22. Chromosome III in H8. Array-CGH profile of Chromosome III in H8 showing copy number gains (blue) and copy number losses (red) with respect to LOG2 ratio for all probes in the region.

H9

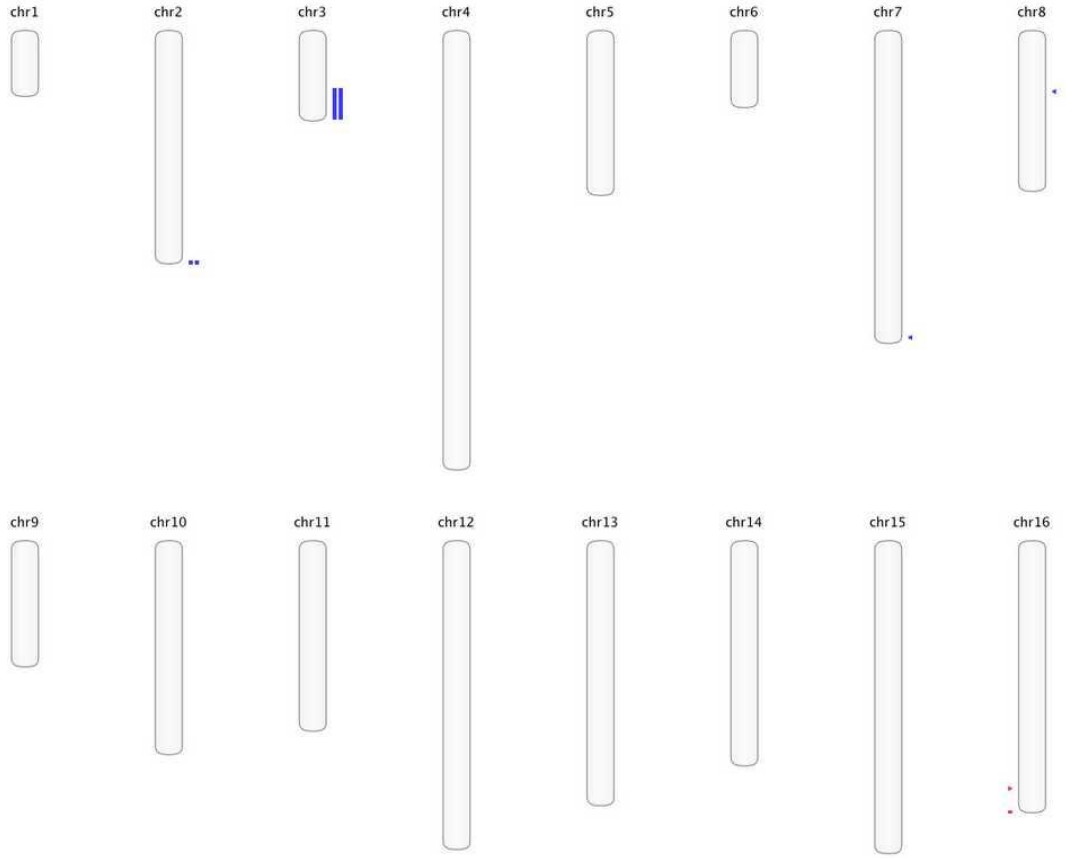

Figure A 23. H9 overview. Array-CGH overview for H9 showing small CNVs in all chromosomes where blue specks on the right side of the chromosome represent copy number gains and red specks on the left side of the chromosome represent copy number losses.

H9

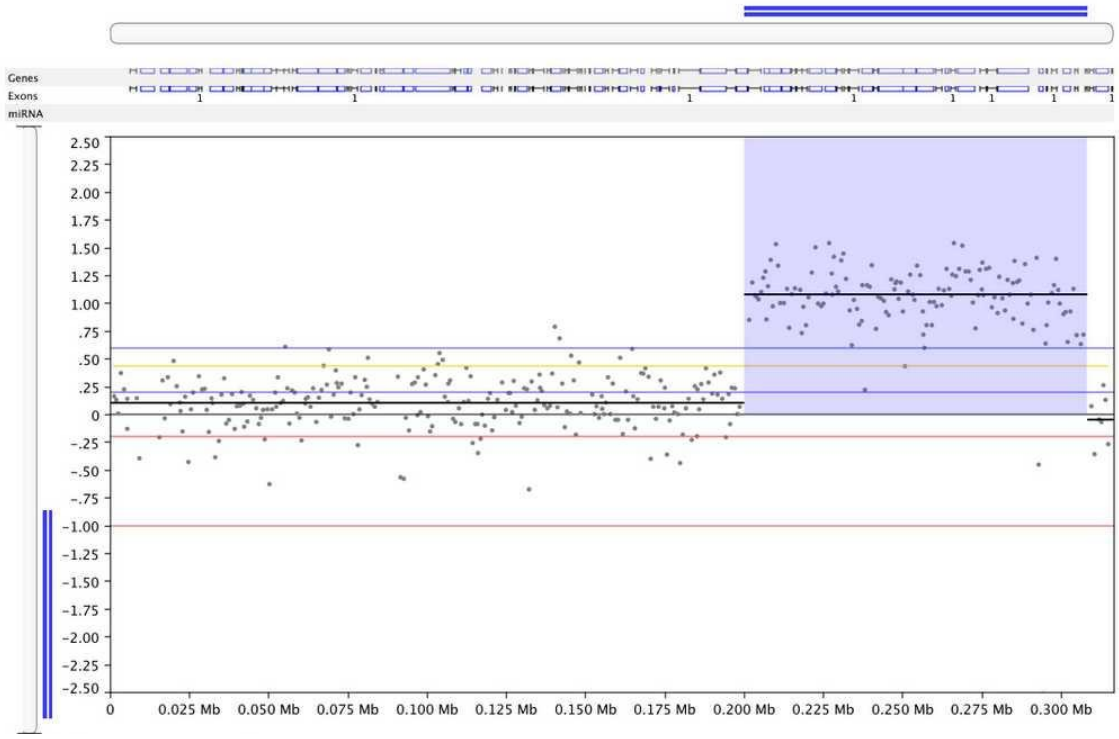

Figure A 24. Chromosome III in H2. Array-CGH profile of Chromosome III in H9 showing a copy number gain (blue) with respect to LOG2 ratio for all probes in the region.

H10

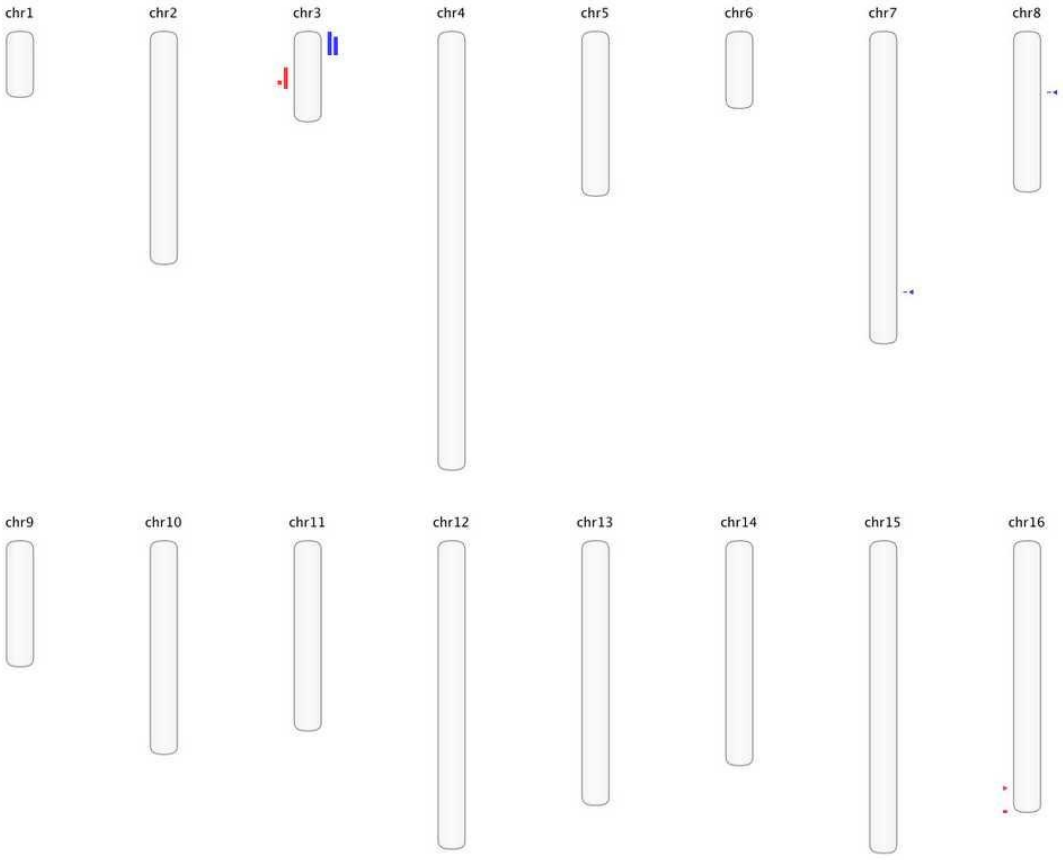

Figure A 25. H10 overview. Array-CGH overview for H10 showing small CNVs in all chromosomes where blue specks on the right side of the chromosome represent copy number gains and red specks on the left side of the chromosome represent copy number losses.

H10

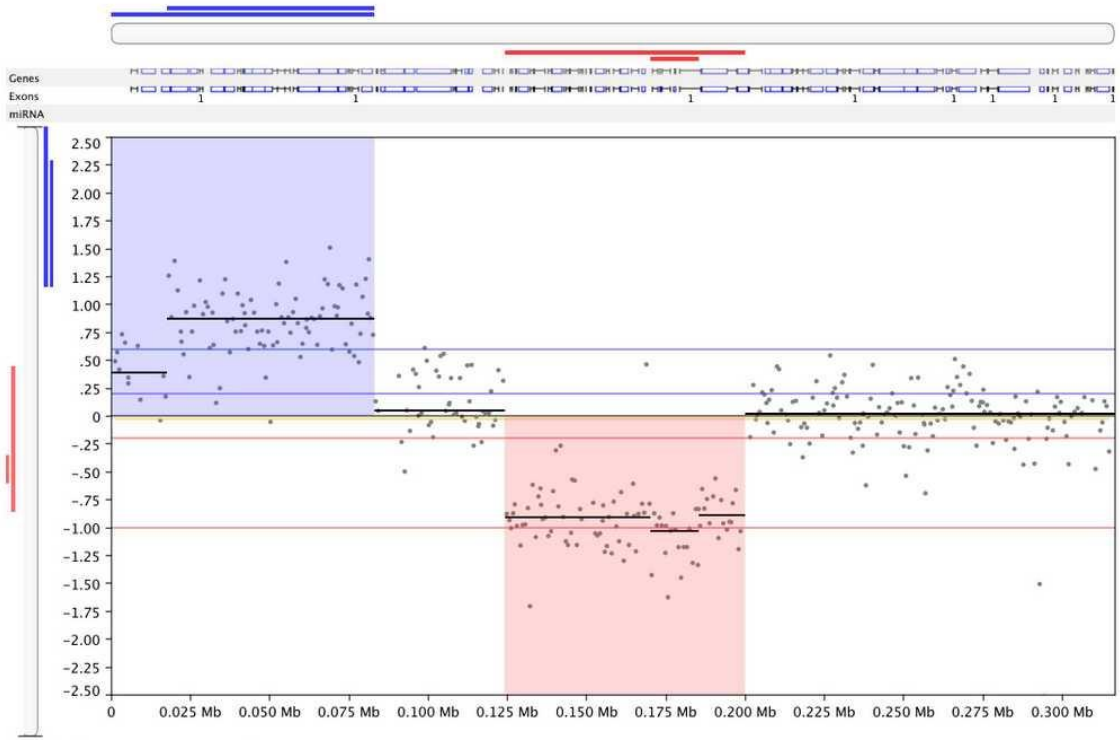

Figure A 26. Chromosome III in H10. Array-CGH profile of Chromosome III in H10 showing copy number gains (blue) and copy number losses (red) with respect to LOG2 ratio for all probes in the region.

H11

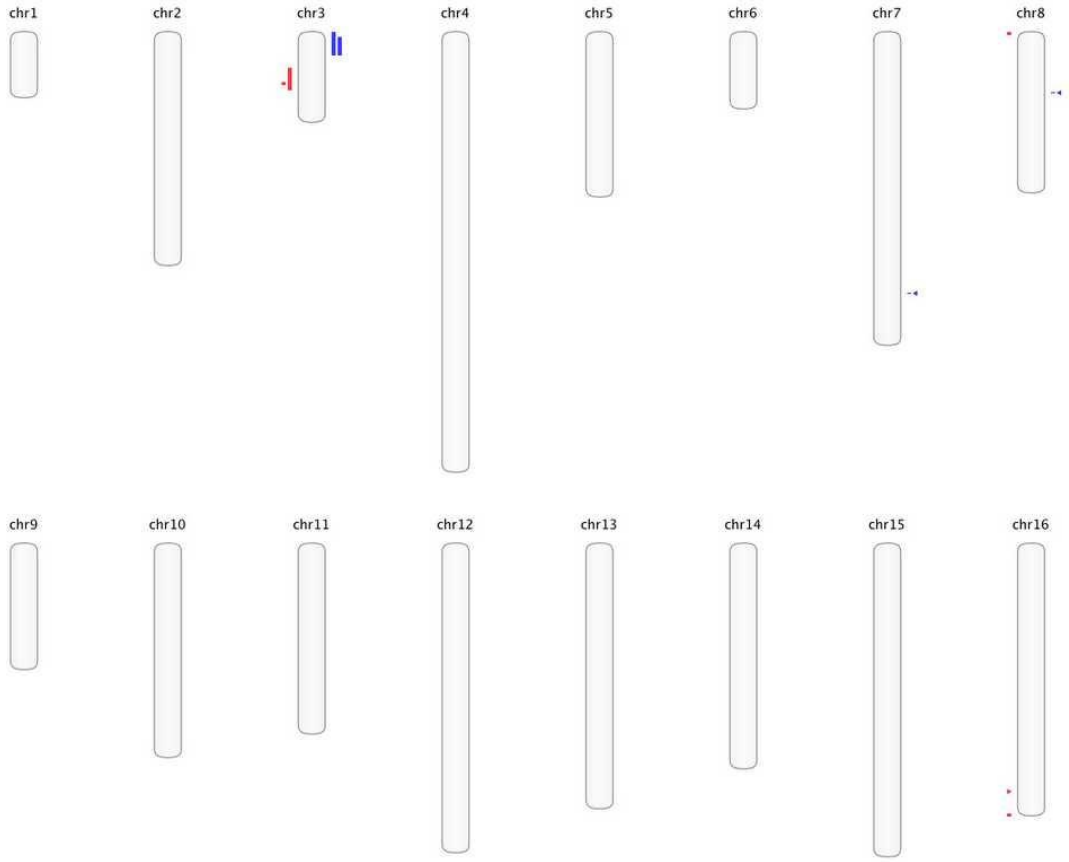

Figure A 27. H11 overview. Array-CGH overview for H11 showing small CNVs in all chromosomes where blue specks on the right side of the chromosome represent copy number gains and red specks on the left side of the chromosome represent copy number losses.

H11

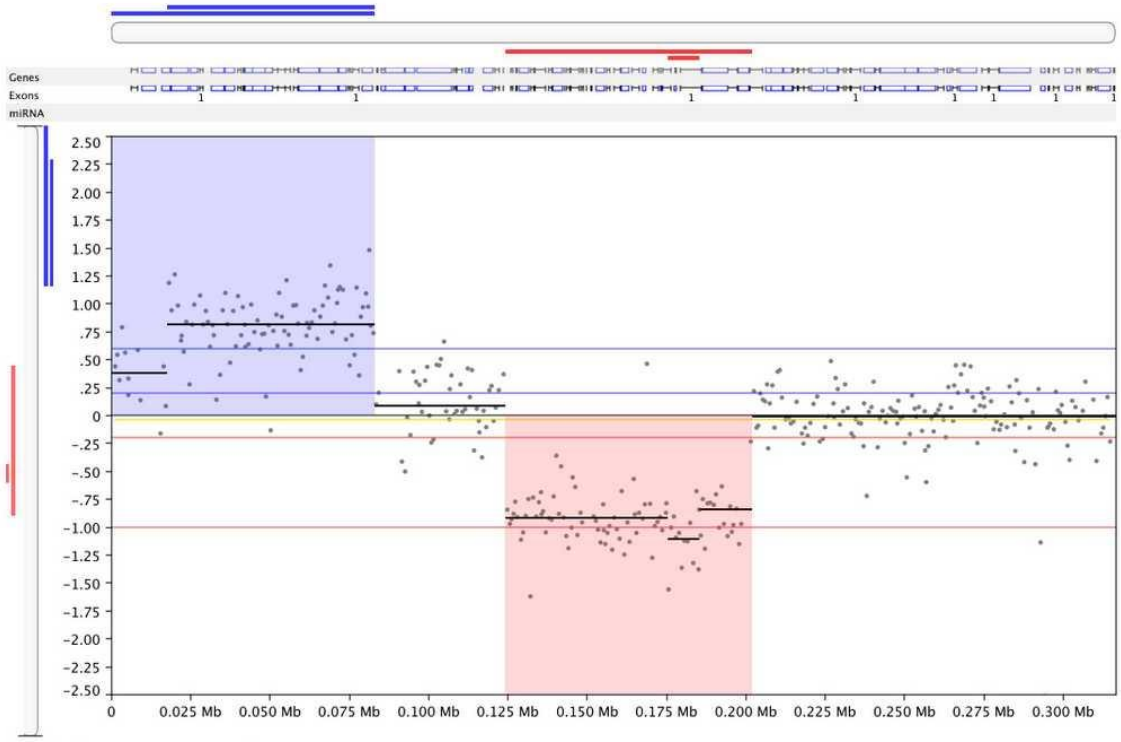

Figure A 28. Chromosome III in H11. Array-CGH profile of Chromosome III in H11 showing copy number gains (blue) and copy number losses (red) with respect to LOG2 ratio for all probes in the region.

H12

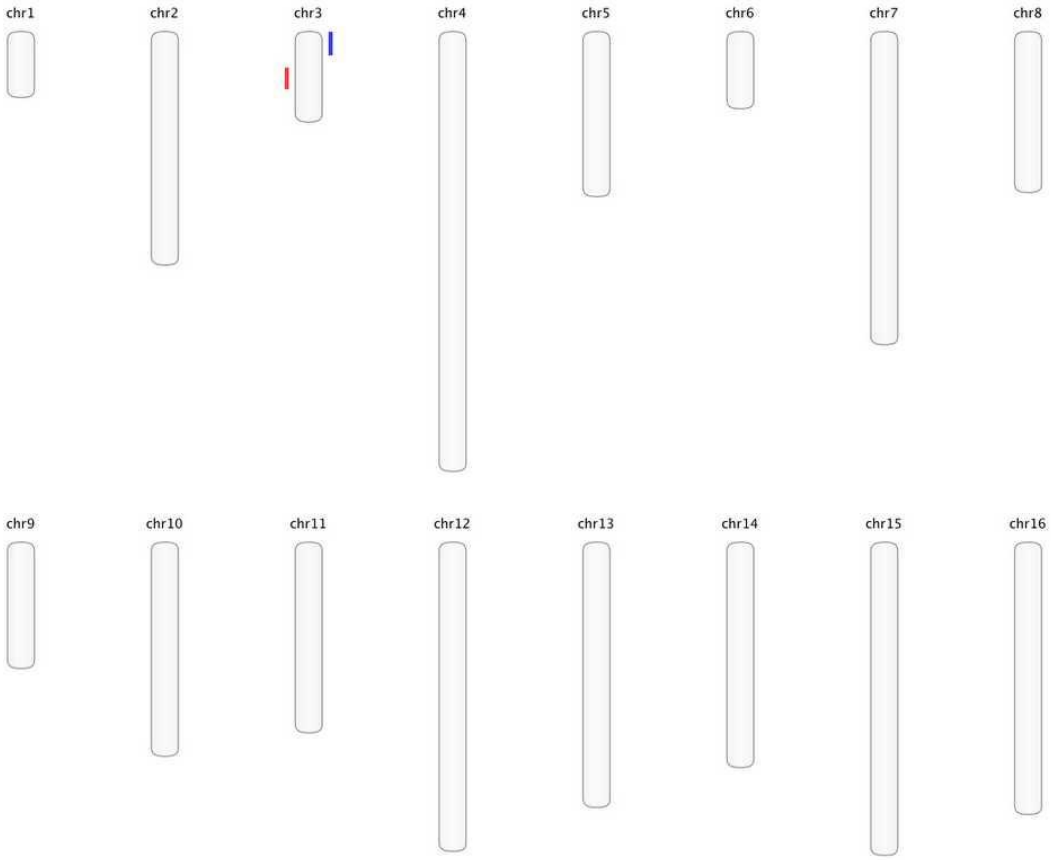

Figure A 29. H12 overview. Array-CGH overview for H12 showing small CNVs in all chromosomes where blue specks on the right side of the chromosome represent copy number gains and red specks on the left side of the chromosome represent copy number losses.

H12

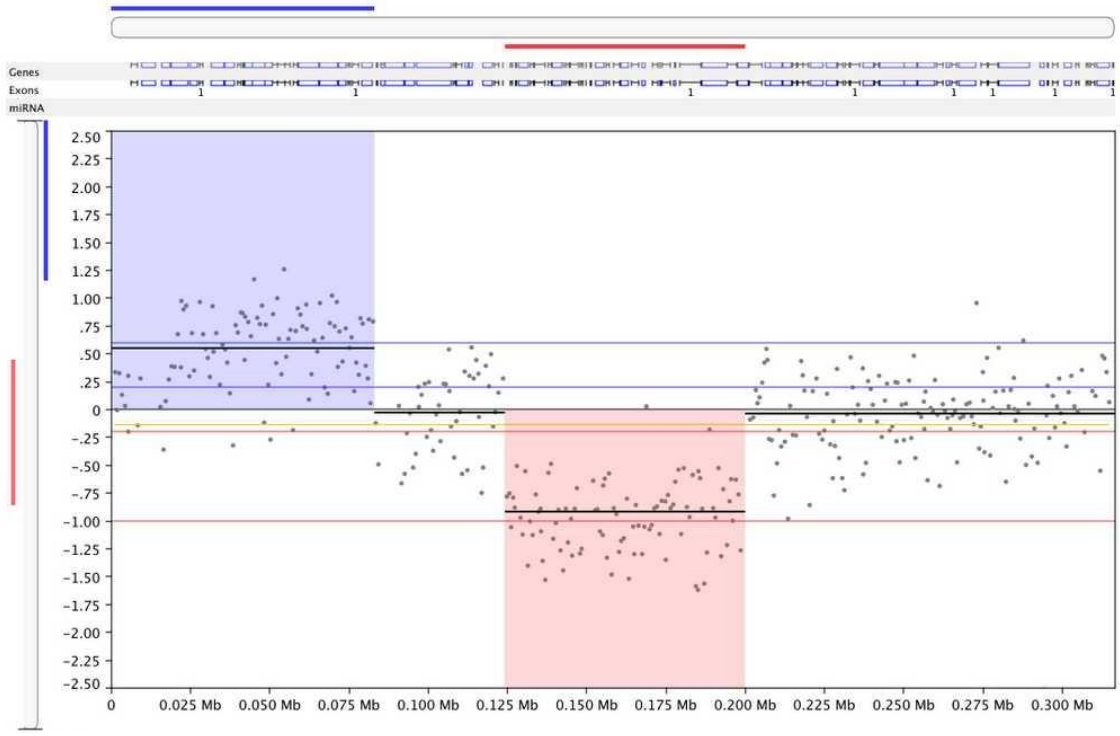

Figure A 30. Chromosome III in H12. Array-CGH profile of Chromosome III in H12 showing copy number gains (blue) and copy number losses (red) with respect to LOG2 ratio for all probes in the region.

H13

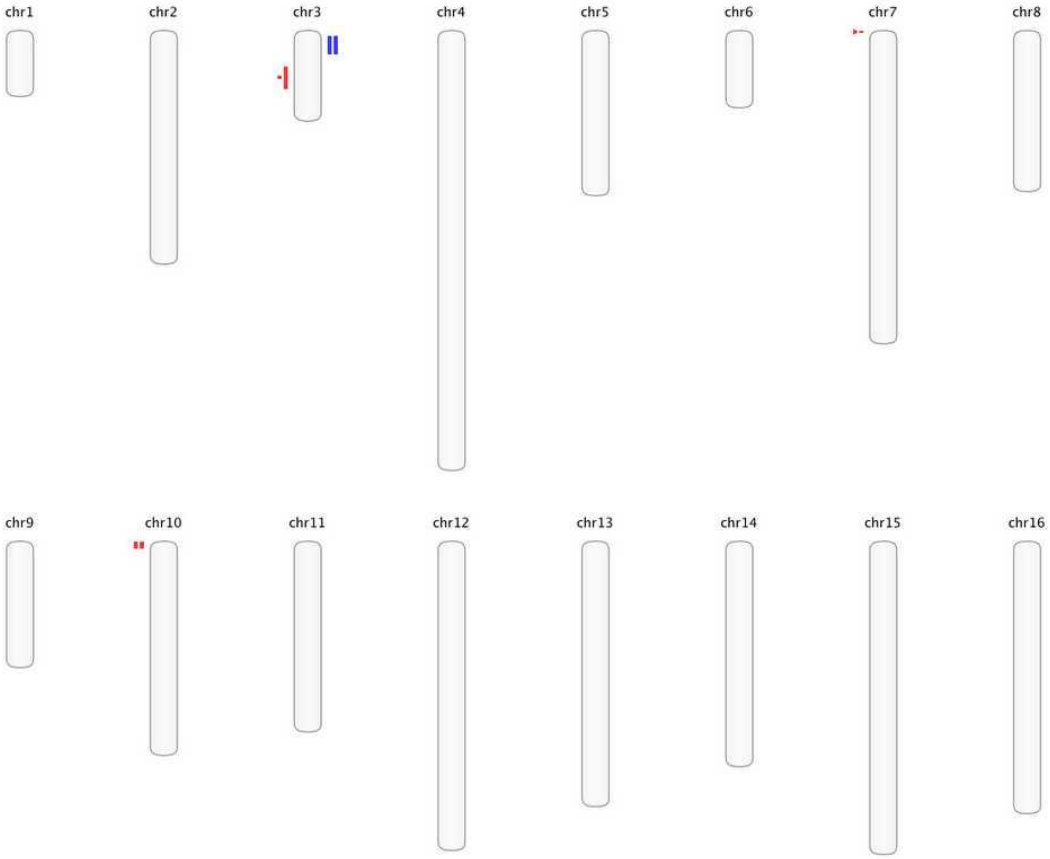

Figure A 31. H13 overview. Array-CGH overview for H13 showing small CNVs in all chromosomes where blue specks on the right side of the chromosome represent copy number gains and red specks on the left side of the chromosome represent copy number losses.

H13

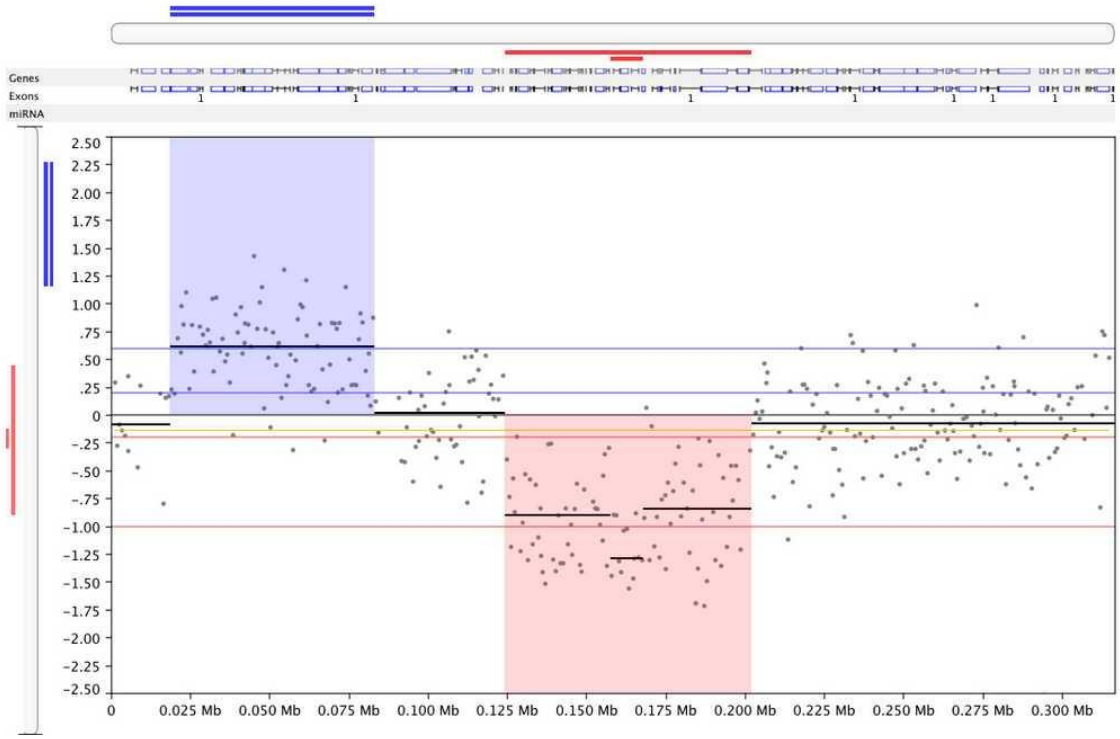

Figure A 32. Chromosome III in H13. Array-CGH profile of Chromosome III in H13 showing copy number gains (blue) and copy number losses (red) with respect to LOG2 ratio for all probes in the region.